CANADIAN THESES

THÈSES CANADIENNES

NOTICE

The quality of this microfiche is heavily dependent upon the quality of the original thesis submitted for microfilming. Every effort has been made to ensure the highest quality of reproduction possible.

If pages are missing, contact the university which granted the degree.

Some pages may have indistinct print especially if the original pages were typed with a poor typewriter ribbon or if the university sent us an inferior photocopy.

Previously copyrighted materials (journal articles, published tests, etc.) are not filmed.

Reproduction in full or in part of this film is governed by the Canadian Copyright Act, R.S.C. 1970, c. C-30. Please read the authorization forms which accompany this thesis.

AVIS

La qualité de cette microfiche dépend grandement de la qualité de la thèse soumise au microfilmage. Nous avons tout fait pour assurer une qualité supérieure de reproduction.

S'il manque des pages, veuillez communiquer avec l'université qui a conféré le grade.

La qualité d'impression de certaines pages peut laisser à désirer, surtout si les pages originales ont été dactylographiées à l'aide d'un ruban usé ou si l'université nous a fait parvenir une photocopie de qualité inférieure.

Les documents qui font déjà l'objet d'un droit d'auteur (articles de revue, examens publiés, etc.) ne sont pas microfilmés.

La reproduction, même partielle, de ce microfilm est soumise à la Loi canadienne sur le droit d'auteur, SRC 1970, c. C-30. Veuillez prendre connaissance des formules d'autorisation qui accompagnent cette thèse.

THIS DISSERTATION HAS BEEN MICROFILMED EXACTLY AS RECEIVED

LA THÈSE A ÉTÉ MICROFILMÉE TELLE QUE NOUS L'AVONS REÇUE

105

NAME OF AUTHOR/NOM DE L'AUTEUR James N. Glosli

TITLE OF THESIS/TITRE DE LA THÈSE Monte Carlo and Renormalization Group Investigation of the Triangular Lattice Gas with Repulsive First and Second Neighbour Interactions

UNIVERSITY/UNIVERSITÉ Simon Fraser University

DEGREE FOR WHICH THESIS WAS PRESENTED/GRADE POUR LEQUEL CETTE THÈSE FUT PRÉSENTÉE Master of Science

YEAR THIS DEGREE CONFERRED/ANNÉE D'OBTENTION DE CE DEGRÉ 1983

NAME OF SUPERVISOR/NOM DU DIRECTEUR DE THÈSE Professor M. Plischke

DATED/DATÉ July 8, 1983 SIGNED/SIGNÉ

PERMANENT ADDRESS/RÉSIDENCE FIXE

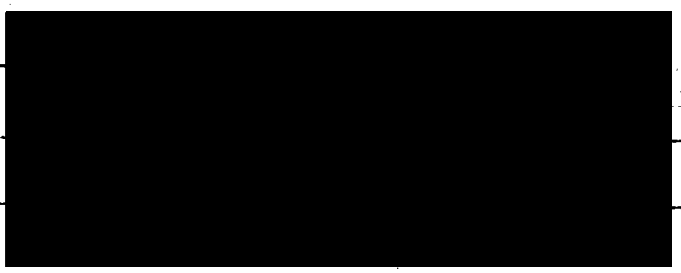

MONTE CARLO AND RENORMALIZATION GROUP INVESTIGATION OF THE TRIANGULAR LATTICE GAS WITH REPULSIVE FIRST AND SECOND NEIGHBOUR INTERACTIONS

by

James N. Glosli

B.Sc., Simon Fraser University, 1981

A THESIS SUBMITTED IN PARTIAL FULFILLMENT OF

THE REQUIREMENTS FOR THE DEGREE OF

MASTER OF SCIENCE

in the Department

of

Physics

SIMON FRASER UNIVERSITY

July 1983

PARTIAL COPYRIGHT LICENSE

I hereby grant to Simon Fraser University the right to lend my thesis, project or extended essay (the title of which is shown below) to users of the Simon Fraser University Library, and to make partial or single copies only for such users or in response to a request from the library of any other university, or other educational institution, on its own behalf or for one of its users. I further agree that permission for multiple copying of this work for scholarly purposes may be granted by me or the Dean of Graduate Studies. It is understood that copying or publication of this work for financial gain shall not be allowed without my written permission.

Title of Thesis/Project/Extended Essay

Monte Carlo and Renormalization Group Investigation of the Triangular Lattice Gas with Repulsive First and Second Neighbour Interactions"

Author:

(signature)

James N. Glosli

(name)

July 8, 1983

(date)

APPROVAL

Name: James N. Glosli

Degree: Master of Science

Title of Thesis: Monte Carlo and Renormalization Group Investigation of the Triangular Lattice Gas with Repulsive First and Second Neighbour Interactions

Examining Committee:

Chairman: B.P. Clayman

M. Plischke
Senior Supervisor

K.S. Viswanathan

J.C. Irwin

L.E. Ballentine
External Examiner
Department of Physics
Simon Fraser University

Approval Date: July 8, 1983

ABSTRACT

The two dimensional lattice gas with repulsive first and second neighbour interactions has been studied on a triangular lattice. To facilitate this study, the lattice gas has been mapped onto the appropriate Ising Hamiltonian and all calculations were carried out for this Ising model. The study employed Monte Carlo and Monte Carlo renormalization group techniques in order to determine the phase diagram, order of the phase transitions and critical exponents of this model. The results are compared with conjecture based on renormalization group calculations.

ACKNOWLEDGEMENTS

I wish to express my sincere gratitude to the many people who assisted and encouraged me in this endeavor. Most deeply, I'd like to recognize and expound on the incredible efforts of time, patience, understanding and endless support given by my advisor, Dr. Michael Plischke. Along with Dr. Plischke, I'd like to thank the rest of my committee; Dr J.C. Irwin, Dr. K.S. Viswanathan, and Dr. L.E. Ballentine, for there critical reading of the thesis and their suggestions.

During both research for and preparation of this thesis I benefitted greatly from discussions with, M.N. Barber, N.A. Berker, M.E. Fisher, David Huse, D.P. Landau, O.G. Mouritsen, M. Schick, J.S. Walker and M. Wortis. I am most appreciated of the effort of a number of people for their technical expertise; namely, Blair McMullin for drafting and figure layout; Glen Miller for his knowledge and assistance with the word proceesing facility generously provided by Microtel Pacific Research.

I would now like to acknowledge the Natural Science and Engineering Reseach Council of Canada for there financial support.

Finally, I wish to tell my wife Chris how much I appreciate her. Though mostly frustrated by this projected, she always supported me in it.

TABLE OF CONTENTS

LIST OF TABLES

LIST OF FIGURES

CHAPTER 1

Introduction

1.1. Model

Two-dimensional models have often been used as a stepping stone towards understanding physically meaningful three-dimensional analogs. Generally the two-dimensional models tend to be more tractable than their three-dimensional counterparts. Hence some exact two-dimensional solutions exist for situations in which the three-dimensional problem remains unsolved.

Recently many two-dimensional models have become physically interesting on their own merits as experimental systems are found which exhibit two-dimensional or quasi two-dimensional behaviour [1,13]. Most experimental work has been on monolayers of atoms or molecules either adsorbed on surfaces or intercalated between layers of crystals. Two examples are helium or other rare gases adsorded on Grafoil or intercalation compounds of noble or alkali metals and host materials such as graphite or transition metal dichalcogenides.

For such systems there exists a substrate potential creating a triangular lattice of highly preferred sites. Therefore a reasonable model for such systems is the triangular lattice gas. The lattice gas Hamiltonian is

$$H=\sum_{i<j} U_{ij} n_i n_j + u^* \sum_i n_i \ , \qquad (1.1.1)$$

where, $n_i=1(0)$ if site i is occupied(unoccupied); U_{ij} is the interaction energy between atoms on sites i and j and u^* is the pseudo chemical potential. u^* includes the perfect lattice chemical potential u plus an additional term to account for thermal vibration of the atoms about the lattice site. For imperfect lattice gases $u^*=u+kT\ln(\lambda^2_T/V_o)$, where,

$\lambda_T^2 = h^2/(2\pi mkT)$ and V_o is the area of the primitive cell of the substrate surface [23,52].

In the lattice gas model, the nearest neighbour interaction U_{nn} would be repulsive for both the rare gas systems on graphite and for intercalation compounds, such as $Ag_x TiS_2$, which we henceforth take as our prototype intercalation compound. For the rare gases the van der Waals potential is the interaction between atoms. This potential is repulsive for nearest neighbour distances of the graphite sites and hence results in a nearest neighbour repulsion U_{nn} . For silver a likely interaction is a screened Coulomb potential and one also expects nearest neighbour repulsion. Both the van der Waals and screened Coulomb potentials fall off quickly and to a first approximation the helium and silver systems can be modeled by a nearest neighbour lattice gas with repulsive interactions. Such a model exhibits an ordered phase with a $(\sqrt{3}\times\sqrt{3})R30^\circ$ structures which would not be present if U_{nn} was attractive [52]. Experimentally such a phase is found for both the rare gas and silver systems supporting the idea of repulsive U_{nn} [29,47,57]. The natural extension is to consider a next nearest neighbour interaction U_{nnn}. For rare gases, in particular Helium, the van der Waals potential is attractive at the nearest neighbour distances with a magnitude approximately 0.1 of the nearest neighbour repulsion [55]. However for silver, the screened Coulomb potential is also repulsive at the next nearest neighbour distance. Interactions mediated by host lattice strains tend to be attractive and will reduce the effect of the Coulomb repulsion. We have not attempted to calculate either the electrostatic or elastic contributions directly. We simply assume that both first and second neighbour interactions are repulsive.

From the above discussion we see that models with either second neighbor repulsion or attraction may be physically interesting. The model with $U_{nnn}=0$ has been studied and is well understood[32,52,56]. The model with second neighbour attraction has also been studied by a number of techniques[31,43].

By examining the possible ground states one finds six interesting cases of next nearest neighbour repulsion. To ennumerate these cases let $a = U_{nnn}/U_{nn}$. The possible cases are:

1. $U_{nn} = 0$ or $a \to \infty$
2. $1 < a$
3. $a = 1$
4. $0.2 < a < 1$
5. $a = 0.2$
6. $0 < a < 0.2$

To the best of the author's knowledge, cases one, four, and five, have not been studied. However, cases two and three have been studied using Monte Carlo, renormalization group, and mean field theory [49,50,63]. Case six is physically the most interesting since the next nearest neighbour interaction is sufficiently small to ensure that the experimentally observed $\sqrt{3} \times \sqrt{3}$ ordered phase is not suppressed.

Walker and Schick have studied some of the features of this case using a finite cluster renormalization group [63]. It is the purpose of this paper to perform a comprehensive study of the phase diagram for fixed a in this range. Because of computing time constraints a typical value of $a = 0.1$ will be chosen in the hope that this will exhibit the qualitative features of the case $a \in (0, 0.2)$.

The lattice gas will not be studied directly but its equivalence to the Ising model enables us to study the corresponding magnetic problem. The lattice gas equivalence to the Ising Model with Hamiltonian

$$H = \sum_{i<j} J_{i,j} s_i s_j + h \sum_i s_i + NC \qquad (1.1.2)$$

is seen by making the following identifications;

$$n_j=\frac{1}{2}(s_j+1),\ h=\frac{1}{4}\sum_{i\neq j}U_{ij}+u^*/2,$$

$$J_{ij}=\frac{1}{4}U_{ij}\ ,\ C=\frac{1}{8}\sum_{i\neq j}U_{ij}+u^*/2$$

where N is the total number of sites and the sums on $i\neq j$ are for fixed i [23,52].

The goals of this study are to find the phase boundaries, order of transitions and critical indices of the antiferromagnetic nearest neighbour and next nearest neighbour triangular Ising model with $a=0.1$.

1.2. Universality

Few models exhibiting a phase transition are exactly solvable. During the 1960's it became clear, from the series expansion calculations of a large number of workers, that the critical properties of many seemingly quite different systems were determined only by the symmetry of the Hamiltonian and the spatial dimensionality of the system. This notion became known as the universality hypothesis. The renormalization group theory of Wilson put this hypothesis on a firm theoretical foundation - a single fixed point in a large Hamiltonian space can attract an infinity of different systems crossing the same critical surface. All these systems will thus display the same critical behaviour [65,66].

The most straight forward way of identifying the universality class of a system is to construct the Landau theory for the system. One writes down an expansion of the free energy in powers of the order parameters allowing all terms which are invariant under the symmetry group of the system. These expansions can then generally be related to the Landau free energies of certain canonical models (eg. the Ising ferromagnet, the Heisenberg ferromagnet, and the q-state Potts model), which are thought to be well understood. In three dimensions this classification scheme has proven to be very successful when combined with a renormalization group treatment of the aforementioned canonical models.

In two dimensions the situation is much more complicated. Many of the "simple" models such as the q-state Potts model have competing fixed points on their critical surface

[42,60]. Thus one needs to know not only what the symmetry of the model is, but which fixed point on the critical surface the renormalized Hamiltonian is attracted to. It is generally not possible to predict this from an examination of the microscopic interaction parameters. Nevertheless, we shall summarize below the results of Landau theory and the predictions of the universality hypothesis.

Before stating the results of Landau theory the nature of the ground state of this model will be discussed. For $h>0$ there exists six possible ground state configurations [33]. These are shown in Fig.1.2.1a-f. There also exists six other ground state configurations for $h<0$. However, the free energy is an even function of h and it suffices to study the $h>0$ case to understand the model for all h.

A point that should be made here is that the 3x1 structure of Fig.1.2.1e and the 3x3 structure of Fig 1.2.1f are thermodynamically equivalent since there exists a one to one mapping between sites of the two structures which are energetically identical.

By comparing the energy of the six structures, one can determine the zero temperature phase diagram as shown in Fig.1.2.2. In this diagram changing h for fixed J_{nn} and J_{nnn} and hence fixed a results in moving along a line of slope a which terminates at the origin. The two special cases $a=0.2$ and $a=1$ are represented on Fig.1.2.2 by the two solid lines. From this we see why the six cases mentioned in section 1.1 are qualitatively different and hence interesting to study.

As mentioned, the case to be studied in this investigation was the small a and repulsive J_{nn} and J_{nnn} model. For this case there exists four ground state configuration and from Fig.1.2.2 we can find the critical fields for the zero temperature transitions. These are displayed in Fig.1.2.3 along with speculative finite temperature phase boundaries. These boundaries have been drawn in only to facilitate a discussion of phase transitions.

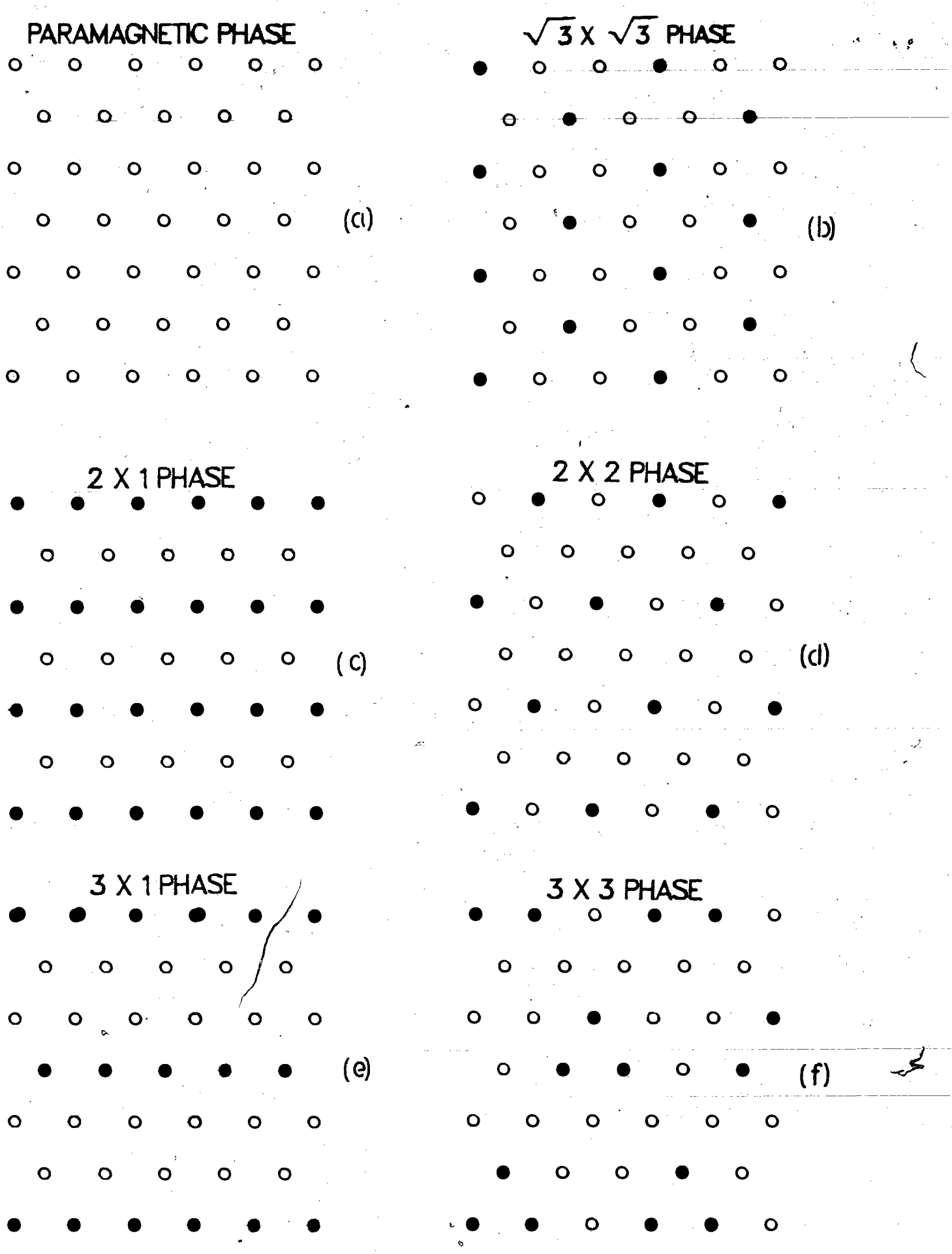

Figure 1.2.1a-f

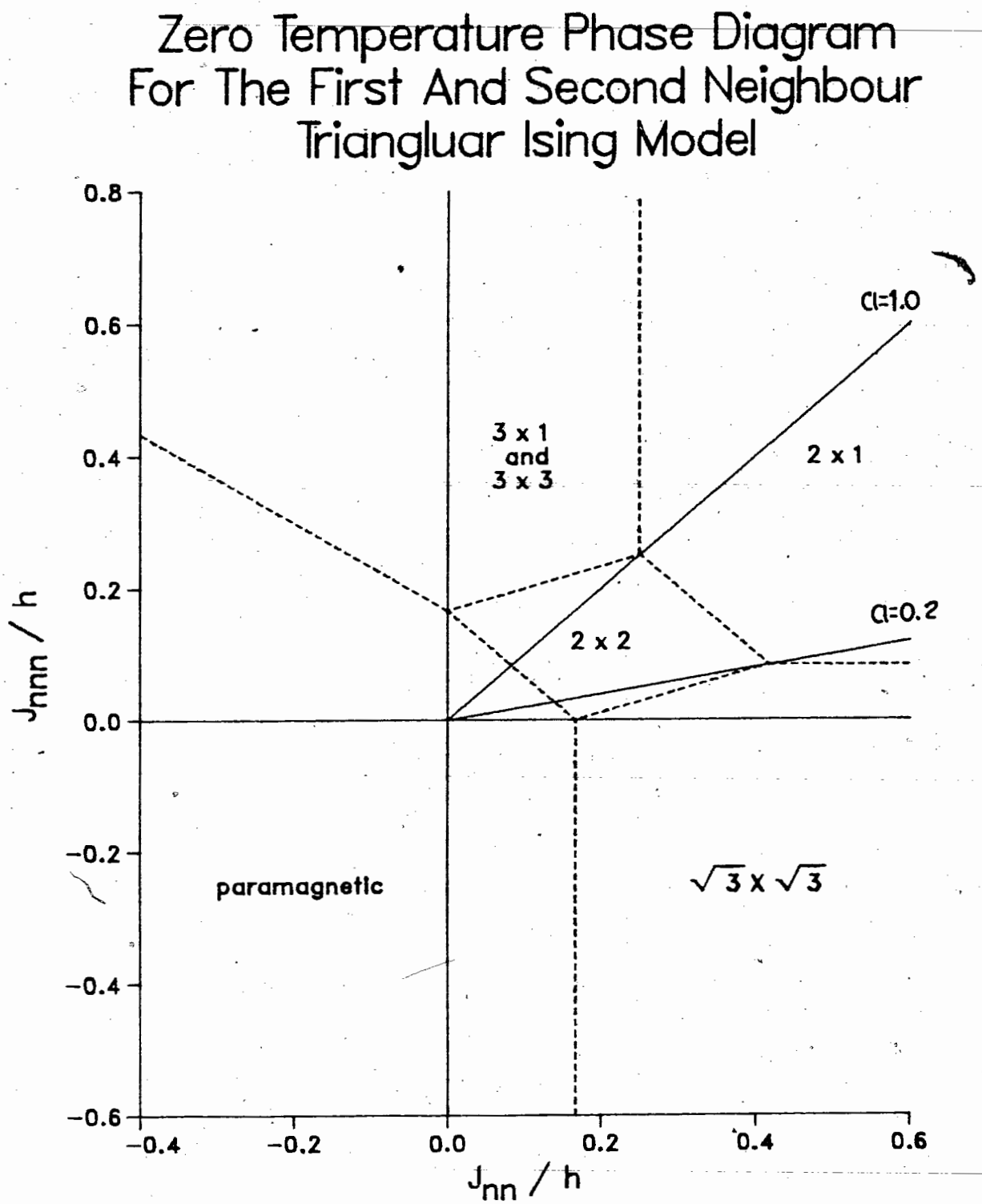
Zero Temperature Phase Diagram
For The First And Second Neighbour
Triangluar Ising Model
0.8
0.6
0.4
0.2
0.0
−0.2
−0.4
−0.6
−0.4
−0.2
0.0
0.2
0.4
0.6
J_{nnn} / h
J_{nn} / h
α=1.0
α=0.2
3 x 1
and
3 x 3
2 x 1
2 x 2
paramagnetic
$\sqrt{3} \times \sqrt{3}$

Figure 1.2.2

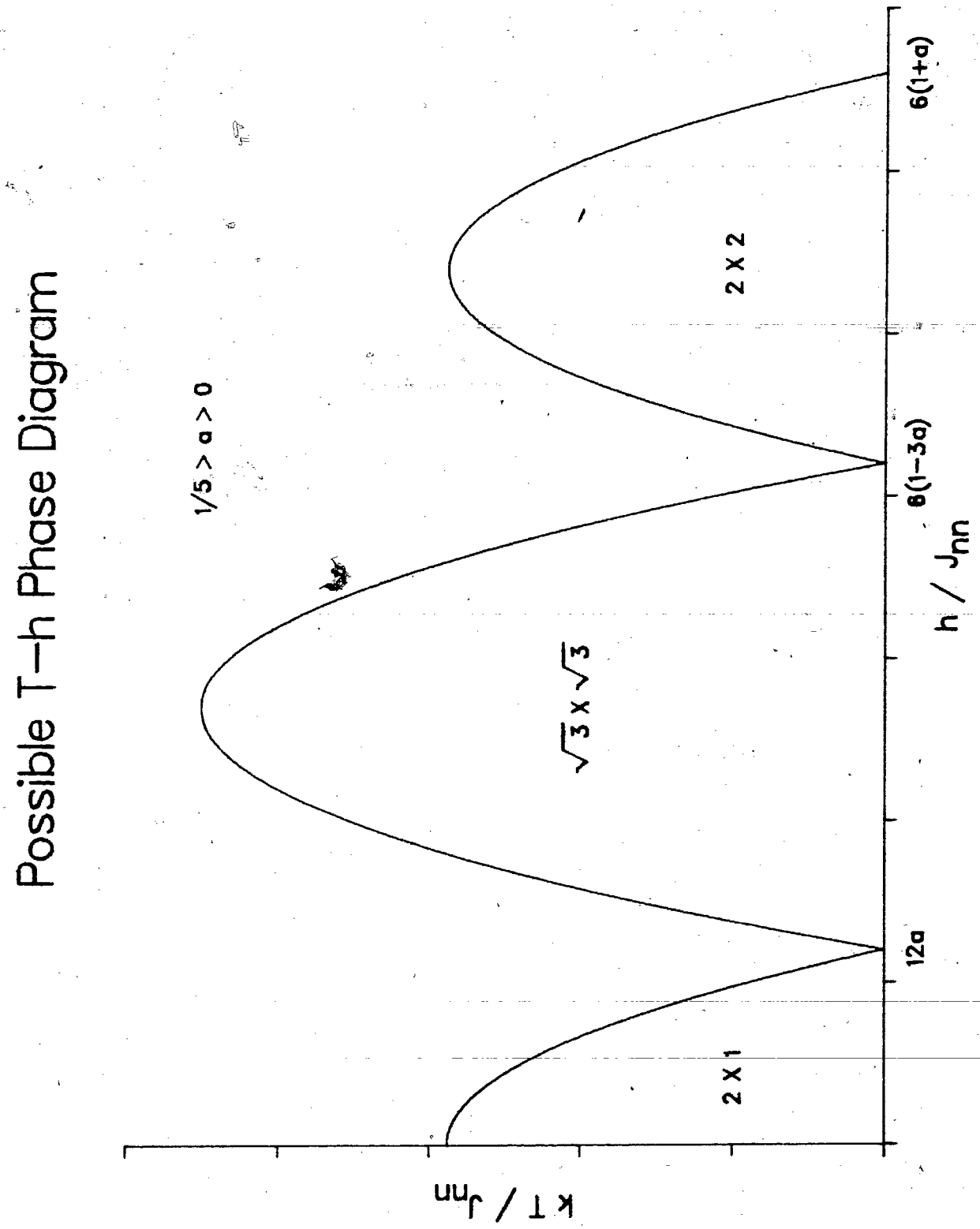
Possible T—h Phase Diagram
1/5 > a > 0
2 X 2
√3 x √3
2 X 1
12a
6(1−3a)
6(1+a)
h / J_nn
k T / J_nn

Figure 1.2.3

This now brings us back to the original discussion of classification of phase transitions. Much work has been done by Schick and his collaborators to classify order-disorder transitions using Landau theory [14,15,51]. Below, the results of their analysis are summarized.

The 2x1 order-disorder transition is found to be in the universality class of the Heisenberg model with face centre cubic anisotropy. The work of Mouritsen, Berlinsky, Bak and Knak-Jensen [35,36] indicates that this Heisenberg model has a first order transition in three dimensions. It is generally believed that the transition will also be first order in two dimensions and we thus expect the 2x1 order-disorder transition to be first order.

The $\sqrt{3}\times\sqrt{3}$ order-disorder transition is found to belong to the same universality class as the three state Potts model and Baxter's hard hexagon model. These models have a continuous transition. Monte Carlo renormalization group studies of the three state Potts model and Baxter's exact solution of the hard hexagon model indicate that the critical exponents for systems in this class will be $\alpha=\frac{1}{3}$ and $\beta=\frac{1}{9}$ [2,48].

The final order-disorder transition is to the 2x2 ordered phase. This transition is in the same class as that of the four state Potts and Baxter-Wu model. Again Monte Carlo renormalization group studies of the four state Potts model and the exact solution of the Baxter-Wu model indicate that the critical exponents for this class are $\alpha=\frac{2}{3}$ and $\beta=\frac{1}{12}$ [3,48,60].

Other possible transitions are between the 2x1 and $\sqrt{3}\times\sqrt{3}$ phases or 2x2 and $\sqrt{3}\times\sqrt{3}$ phase. The symmetry of the 2x1 or 2x2 phase is not a subgroup of the $\sqrt{3}\times\sqrt{3}$ symmetry. Neither is the converse true. These transitions are therefore expected to be first order. Much of the remaining work of this paper will be devoted to testing these predictions.

CHAPTER 2

Theory

2.1. Renormalisation Group

Often group theory is used to study the nature of the perturbation problem whose Hamiltonian has the form

$$H = H_0 + H_1 ,$$

where H_1 is a small perturbation of H_0 and has a lower symmetry. Much of the success in applying this approach depends on finding an H_0 with the highest possible symmetry that still ensures that H_1 is a small perturbation. Some of the symmetries that often occur in physical problems are continuous translation or rotations as well as their discrete counterparts as defined on lattices.

However, in critical phenomena a new symmetry operation must be found to exploit the ideas of group theory in critical systems. To find this symmetry the physics of the problem will be considered. Experimentally, it is found that the correlation length of the system diverges as it approaches criticality. If the assertion is made, now called the scaling hypothesis, that the only relevant length governing the singular behaviour near the critical point (T_c) is the correlation length (ξ), we find the system depends little on microscopic detail and is therefore independent of the length scale chosen. This follows because the only way a length (l) enters the problem is as l/ξ (scaling hypothesis) and as $T_c \to 0$, $\xi \to \infty$ which implies $l/\xi \to 0$ for all finite l.

Now with an invariance discovered, a group operation which exploits this invariance must be found. A possible operation could consist of the following steps:

1. "Average" over a set of microscopic degrees of freedom and assign an effective degree of freedom to this set.

2. Then "rescale" all lengths in the new problem of effective degrees of freedom to make it isomorphic to the original problem.

Since the critical system is assumed independent of microscopic detail and length scales, this operation should be an invariant symmetry operation. These ideas, which form the basis of the renormalization group (R.G.), are due to Kadanoff [24]. Wilson formalized these ideas into the modern theory of renormalization group [65,66]. Niemeijer and van Leeuwen applied the theory of Wilson to spin systems [16,38,39]. The approach of the latter authors is used below to precisely define the operations of the R.G. for Ising spin systems.

Imagine a lattice of Ising Spins (s) with Hamiltonian $H(s)$. Subdivide this system into blocks of spins and choose an "averaging rule" to assign an effective Ising spin to each block, based on the spin configuration of the block. This will be called the block spin (s'). Next, rescale the lengths of the blocked system to match those of the spin system. This defines the block Hamiltonian $H'(s')$ that governs the action of the block spins. Though Kadanoff was unable to construct the relationship between H and H', he was able to develop a scaling theory with these intuitive operations and the notion of scale invariance. Scaling theory will not be discussed here though it will be shown to follow naturally from the renormalization group. The next step in R.G. theory is to derive the relationship between H and H'. However, to do this we must be able to characterize these Hamiltonians by a set of parameters. Instead of H, the dimensionless Hamiltonian $\tilde{H} = -H/kT$ will be used in the remaining analysis. To characterize this Hamiltonian, some definitions are needed. Let s_i be the spin at site i of a d-dimensional lattice (Q) of N points. Then let a be a subset of Q and $A = \{a \mid \text{for } \textit{all subsets } a \in Q\}$. Let $S_a = \prod_{i \in a} s_i$. Then the most general Ising Hamiltonian has the form;

$$\tilde{H}(s)=\sum_{a\in A} K_a S_a \ , \tag{2.1.1}$$

where $s=\{s_i \mid \text{for } all\ i\in Q\}$ and K_a is a set of parameters.

In this paper only homogeneous Hamiltonians will be considered. A homogeneous Hamiltonian is defined as : If $a,b\subset Q$ and if there exists a symmetry operation R of the lattice space group such that $a=Rb \Rightarrow K_a=K_b$, then the Hamiltonian is homogeneous and can be written as;

$$\tilde{H}(s)=\sum_{w\in B} K_w \sum_{a\in w} S_a \ , \tag{2.1.2}$$

where w is the class of all subsets such that $a,b\subset w$ if and only if there exists a lattice transformation R such that $a=Rb$ with, $K_a=K_b=K_w$ and $B=\{w \mid \text{for } all\ such\ classes\}$. If $\tilde{H}(s)$ is written out explicitly it has a more familiar form;

$$\tilde{H}(s)=K_{nag}\sum_i s_i+K_{nn}\sum_{nn} s_i s_j+K_\Delta\sum_\Delta s_i s_j s_k+\cdots \ . \tag{2.1.3}$$

From the above we see that all that is needed to describe the Hamiltonian is the set of coupling constants K_a. Therefore, each Ising-like Hamiltonian can be represented by a a point in some infinite dimensional space. This space is called the Hamiltonian or parameter space. Initially, it was the relationship between $\tilde{H}(s)$ and $\tilde{H}'(s')$ which was sought. However, if we write

$$\tilde{H}=\sum_{w\in B} K_w \sum_{a\in w} S_a \tag{2.1.4}$$

and

$$\tilde{H}'(s')=\sum_{w\in B} K_w' \sum_{a\in w} S_a' \ , \tag{2.1.5}$$

this translates into finding the functions $R_a(K)$ such that $K_a'=R_a(K)$.

To calculate R the "average rule" must be clearly defined. The average rule can be thought of as a conditional probability $P(s_i',\bar{s}_i)$, which is the probability that the block spin of the i^{th} block has the value s_i' given that the configuration of spins in the i^{th} block is $\bar{s}_i$. This now defines the conditional Probability $P(s';s)$ between the block spin configuration s' and spin configuration s as,

$$P(s';s)=\prod_{i}^{N'} P(s_i',\bar{s}_i)>0\,, \tag{2.1.6a}$$

with

$$\sum_{s'} P(s';s)=1\,, \tag{2.1.6b}$$

where N' is the number of blocks. Therefore the Probability $P'(s')$ of a block spin configuration s', is

$$P'(s')=\sum_{s} P(s';s)P(s)\,, \tag{2.1.7}$$

where $P(s)$ is the probability of the spin configuration given by

$$P(s)=\exp\{\tilde{H}(s)\}/\sum_{s}\exp\{\tilde{H}(s)\}\,. \tag{2.1.8}$$

By analogy to 2.1.8 we seek $\tilde{H}'(s')$ such that

$$P'(s')=\exp\{\tilde{H}'(s')\}/\sum_{s'}\{\tilde{H}'(s')\}\,, \tag{2.1.9}$$

By combining 2.1.7, 2.1.8a, 2.1.9a and defining a function $G(K)$ as;

$$\exp\{G(K)\}=\sum_{s}\exp\{\tilde{H}(s)\}/\sum_{s'}\exp\{\tilde{H}'(s')\}\,,$$

we find that

$$\exp\{G(K)+\tilde{H}'(s')\}=\sum_{s}P(s';s)\exp\{\tilde{H}(s)\}\,. \tag{2.1.10}$$

This relationship between $\tilde{H}$ and $\tilde{H}'$ in principle determines the function $K_a'=R_a(K)$ More generally it follows that

$$K^{(n)}=R(K^{(n-1)})=R(R\ldots R(K)\cdots)=R^{(n)}(K) \tag{2.1.12}$$

where $K^{(n)}$ is the coupling constant of the system which has been blocked n times. Notice that equation 2.1.12 can be thought of as a recursion relation. From this point of view the topology of the flows, defined by R , in the Hamiltonian space becomes interesting. In light of the assertion that a critical system be invariant under the renormalization group transformation (ie. $K'=K=K^*$) the fixed points of R (i.e. $K^*=R(K^*)$) are particularly interesting and correspond to sinks or sources of the flow of coupling constants through Hamiltonian space.

A number of questions can be asked about the relationship between fixed points of R and criticality of a system.

1 Do all fixed points correspond to a critical system?

2 Is a critical system a fixed point of $R(K)$?

To answer these questions the effect of the topology of the flows in the neighbourhood of the fixed point K^* on the free energy must be studied. The effect of the flows on the free energy is most easily seen if a recursion relation between the free energies of the block and spin systems $F'(K')$ and $F(K)$ respectively, is derived. The derivation is as follows.

If 2.1.10 is summed over s' on both sides and the sums s and s' of the right hand side are interchanged then

$$\sum_{s'}\exp\{G(K)+\tilde{H}'(s')\}=\sum_{ss'}P(s';s)\exp\{\tilde{H}(s)\}\,.$$

However by 2.1.6b this reduces to

$$\exp\{G+F'(K')\}=\exp\{F(K)\}$$

or

$$G(K)+F'(K')=F(K)\,.$$

Now let $N=$ number of particles of spin system, $N'=$ number of particles of block system, and $N'/N=l^{-d}$. We expect G,F, and F', to be extensive quantities. Therefore, as $N\to\infty$, $G(K)\to Ng(K)$, $F(K)\to Nf(K)$ and $F'(K')\to N'f(K')$. The relationship

$$f(K)=g(K)+l^{-d}f(K') \qquad (2.1.14)$$

is found. Using this relationship the free energy can be expressed as a sum of terms:

$$f(K)=\sum_{n=0}^{m-1}l^{-nd}g(K^{(n)})+l^{-md}f(K^{(m)})\,. \qquad (2.1.15a)$$

This finite sum may be extended to infinity if

$$\lim_{n\to\infty}l^{-nd}f(K^{(n)})=0\,. \qquad (2.1.15b)$$

A word of caution should be introduced here. In the remaining analysis we assume that $g(K)$ and $R(K)$ are analytic functions of their arguments. This imposes further restrictions on $P(s';s)$. One of the restrictions is that if s_g is the ground state configuration of the spin system with symmetry ω then the ground state configuration of the block system s_g' must have the same symmetry ω. It should be noted that this is only a necessary condition and not a sufficient condition for analyticity. The analyticity assumption is of no small concern and has been one of the weak points of the R.G. arguments [22].

Now consider the recursion relations R in the neighbourhood of a fixed point K^*. Let

$$T^*_{ab}=\frac{\partial K_a'}{\partial K_b}|_{K_b=K_b^*} \tag{2.1.16}$$

then for small $K_b-K_b^*$

$$K_a'-K_a^*=\sum_b T^*_{ab}(K_b-K_b^*)\ . \tag{2.1.17}$$

Let λ_i be the eigenvalues with associated left eigenvectors V^i_a of T^*_{ab} such that

$$\sum_a V^i_a T^*_{ab}=\lambda_i V^i_b$$

Then define the functions u_i and u_i' as:

$$u_i=\sum_a V^i_a(K_a-K_a^*) \tag{2.1.18a}$$

$$u_i'=\sum_a V^i_a(K_a'-K_a^*) \tag{2.1.18b}$$

The u_i and u_i' are called the first order scaling fields of the fixed point K^*. From the above definitions it is easy to see that

$$u_i'=\sum_a V^i_a(K_a'-K_a^*)=\sum_{ab} V^i_a T^*_{ab}(K_b-K_b^*)=\lambda_i\sum_b V^i_b(K_b-K_b^*)=\lambda_i u_i$$

Therefore

$$u_i(K')=\lambda_i u_i(K) \tag{2.1.19}$$

The scaling fields can be generalized such that equation 2.1.19 is true not only for infinitesimal u_i but also for all finite u_i [16]. If $|\lambda_i|>1$ the scaling field u_i is called relevant, if $|\lambda_i|<1, u_i$ is called irrelevant and if $\lambda_i=1$, u_i is called marginal. These

definitions become more meaningful in what follows.

Consider g and f as functions of the scaling fields u_i. Since g is an analytic function of K_a, and hence of u_i, it can be expanded as a power series in u_i

$$g(u_1,u_2,\cdots)=\sum_{\underline{n}=0}^{\infty} g_{\underline{n}} u_1^{n_1}u_2^{n_2}\cdots \tag{2.1.20}$$

where $\underline{n}=(n_1,n_2,\cdots)$. We now perform the above sum in two parts. The first part, $\sum_{lesser}$ which represents the sum over all $\underline{n}$ such that $\lambda_1^{n_1}\lambda_2^{n_2}\cdots<l^d$ and the other part $\sum_{greater}$ which represents the sum over all $\underline{n}$ such that $\lambda_1^{n_1}\lambda_2^{n_2}\cdots\geq l^d$. Therefore we can write g as:

$$g(u_1,u_2,\cdots)=\sum_{lesser} g_{\underline{n}} u_1^{n_1}u_2^{n_2}\cdots+\sum_{greater} g_{\underline{n}} u_1^{n_1}u_2^{n_2}\cdots .$$

By substituting this in equation 2.1.15a and assuming 2.1.15b we find that

$$\begin{aligned} f(u_1,u_2,\cdots)&=\sum_{n=0}^{\infty} l^{-nd} g(\lambda_1^n u_1,\lambda_2^n u_2,\cdots)\\ &=\sum_{n=0}^{\infty} l^{-nd}\sum_{lesser} g_{\underline{n}}(\lambda_1^n u_1)^{n_1}(\lambda_2^n u_2)^{n_2}\cdots\\ &+\sum_{n=0}^{\infty} l^{-nd}\sum_{greater} g_{\underline{n}}(\lambda_1^n u_1)^{n_1}(\lambda_2^n u_2)^{n_2}\cdots \end{aligned} \tag{2.1.21}$$

In the first term of the above equation $\lambda_1^{n_1}\lambda_2^{n_2}\cdots<l^d$ which ensures that the sum is uniformly convergent allowing the sums over n and $\underline{n}$ to be interchanged. However such is not the case for the second term. We define the function g_{rem} to be:

$$g_{rem}(u_1,u_2,\cdots)=\sum_{greater} g_{\underline{n}} u_1^{n_1}u_2^{n_2}\cdots \tag{2.1.22}$$

Making use of the discussion and the above definition one may rewrite equation 2.1.21 in the form:

$$f(u_1,u_2,\cdots)=\sum_{lesser}\frac{(g_{\underline{n}}u_1^{n_1}u_2^{n_2}\cdots\cdots)}{(1-l^{-d}\lambda_1^{n_1}\lambda_2^{n_2}\cdots)}+\sum_{n=0}^{\infty} l^{-nd} g_{rem}(\lambda_1^n u_1,\lambda_2^n u_2,\cdots) \tag{2.1.23}$$

Next notice that

$$\sum_{n=0}^{\infty} l^{-nd} g_{rem}(\lambda_1^n u_1, \lambda_2^n u_2, \cdots) = \sum_{n=-\infty}^{\infty} l^{-nd} g_{rem}(\lambda_1^n u_1, \lambda_2^n u_2, \cdots) - \sum_{n=-\infty}^{-1} l^{-nd} g_{rem}(\lambda_1^n u_1, \lambda_2^n u_2, \cdots)$$

and also if we write g_{rem} out explicitly that

$$-\sum_{n=-\infty}^{-1} l^{-nd} g_{rem}(\lambda_1^n u_1, \lambda_2^n u_2, \cdots) = -\sum_{n=-\infty}^{-1} l^{-nd} \sum_{greater} g_{\underline{n}} (\lambda_1^n u_1)^{n_1} (\lambda_2^n u_2)^{n_2} \cdots$$

If we assume that $\lambda_1^{n_1}\lambda_2^{n_2}\cdots l^{-d} \neq 1$ then the above series is uniformly convergent for all u_i and the order of summation can be interchanged such that it can be written as:

$$\sum_{greater} (g_{\underline{n}} u_1^{n_1} u_2^{n_2} \cdots)/(1 - l^{-d}\lambda_1^{n_1}\lambda_2^{n_2}\cdots)$$

Therefore

$$f(u_1, u_2, \cdots) = \sum_{n=0}^{\infty} \frac{(g_{\underline{n}} u_1^{n_1} u_2^{n_2} \cdots)}{(1 - l^{-d}\lambda_1^{n_1}\lambda_2^{n_2}\cdots)} + \sum_{n=-\infty}^{\infty} l^{-nd} g_{rem}(\lambda_1^n u_1, \lambda_2^n u_2, \cdots) \quad (2.1.24)$$

or

$$f(u_1, u_2, \cdots) = f_{reg}(u_1, u_2, \cdots) + f_{sing}(u_1, u_2, \cdots) \quad (2.1.25)$$

$$f_{reg}(u_1, u_2, \cdots) = \sum_{n=0}^{\infty} \frac{(g_{\underline{n}} u_1^{n_1} u_2^{n_2} \cdots)}{(1 - l^{-d}\lambda_1^{n_1}\lambda_2^{n_2}\cdots)} \quad (2.1.26)$$

$$f_{sing}(u_1, u_2, \cdots) = \sum_{n=-\infty}^{\infty} l^{-nd} g_{rem}(\lambda_1^n u_1, \lambda_2^n u_2, \cdots) \quad (2.1.27)$$

from equation 2.1.27 we can see that

$$f_{sing}(\lambda_1 u_1, \lambda_2 u_2, \cdots) = \sum_{n=-\infty}^{\infty} l^{-nd} g_{rem}(\lambda_1^{n+1} u_1, \lambda_2^{n+1} u_2, \cdots)$$

$$= l^{d} \sum_{n=-\infty}^{\infty} l^{-(n+1)d} g_{rem}(\lambda_1^{n+1} u_1, \lambda_2^{n+1} u_2, \cdots)$$

by making the index shift, $n+1 \rightarrow n$, in the above sum we find that

$$f_{sing}(\lambda_1 u_1, \lambda_2 u_2, \cdots) = l^{d} \sum_{n=-\infty}^{\infty} l^{-nd} g_{rem}(\lambda_1^n u_1, \lambda_2^n u_2, \cdots)$$

hence

$$f_{sing}(\lambda_1 u_1, \lambda_2 u_2, \cdots) = l^{d} f_{sing}(u_1, u_2, \cdots) \quad (2.1.28)$$

This form of the singular part of the free energy is called a scaling form. It was postulated some years before the discovery of the R.G. What has been shown here is that it follows naturally from the flows in Hamiltonian space of a system near a fixed point. This singular piece is analyzed in more detail below and it is shown that the relation 2.1.28 implies that at a critical point thermodynamic quantities will have power law singularities.

To analyse the singular part of the free energy it is useful to define a function A as:

$$A(v_2, v_3, \cdots; u_1) = |u_1|^{-\frac{d}{y_1}} \sum_{n=-\infty}^{\infty} l^{-nd} g_{rem}(\lambda_1^n u_1, \lambda_2^n v_2 |u_1|^{y_2/y_1}, \lambda_3^n v_3 |u_1|^{y_3/y_1}, \cdots)$$

where $u_i = v_i |u_1|^{y_i/y_1}$ with $\lambda_i = l^{y_i}$ and u_1 is assumed to be a relevant scaling field. It is easy to show that

$$A(v_2, v_3, \cdots; \lambda_1 u_1) = A(v_2, v_3, \cdots; u_1)$$

hence A is a periodic function of $\ln|u_1|$ with period $\ln\lambda_1$. This enables us to expand A in a Fourier series as:

$$A(v_2, v_3, \cdots; u_1) = \sum_{n=-\infty}^{\infty} A_n^{\pm} \exp\{2\pi i n \ln|u_1| / \ln\lambda_1\}$$

$$= \sum_{n=-\infty}^{\infty} A_n^{\pm} |u_1|^{\{2\pi i n/\ln\lambda_1\}}$$

The $\pm$ signs are introduced to distinguish the two cases $u>0$ and $u<0$. The Fourier coefficients $A_m^{\pm}$ can be written as;

$$A_m^{\pm} = \frac{1}{\ln\lambda_1} \int_0^{\ln\lambda_1} d(\ln|u_1|) |u_1|^{-\{2\pi i m/\ln\lambda_1\}} |u_1|^{-\frac{d}{y_1}} \times \sum_{n=-\infty}^{\infty} l^{-nd} g_{rem}(\lambda_1^n u_1, \lambda_2^n v_2 |u_1|^{y_2/y_1}, \lambda_3^n v_3 |u_1|^{y_3/y_1}, \cdots)$$

By making the substitution $l = \lambda_1^n |u_1|$ in the n^{th} term we find, after performing the sum, that

$$A_m^{\pm} = \frac{1}{\ln\lambda_1} \int_0^{\infty} \frac{dl}{l^{1+d/y_1}} g_{rem}(\pm l, v_2 l^{y_2/y_1}, v_3 l^{y_3/y_1}, \cdots) l^{-\{2\pi i m/\ln\lambda_1\}}.$$

The common assumption made here is that $A_m^{\pm} = 0$ for all $n \neq 0$. This implies that

$$A(v_2, v_3, \cdots; u_1) = A_0^{\pm}(v_2, v_3, \ldots).$$

or that

$$f_{sing}(u_1,u_2,\cdots)=|u_1|^{\frac{d}{y_1}}A_0^{\pm}\left(\frac{u_2}{|u_1|^{y_2/y_1}},\frac{u_3}{|u_1|^{y_3/y_1}},\cdots\right) \qquad (2.1.29)$$

Physically this assumption seems reasonable because if it were not true the singular part of the free energy would have oscillatory terms superimposed on the $|u_1|^{\frac{d}{y_1}}$ behaviour. For more discussion on this point see the article by Th. Niemeijer and and J. M. J. van Leeuwen in reference [16].

Next consider the effects of the relevant and irrelevant fields. To do so consider equation 2.1.29 where labels for the scaling fields have been chosen such that u_i for $1\leq i\leq k$ are relevant fields and all other u_i are irrelevant. Notice we have excluded the case of marginal fields. In fact, this assumption was implicitly made when we assumed $\lambda_1^{n_1}\lambda_2^{n_2}\cdots\neq l^d$. For a discussion of this case, again see the article mentioned above. Notice that $y_i/y_1<0$, for all $i>k$. Therefore as $|u_1|\to 0$, $\frac{u_i}{|u_1|^{y_i/y_1}}\to 0$ for all $i>k$ and hence

$$f_{sing}(u_1,u_2,\cdots)\to|u_1|^{\frac{d}{y_1}}A_0^{\pm}\left(\frac{u_2}{|u_1|^{y_2/y_1}},\cdots,\frac{u_k}{|u_1|^{y_k/y_1}},0,0,\cdots\right)$$

Therefore to, leading order, f_{sing} is independent of the irrelevant fields. This is the reason for the distinction between relevant and irrelevant fields.

This brings us to the idea of universality. Previous to the development of the renormalization group it was found that many systems displayed the same critical behaviour. Classification of these groups of systems into classes become known as the universality scaling hypothesis. In the above analysis we were initially concerned with the critical behaviour in the neighbourhood of the fixed point. However, we see that there exists a hypersurface defined by setting all the relevant fields to zero. In the neighbourhood of this surface the singular behaviour of the free energy is universal, to leading order. Therefore in terms of renormalization group theory, a universality class consists of all systems described by a point on this hypersurface. Because of its critical properties the hypersurface is called the surface of criticality. We define this hypersurface to be the domain of attraction of the

fixed point. This means that all systems in this domain will be mapped towards the fixed point under renormalization group transformation. Universality is therefore a natural consequence of the renormalization group.

Widom's [64] static scaling hypothesis is usually written as;

$$f_{sing}(\chi^{a_\tau}\tau,\chi^{a_h}h)=\chi f_{sing}(\tau,h)\ .$$

This can be related to equation 2.1.30 if we assume that there are only two relevant variables u_1 and u_2 which are temperature-like and field-like respectively and then invoke the universality of the critical surface to apply the scaling analysis at an arbitrary point on the critical surface.

In summary renormalization group theory has provided the mathematical tools and concepts that enable us to understand these conjectures of early workers in critical phenomena. The renormalization group also provides calculational tools useful in determining the singular behaviour of specific systems.

2.2. The Monte Carlo Method

In classical equilibrium Statistical Mechanics one is often interested in the calculation of the expectation of a function of random variables. In the canonical ensemble the expectation of A is written as

$$<A>=\frac{\int d\underline{x}A(\underline{x})\exp\{-H(\underline{x})/kT\}}{\int \exp\{-H(\underline{x})/kT\}} \qquad (2.2.1)$$

for functions of continuous random variables and as

$$<A>=\frac{\sum_{\underline{x}}A(\underline{x})\exp\{-H(\underline{x})/kT\}}{\sum_{\underline{x}}\exp\{-H(\underline{x})/kT\}} \qquad (2.2.2)$$

for function of discrete random variables.

For the purpose of this paper, only functions of spin $\frac{1}{2}$ variables be considered; therefore, equation (2.2.2) reduces to

$$<A>=\frac{\sum_{s_1=\pm 1}\cdots\sum_{s_N=\pm 1}A(s_1,\ldots,s_N)\exp\{-H(s_1,\ldots,s_N)/kT\}}{\sum_{s_1=\pm 1}\cdots\sum_{s_N=\pm 1}\exp\{-H(s_1,\ldots,s_N)/kT\}} \qquad (2.2.3)$$

for a N particle system.

Though the formalism of Monte Carlo will be developed for spin $\frac{1}{2}$ systems it can be easily generalized to systems of other degrees of freedom.

In the evaluation of (2.2.3), 2^{N+1} terms must be calculated and summed together. Even for small systems this can be a difficult task. For example, to evaluate (2.2.3) for a 2-dimensional 5×5 particle system, approximately 10^8 terms must be evaluated. Therefore, in the thermodynamic limit as $N\to\infty$ the straight forward approach of summing the series directly becomes hopeless. Apart from a few special Hamiltonians, $<A>$ can only be approximated.

One of the simplest approximations is called Monte Carlo importance sampling [4]. It is based on the result of probability theory that the arithmetic mean of an infinite sequence of independent random variables having a common distribution converges to the expectation. Therefore to approximate $<A>$, a long sequence of independent random spin configurations is generated from the distribution $P(s)$.

$$P(s)=\frac{\exp\{-H(s)/kT\}}{\sum_{s_1=\pm 1}\cdots\sum_{s_N=\pm 1}\exp\{-H(s_1,\ldots,s_N)/kT\}} \qquad (2.2.4)$$

from which $<A>$ is approximated as

$$<A>\approx\frac{1}{m}\sum_{v=1}^{m}A(s^v) \qquad (2.2.5)$$

where s^v, is the v^{th} spin configuration of the sequence and m is the number of configurations in the sequence.

This method proves to be much more efficient than trying to sum the series (2.2.3) directly. The reason for this is that there tends to be only a small subset of the 2^N possible spin configurations that occurs with any appreciable probability. So for m of the order of

the number of elements of this subset, the approximation (2.2.5) is generally good. Though the above ideas are simple, the realization is not so trivial. The generation independent random variables is not a straightforward task since the calculation of the distribution (2.2.4) is nearly as difficult as trying to evaluate $<A>$ by summing the series (2.2.3). However, the theory of Markov chains provides a method for generating variables of a given distribution. Markov theory consists of the study of a special stochastic chain of events where the outcome of the n^{th} event of the chain depends only on the $(n-1)^{th}$ event of the chain. Moreover, the transition probability is independent of step n. To define the Markov Chain one defines the conditional probability

$$P_{ij}=Prob\,(X^{n+1}=j\,|X^{n}=i)$$

which reads as the probability that event $n+1$ has value "j" given that the event n had value "i". This matrix is called the one step transition probability matrix. Next the m step transition matrix is defined as

$$P_{ij}^{(m)}=Prob\,(X^{n+m}=j\,|X^{n}=i)\ .$$

From these definitions it is easy to see that

$$P_{ij}^{(m)}=\sum_{k_1,\ldots,k_m} P_{ik_1}P_{k_1k_2}\cdots P_{k_mj}\ .$$

If the conditions

$$P_{ij}>0 \quad \text{for } all\ i,j \tag{2.2.6}$$

are imposed and if there exist some numbers $\pi_j>0$ such that

$$\sum_j \pi_j=1 \tag{2.2.7a}$$

and

$$\pi_j=\sum_i \pi_i P_{ij}\ . \tag{2.2.7b}$$

then the limit of $P_{ij}^{(m)}$ as $m\to\infty$ exists, and is such that

$$\lim_{m\to\infty} P_{ij}^{(m)}=\pi_j\ . \tag{2.2.8}$$

The above statement (2.2.8) can also be interpreted as saying that the long run distribution of states of the Markov process is independent of initial state and is equal to π_j. Therefore, to generate any particular sequence of random variables whose distribution is π_j we merely must find a P_{ij} such that

$$\lim_{m\to\infty} P_{ij}^{(m)}=\pi_j$$

What is sought; therefore, is a matrix P_{ij} such that π_j is the Boltzmann distribution (2.2.4) of the states j. With this P_{ij} the long run distribution of states of the Markov chain will have the desired Boltzmann distribution. Therefore, to approximate $<A>$ one merely averages $A(s)$ over the states generated by the Markov Process.

The task now is to find P_{ij} with the desired properties

$$P_{s's}>0 \qquad (2.2.9a)$$

$$\exp\{-H(s)/kT\}=\sum_{s'} P_{s's}\exp\{-H(s')/kT\} \qquad (2.2.9b)$$

If the detailed balance condition

$$P_{ss'}\exp\{-H(s)/kT\}=P_{s's}\exp\{-H(s')/kT\} \qquad (2.2.10)$$

is imposed, both of the above conditions are satisfied. From (2.2.10) we have

$$(P_{s's}/P_{ss'})=\exp\{-(H(s)-H(s'))/kT\}$$

$$=\exp\{-\delta H_{s's}/kT\}>0 \text{ for } all\ s',s$$

where $\delta H_{s's}=(H(s)-H(s'))$, hence $P_{s's}>0$ which is which is condition (2.2.9a). Also from (2.2.10) it can be seen that by summing over s' on both sides of the equation

$$\exp\{-H(s)/kT\}\sum_{s'} P_{ss'}=\sum_{s'} P_{s's}\exp\{-H(s')$$

but, $\sum_{s'} P_{ss'}=1$, therefore it is easy to see that condition 2.2.9b is also satisfied

Even at this point there is some arbitrariness in the choice of $P_{s's}$. Some of the common choices are [4,11];

$$P_{s's}=\{1-\tanh(\delta H_{s's}/2kT)\} \qquad (2.2.11a)$$

$$P_{s's} = \begin{cases} \exp\{-\delta H_{s's}/kT\} & \text{if } \delta H_{s's} > 0 \\ 1 & \text{otherwise} \end{cases} \qquad (2.2.11b)$$

In this work we have consistently used formula 2.2.11a

We now consider how the Monte Carlo scheme is realized in practice. The first step is to choose some initial configuration s. The choice of this configuration is in general arbitrary. However, to decrease the number of samples needed for convergence of (2.2.5) one may bias the selection. Then one selects, either systematically or randomly, one or more of the spins of the current configuration and calculates the energy change δH which would occur if these spins were flipped. This energy change determines the probability of such a transition. This probability is compared to a random number (usually a pseudo-random number generated on a computer), and the new configuration is either rejected, in which case s remains unchanged, or accepted, in which case s will change by the flipping of these spins. The process is repeated q times where q is sufficiently large that all states are possible. This then is what is called one Markov step.

For a sequence of such configurations $\{s^v | v=1,m\}$, $<A>$ is calculated as:

$$<A> \approx \frac{1}{t}\sum_{i=1}^{t} A(s^{(m)}) , \qquad (2.2.12)$$

where $m=wt$ and w is chosen typically between 2 and 10 to enhance the independence of the set of configuration A is averaged over.

Having described the basics of Monte Carlo importance sampling, we now discuss the difficulties of the technique.

The first problem to consider is that of finite size. Generally one is interested in the thermodynamic limit as the number of particles $N \to \infty$. However, Monte Carlo can only be performed on finite systems. This is not to be a problem for noncritical systems. However, as a phase transition is approached, difficulties are encountered. At a phase transition, one is interested in the singular behaviour of various thermodynamic functions, but for finite

systems the free energy is analytic and these singularities are not present. To overcome this problem, Monte Carlo calculations are performed on a number of systems of increasing size to see if the analytic functions of the finite system tend to a singular limit as N increases. In this way the Monte Carlo results may be extrapolated to the thermodynamic limit.

Next, the influence of the starting configuration on the convergence rate of the sum (2.2.12) will be considered. In the limit as $m \to \infty$ the initial configuration is of no consequence. However, one is unable to perform an infinite number of Monte Carlo steps, so the initial configuration does play a role. Ideally, one would like to start with a typical configuration. In general though, one does not have this information. A technique called thermalization can be used to attempt to generate one of these typical configurations. The technique simply allows the Monte Carlo process to iterate many times before averaging, allowing the Markov process to drive the spin configuration towards a typical state. Again this works well for noncritical systems; however, for a second order transition the relaxation time to thermalize the system diverges. For finite systems the relaxation time remains finite which helps somewhat, but it still can be very large.

Statistical errors also will play their usual role in the evaluation of $<A>$ and to a large extent are handled by "eyeballing" the data although more sophisticated techniques do exist . Other problems also exist such as the generation of pseudo-random number and the choice of boundary conditions. For a discussion of these see the article by Binder in Monte Carlo Methods in Statistical Physics (ref. [4]).

2.3. Monte Carlo Renormalization Group

In the renormalization group theory the expression of interest is the recursion relationship $K_a' = R_a(K)$ and in particular

$$T^{*}_{ab}=\frac{\partial K_a'}{\partial K_b}\Big|_{K_i=K_i^{*}}, \qquad (2.3.1)$$

where K^{*} is a fixed point of the recursion relationship. It was not mentioned in the discussion of the general theory that for most models one is unable to derive exact expressions for these functions. The main stumbling block in the calculation is the fact that K is an infinite dimensional vector.

Prior to the development of Monte Carlo renormalization group, one would attempt to calculate R_a by assuming that only a only a finite number of coupling constants K_a affected the critical behaviour of the system.

Two different finite lattice methods have been commonly used in closed-form renormalization group approximation. The first is called the cumulant approximation The essence of this approximation is to find a Hamiltonian H_o for which the recursion relations are known and such that the original Hamiltonian H can be expressed as, $H=H_o+V$ where V is a small perturbation. Then the recursion relationships of H are truncated by only keeping terms to some desired order in V. This technique has produced reasonable values for critical exponents in two dimensional systems but becomes unwieldy for three dimensional systems or systems with interactions of greater range than nearest neighbour.

The next method is the finite cluster approximation. To make this approximation one begins by blocking a sufficiently small lattice such that the probability distribution of states of the blocked and unblocked system can be calculated exactly. From these distributions one obtains R_a. This R_a is assumed to mimic the behaviour of the corresponding R_a for the infinite systems. This method has produced good results for a number of two dimensional systems.

To overcome the effects of truncation of the dimension of the recursion relation, Swendsen, in 1979, proposed a method combining Monte Carlo simulation and renormalization group called Monte Carlo renormalization group (MCRG) [10,58-61]. MCRG theory makes use of the fact that the matrix

$$T_{ab}^{(n)}=\frac{\partial K_a^{(n)}}{\partial K_b^{(n-1)}} \tag{2.3.2}$$

can be related to correlation functions which can be calculated approximately by Monte Carlo simulation.

Recall from equations 2.1.1 and 2.1.10 that the Hamiltonian, after n renormalization group transformations, can be written as

$$\tilde{H}^{(n)}=\sum_{a\in A} K_a^{(n)} S_a^{(n)} \tag{2.3.3a}$$

where the relationship between the n^{th} and $(n-1)^{th}$ Hamiltonian is given by

$$\exp\{G(K^{(n-1)})+\tilde{H}^{(n)}\}=\sum_{s^{n-1}} P(s^{(n)};s^{(n-1)})\exp\{\tilde{H}^{(n-1)}\} \tag{2.3.3b}$$

We begin the derivation by considering a relationship that follows from the chain rule

$$\frac{\partial<S_c^{(n)}>}{\partial K_b^{(n-1)}}=\sum_a \frac{\partial<S_c^{(n)}>}{\partial K_a^{(n)}}\frac{\partial K_a^{(n)}}{\partial K_b^{(n-1)}} \tag{2.3.4}$$

Notice that

$$\frac{\partial<S_c^{(n)}>}{\partial K_a^{(n)}}=\frac{\partial}{\partial K_a^{(n)}}\frac{\sum_{s^n} S_c^{(n)}\exp\{\tilde{H}^{(n)}\}}{\sum_{s^n}\exp\{\tilde{H}^{(n)}\}}$$

$$=<S_c^{(n)}S_a^{(n)}>-<S_c^{(n)}><S_a^{(n)}> \tag{2.3.5}$$

and by using (2.3.3b)

$$\frac{\partial<S_c^{(n)}>}{\partial K_a^{(n-1)}}=\frac{\partial}{\partial K_a^{(n-1)}}\frac{\sum_{s^n s^{n-1}} S_c^{(n)}P(s^{(n)};s^{(n-1)})\exp\{\tilde{H}^{(n-1)}-G\}}{\sum_{s^n s^{n-1}} P(s^{(n)};s^{(n-1)})\exp\{\tilde{H}^{(n-1)}-G\}}$$

$$=\frac{\sum_{s^n s^{n-1}} S_c^{(n)}S_a^{(n-1)}P(s^{(n)};s^{(n-1)})\exp\{\tilde{H}^{(n-1)}\}}{\sum_{s^{n-1}}\exp\{\tilde{H}^{(n-1)}\}}-\frac{\sum_{s^n} S_c^{(n)}\exp\{\tilde{H}^{(n)}\}\sum_{s^{n-1}} S_a^{(n-1)}\exp\{\tilde{H}^{(n-1)}\}}{\sum_{s^n}\exp\{\tilde{H}^{(n)}\}\times\sum_{s^{n-1}}\exp\{\tilde{H}^{(n-1)}\}}$$

Note that the fact that

$$\sum_{s^n} P(s^{(n)};s^{(n-1)}) = 1$$

was used in the above calculation. Next notice that

$$\sum_{s^n} S_c^{(n)} S_a^{(n-1)} P(s^{(n)};s^{(n-1)})$$

is the conditional expectation of $S_c^{(n)} S_a^{(n-1)}$ given $s^{(n-1)}$, since $P(s^{(n)};s^{(n-1)})$ is the conditional probability of s^n given $s^{(n-1)}$. Hence,

$$\frac{\partial \langle S_c^{(n)} \rangle}{\partial K_a^{(n-1)}} = \langle S_c^{(n)} S_a^{(n-1)} \rangle - \langle S_c^{(n)} \rangle \langle S_a^{(n-1)} \rangle \qquad (2.3.6)$$

Combining (2.3.2), (2.3.4), (2.3.5), and (2.3.6) we obtain the relationship

$$\langle S_c^{(n)} S_b^{(n-1)} \rangle - \langle S_c^{(n)} \rangle \langle S_a^{(n-1)} \rangle = \sum_a \langle S_c^{(n)} S_a^{(n)} \rangle - \langle S_c^{(n)} \rangle \langle S_a^{(n)} \rangle T_{ab} \ . \qquad (2.3.7)$$

This can be put into matrix notation by defining matrixes

$$(\tilde{S}^{(n,m)})_{ab} = \langle S_a^{(n)} S_b^{(m)} \rangle - \langle S_a^{(n)} \rangle \langle S_b^{(m)} \rangle$$

$$(\tilde{T}^{(n)})_{ab} = T_{ab}^{(n)}$$

Hence, equation (2.3.7) reads as;

$$\tilde{S}^{(n,n-1)} = \tilde{S}^{(n,n)} \tilde{T}^{(n)} \ ,$$

therefore

$$\tilde{T}^{(n)} = (\tilde{S}^{(n,n)})^{-1} \tilde{S}^{(n,n-1)} \ .$$

In general $\tilde{S}^{(n,n)}$ is an infinite dimensional matrix which might be difficult to invert, let alone to calculate by Monte Carlo. However, since it is only the largest few eigenvalues of $\tilde{T}^{(n)}$ that are sought, only a small part of $\tilde{S}^{(n,n)}$ has to be inverted to find these eigenvalues with a good degree of accuracy. This is, of course, an assumption, but using MCRG one can add more and more coupling constants with relatively little effort.

What is of most interest are the eigenvalues at the fixed point K^*. We can find these by making use of the fact that for a set of parameters K^o on the critical surface $K^{(n)} \to K^*$ and hence $T_{ab}^{(n)} \to T_{ab}^*$ as $n \to \infty$.

To find T'_{ab} one merely performs Monte Carlo simulation on a critical system, and performs the renormalization group transformation a number of times on each configuration thus generating a sequence of configurations of the blocked system. The distribution of these block configurations will be the same as if an exact renormalization group had been applied to the original Hamiltonian. Therefore, the Monte Carlo simulation will approximate the correlation functions $\tilde{S}^{(n,n-1)}$, $\tilde{S}^{(n,n)}$ determined from exact renormalization group transformation. The sequence $\{\tilde{S}^{(n,n-1)}, \tilde{S}^{(n,n)} | n=1,2,3\cdots\}$ generated will tend towards the fixed point value of this function for increasing n. In this way T'_{ab} can be approximated.

We now mention some of the limitations of this method and some consistency requirements. Apart from the standard problem of finite size statistics, as found in all Monte Carlo simulations, a number of new difficulties appear. The problem associated with only calculating a finite number of elements of the matrixes $\tilde{S}^{(n,n-1)}$, $\tilde{S}^{(n,n)}$ has already been mentioned. In principle, this is a problem. In practice, however, it is easy to test if enough elements have been calculated by varying the number of interactions used in the calculation of the eigenvalues of T'_{ab}. Convergence as a function of this number has been found to be quite rapid.

The next difficulty arises from the use of finite lattices. Because of this, only a finite number of iterations of the renormalization group transformation can be performed. So the question arises: is $K^{(n)}$ sufficiently close to K^* ? There tend to be, in many cases, a large region about K^* in which the flows are linear; therefore, all that is needed is for $K^{(n)}$ to be in the linear region. This condition can be checked by seeing if the eigenvalues are stationary for the last couple of iterations.

The last point to be made on the limitations, is the question concerning accurate location of a point on the critical surface so that the renormalization group transformation drives the Hamiltonian to the critical fixed point. This process is normally done in two

stages. The first stage is to examine the flows of the expectations $<S_c^{(n)}>$, which tends to flow to the ground state or infinite temperature fixed point values very quickly for points not too close to the critical surface. By looking for the bifurcation of these flows one is able to determine the phase boundary normally to about one percent. The second stage is to sample this one percent tolerance region such that the variation of the eigenvalues is minimized under renormalization group transformation.

In summary, Monte Carlo Renormalization group provides a very general scheme for performing exact renormalization group transformations with several self consistency checks.

CHAPTER 3

Calculation

It is the purpose of this investigation to examine the effects of the addition of a small (repulsive) next nearest neighbour interaction to the triangular nearest neighbour Ising antiferromagnet. The resulting Hamiltonian for this model is

$$H = J_{nn}\sum_{nn} s_i s_j + J_{nnn}\sum_{nnn} s_i s_j + h\sum_i s_i ,$$

where *nn* and *nnn* represents nearest and next nearest neighbour pair respectively. In particular, the case to be studied is $J_{nn}>0$ and $J_{nnn}>0$ with the ratio $a = J_{nnn}/J_{nn} = 0.1$.

The study has three objectives:

1 To determine the phase boundaries in the T-h plane for fixed $a = 0.1$.

2 To determine the order of the transition along these boundaries.

3 To determine the critical indices of the phase transitions.

Objectives one and three will be realized by MCRG Techniques and objective two will be obtained by Monte Carlo sampling of the energy, order parameter and free energy functional $F(\psi)$. $F(\psi)$ will be defined and discussed below.

Before any RG calculation can be performed the ground state configurations must be identified. Next a RG Transformation must be found such that the ground state symmetry is preserved under this operation.

For this model (i.e. $a = 0.1$) the ground state phase diagram is in shown in Fig. 1.2.2 . Ideally, one would seek a RG Transformation that would preserve the symmetry of all four phases simultaneously. However, in the attempt to do so, the only such transformation found produced a blocked Hamiltonian with very anisotropic coupling constants. In order to keep the blocked Hamiltonian (approximately) isotropic, the idea of a single RG

Transformation for the entire phase diagram was abandoned and two separate RG Transformations were used.

A four spin block was used to study the $\sqrt{3}\times\sqrt{3}$ phase as shown in Fig. 3.1 with projection matrix defined as

$$P(s';s)=\prod_i P(s_i';s_i^1,s_i^2,s_i^3,s_i^4)$$

$$P(s_i';s_i^1,s_i^2,s_i^3,s_i^4)=\begin{cases}1 & \text{if} \quad (s_i^1+s_i^2+s_i^3)/s_i' \quad >0\\ 0 & \textit{otherwise}\end{cases}$$

For the 2×1 and 2×2 phase a common three spin block was used as shown in Fig. 3.2 with projection matrix defined as

$$P(s';s)=\prod_i P(s_i';s_i^1,s_i^2,s_i^3)$$

$$P(s_i';s_i^1,s_i^2,s_i^3)=\begin{cases}1 & \text{if} \quad (s_i^1+s_i^2+s_i^3)/s_i' \quad >0\\ 0 & \textit{otherwise}\end{cases}$$

The use of two different blocking schemes is a cause for concern only near a transition between 2×1 and $\sqrt{3}\times\sqrt{3}$ phases or 2×2 and $\sqrt{3}\times\sqrt{3}$ phases. We expect these transitions to be first order and we can use other Monte Carlo methods to find the coexistence curves.

The first part of the study is to locate the phase boundaries by using the above blockings in a MCRG scheme. Under successive RG Transformation, the Hamiltonian initially in a given phase will flow such that the block spin configuration will tend towards the ground state configuration of that phase. Then

$$\lim_{n\to\infty}\langle S_a^{(n)}\rangle=\langle S_a^f\rangle$$

where $\langle S_a^f\rangle$ is the average of S_a evaluated over the ground state configurations. So, by

R.G. blocking scheme for the

$\sqrt{3} \times \sqrt{3}$ phase

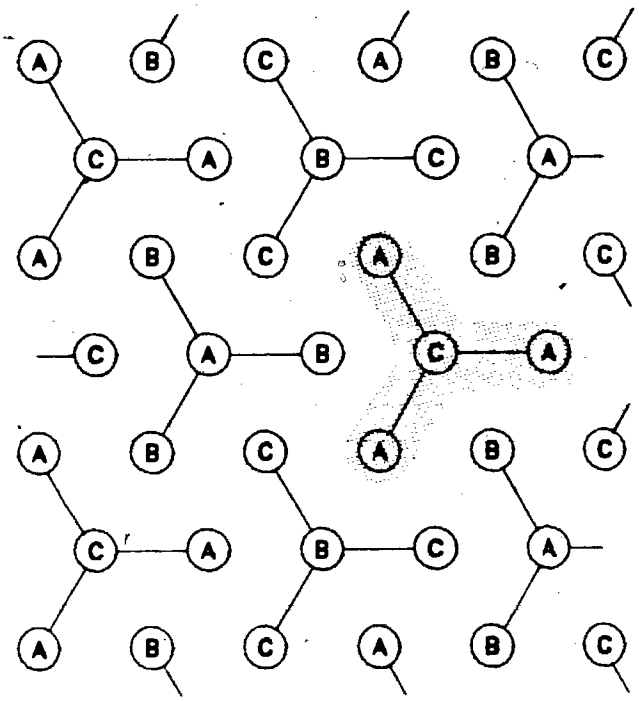

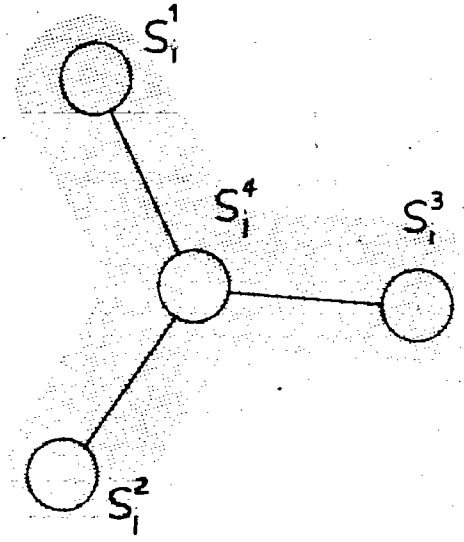

Figure 3.1

R.G. blocking scheme for the 2x2 and 2x1 phases

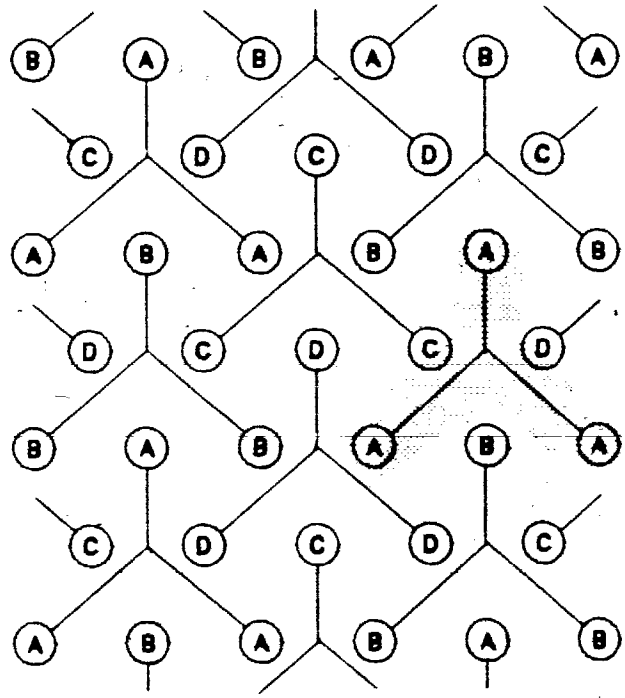

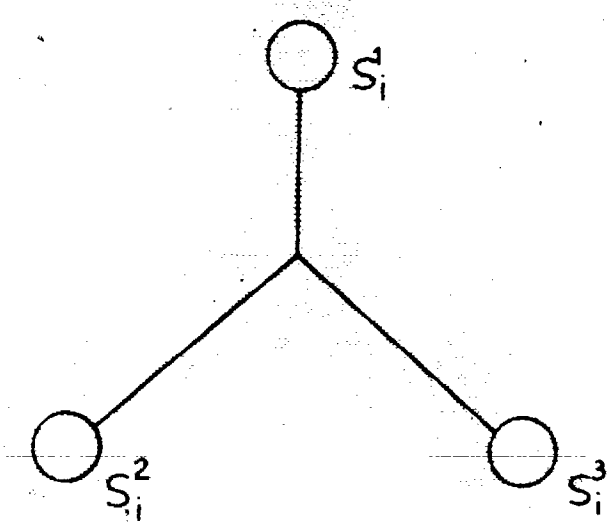

Figure 3.2

looking for the bifurcation of the sequence $<S_a^{(n)}>$ the phase transition can be located. In practice, the finite lattice used can only be iterated a limited number of times. Therefore, this restricts the accuracy to which the phase boundary can be located. However, even for relatively small lattices (30×30) the uncertainty in many cases is less than 2%.

In this study relatively small lattices were used to find the phase boundaries. For the $\sqrt{3}\times\sqrt{3}$ phase a 32×48 spin lattice was most frequently used whereas for the 2×1 and 2×2 phase we generally performed the calculations on a 36×36 lattice. The initial configuration was thermalized 2000-20,000 MCS/Spin before sampling, and the averages evaluated over every fifth MCS/Spin of runs 5,000-30,000 MCS/Spin. Close to the phase boundary a number of different runs were made to check for metastability. These numbers may seem small when compared to other MCRG studies. Most of these studies are concerned with the determination of the of the critical indices which require the accurate evaluation of the correlation functions $<S_a^{(n)}S_b^{(n-1)}>-<S_a^{(n)}><S_b^{(n-1)}>$ on the phase boundaries. However, to determine the phase boundaries only the expectations $<S_a>$ are sought for points near the phase boundaries but not necessarily on these boundaries. Therefore, convergence in the determination of the phase boundaries is much faster than the calculation of the critical indices.

We attempted to estimate the effect of the finite lattice size by carrying out the calculations on larger lattices for a few select points along the phase boundaries. For the $\sqrt{3}\times\sqrt{3}$ phase the larger lattice sizes were 64x48 and 64x96 and for the 2x1 and 2x2, 36x54 and 72x54. In all cases the changes were found to be less than 2%. To determine the nature of the phase transition we have evaluated the Landau-like free energy $F(\psi)$ for points along the phase boundaries by Monte Carlo simulation. More explicitly we evaluated the function

$$F(\psi)-F_o=-\ln\{Prob(|\psi-\psi_o|<\delta/2)\},$$

where the right hand side reads as the negative logarithm of the probability that the magni-

tude of the order parameter ψ_o is within a $\delta/2$ neighbourhood of the number ψ. F_o is the total free energy of the system. The order parameter definition depends on which phase is being sampled. For the 2×1 and the 2×2 phases a three component order parameter (ψ_1,ψ_2,ψ_3) is defined for the system as:

$$\psi_o=\sqrt{\psi_1^2+\psi_2^2+\psi_3^2}$$

$$\psi_1=\frac{1}{N}(M_A-M_B-M_C+M_D)$$

$$\psi_2=\frac{1}{N}(M_A-M_B+M_C-M_D)$$

$$\psi_3=\frac{1}{N}(M_A+M_B-M_C-M_D)$$

where M_α is the total magnetization on the α sublattice (see figure 3.2 α = A,B,C,D) and N is the total number of lattice sites. For the $\sqrt{3}\times\sqrt{3}$ a two component order parameter is defined as:

$$\psi_o=\sqrt{\psi_1^2+\psi_2^2}$$

$$\psi_1=\frac{3}{2N}\left[M_a-\frac{1}{2}(M_b+M_c)\right]$$

$$\psi_2=\frac{3\sqrt{3}}{4N}\left[M_b-M_c\right]$$

where M_α is the total magnetization on the α sublattice (see figure 3.1 α = A,B,C) and N is the total number of lattice sites.

The classification of the order of the transition is based on the shape of this function. For example Fig 3.3a would be called a first order transition because of the dual absolute minimum that $F(\psi)$ manifests. On the other hand, Fig 3.3b would represent a second or higher order transition because of the flatness of the curve. It is surprising that this technique is not more widely used in this type of study since many of the techniques previously used in the classification of the order of phase transitions can be explained in terms of this function. One of the main advantages derived from the use of this function, is that finite size rounding has no effect in the classification scheme, though other finite size effects may

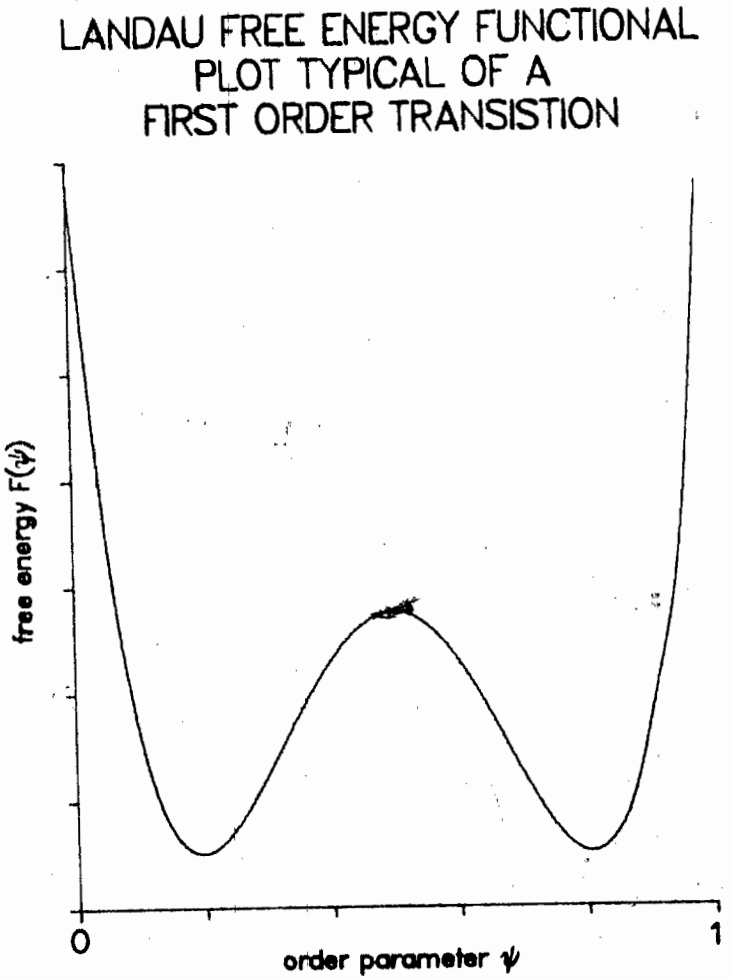
LANDAU FREE ENERGY FUNCTIONAL
PLOT TYPICAL OF A
FIRST ORDER TRANSISTION
free energy F(ψ)
0
1
order parameter ψ
(a)

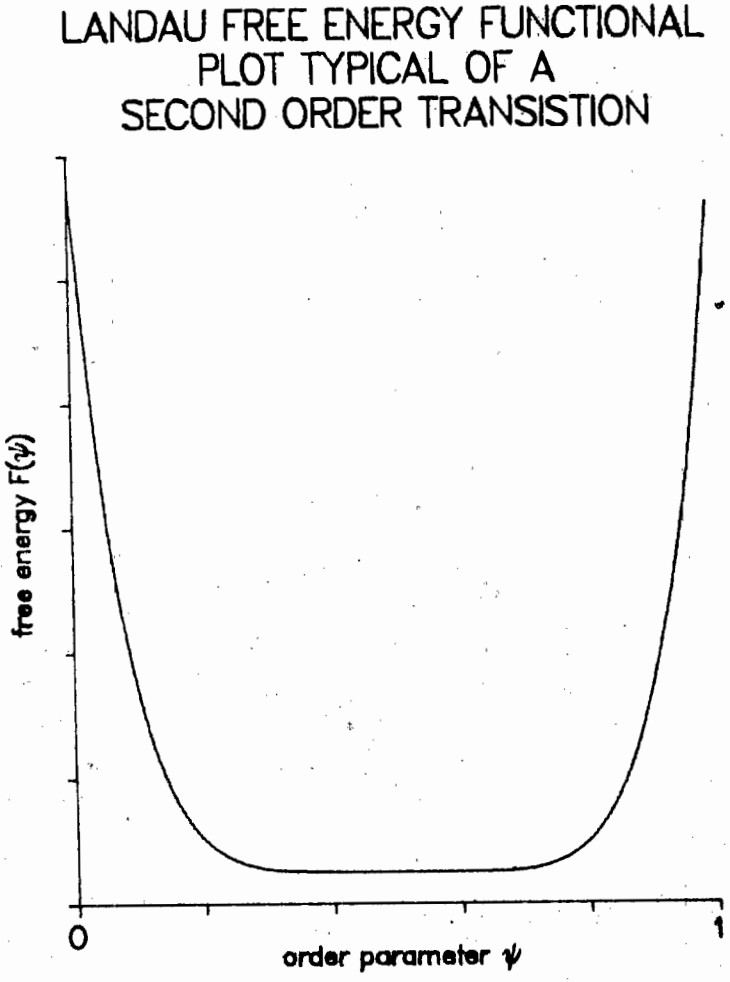
LANDAU FREE ENERGY FUNCTIONAL
PLOT TYPICAL OF A
SECOND ORDER TRANSISTION
free energy F(ψ)
0
1
order parameter ψ
(b)

Figure 3.3a-b

play a role. One drawback to the technique is that it requires very long running times. This is compensated though, by the fact that the function need only be evaluated at one temperature to determine the order of the transition if T_c is known accurately. Typically, T_c is not known to sufficient accuracy and the function $F(\psi)$ must be calculated for a small number of parameter values. However, the number of points for which $F(\psi)$ is evaluated is normally much smaller than the number of points that must be sampled in other Monte Carlo techniques to determine the order of the transition. For example, in this study, by using T_c as determined by the bifurcation of the Monte Carlo renormalization group flows as a starting point, we are able to determine the order of the transition by evaluating $F(\psi)$ for two to four values of the temperature.

In the calculation of $F(\psi)$ the bulk of the simulation was done on a 36×36 lattice when considering the 2x1 and 2x2 order-disorder transitions and 32x48 lattice for the $\sqrt{3}\times\sqrt{3}$ order-disorder transitions.

Finite size effects on $F(\psi)$ were checked on a 36x54 lattice for the 2x1 and 2x2 phases, and a 64x48 lattice for the $\sqrt{3}\times\sqrt{3}$ lattice. If the results were ambiguous after these runs then further calculation were carried out on a 72x54 lattice for the 2x1 and 2x2 and 64x96 for the $\sqrt{3}\times\sqrt{3}$. All runs were initially run for 90-180,000 MCS/Spin after 20,000 MCS/Spin were deleted for thermalization. The runs were broken up into 10,000-30,000 MSC/Spin segments so that the thermalization and convergence could be checked, and extra steps deleted or added if necessary. The increment δ was chosen to be 1/100.

The scaling of the functional with size was not as clear as we originally expected. It was initially thought that a bump in the free energy functional, which we are using as the signature of a first order transition, would increase with lattice size, but such was not the case. Because of this, we decided to compare the functional method with more conventional methods of determination of first order transition. The first method chosen tests for hysteresis of various thermodynamical quantities (i.e internal energy, order parameter, etc.) as

a signature of a first order transition[4]. Following a suggestion by Mouritsen, we looked at the time series of a coarse grain average ψ_{cg} of the order parameter at a few points, however the hysteresis calculation was the more extensive study. We chose to compare the hysteresis calculation results with those based on the free energy functional, along the 2x2 boundary because it appears to exhibit a weakening first order transition with increasing field that may eventually be driven second order.

We began at a point on the boundary which we felt was strongly first order using a 36x36 lattice. The possibility of hysteresis was explored by varying the temperature at fixed field. This was repeated for successively larger values of the field. As the field was increased the system appeared to become more critical causing the system to jump back and forth between the ordered and disordered phases. To suppress this oscillation the lattice size was increased to 72x54 for all points tested with $H/J_{nn} \geq 4.75$ The internal energy and order parameter were calculated on each sweep by sampling every MCS/Spin for a total of 3000 MCS/Spin. The system was allowed to thermalize for 1000 MCS/Spin between successive points of the sweeps.

CHAPTER 4

Results

4.1. Phase Diagrams

The results of the MCRG study of the phase diagram are summarized by Fig. 4.1.1a. The errors in the location of the boundary, which are of the size of of the plotted data points, are due to the indeterminacy of the MCRG Flows. From the several points that we checked for finite size effects no qualitative changes to phase boundaries were found with increasing lattice size, though transition temperatures seem to decrease slightly.

The two most interesting features of Fig. 4.1.1a are the apparent depression of the transition temperation to zero at $h/J_{nn}=\pm 2a=1.2$ and the existence of a finite temperature phase transition between the $\sqrt{3}\times\sqrt{3}$ and 2×2 ordered phases. The depression of the transition to zero temperature is conjectured since Monte Carlo work becomes extremely difficult at low temperatures. Metastability problems tend to become more severe as the temperature is decreased.

However even with very long Monte Carlo runs of 90,000 MCS/spin after 20,000 MCS/spin thermalization the qualitative features of the phase diagram remained unchanged. The plot of magnetization versus temperature for $h/J_{nn}=1.2$ (see fig. 4.1.2) seems to be a smooth function indicating that for kT/J_{nn} as low as 0.25 the system is still paramagnetic.

It was hoped that the apparent depression of T_c to zero at $|h|/J_{nn}=\pm 2a$ could be proven analytically. In our attempts, we were unable to produce a rigorous proof of this, however we did find some properties of the ground state, suggest that both the 2×1 and $\sqrt{3}\times\sqrt{3}$ are unstable at finite temperature at $|h|/J_{nn}=\pm 2a$. A discussion of this, along

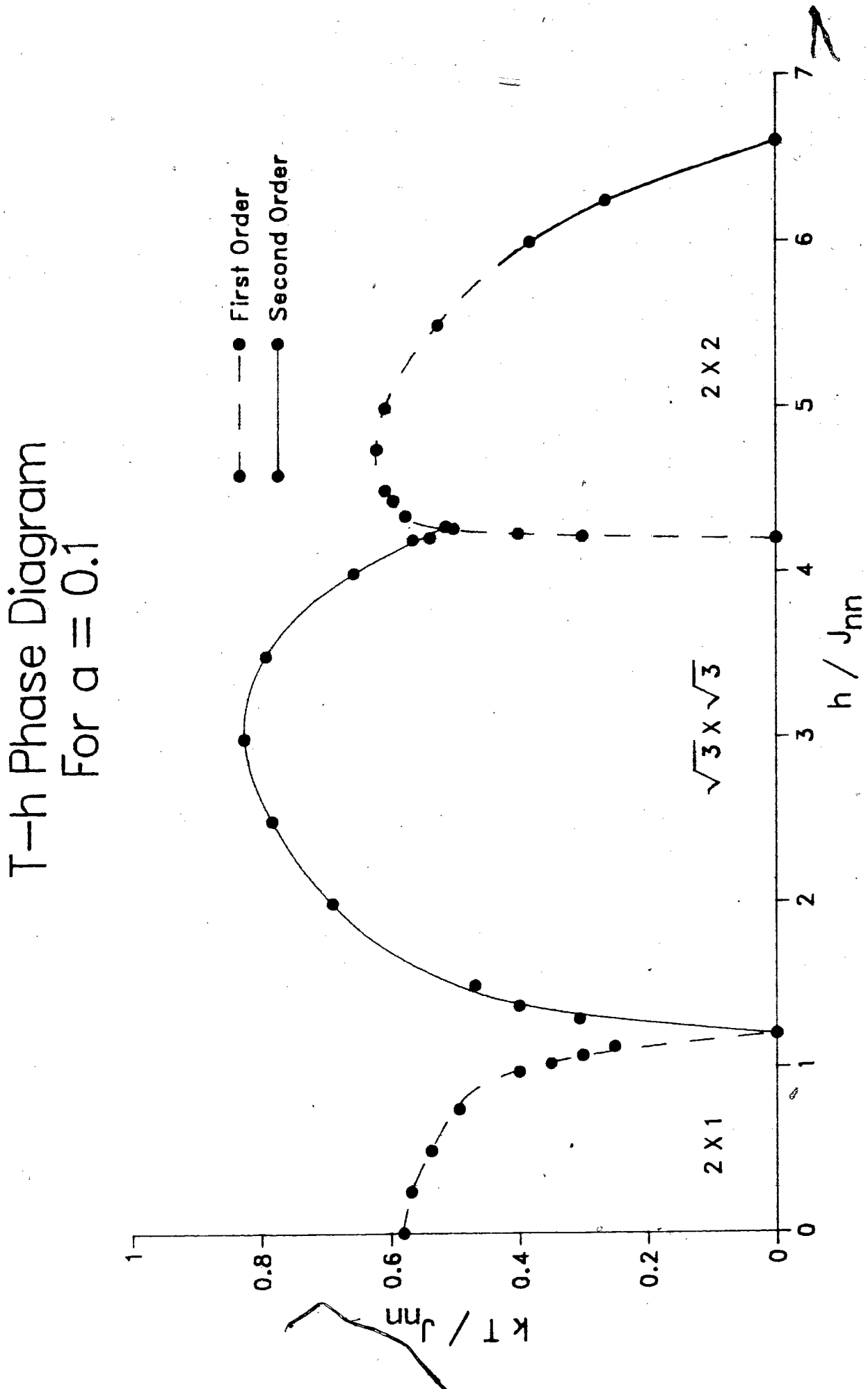
T–h Phase Diagram
For a = 0.1
First Order
Second Order
2 X 2
√3 X √3
2 X 1
k T / J_nn
h / J_nn
0
0.2
0.4
0.6
0.8
1
0
1
2
3
4
5
6
7

Figure 4.1.1a

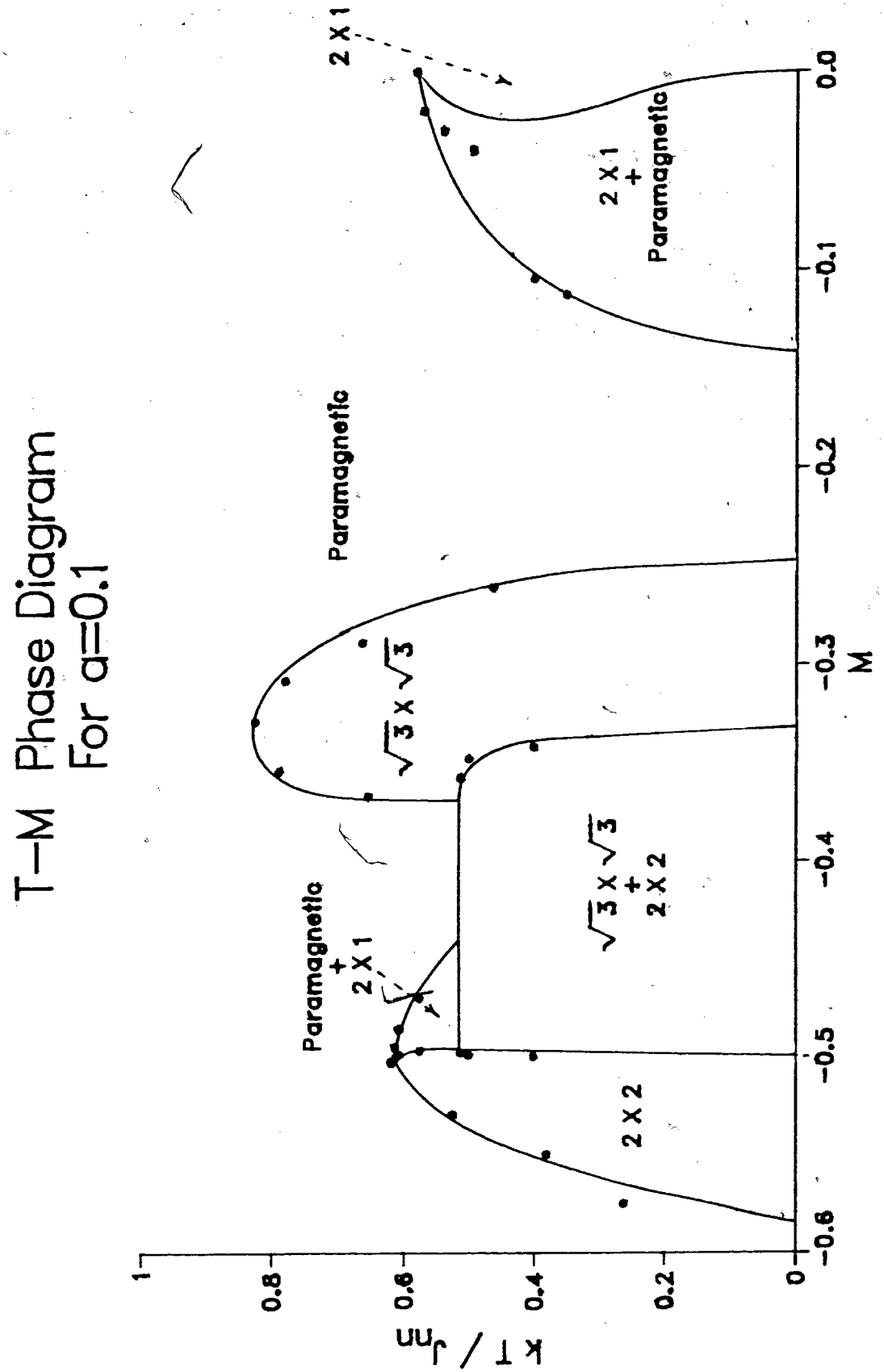
T–M Phase Diagram
For a=0.1
Paramagnetic
2 X 1
Paramagnetic
+
2 X 1
√3 x √3
√3 x √3
+
2 X 2
Paramagnetic
+
2 X 1
2 X 2
K T / J_nn
M
0
0.2
0.4
0.6
0.8
1
0.0
-0.1
-0.2
-0.3
-0.4
-0.5
-0.6

Figure 4.1.1b

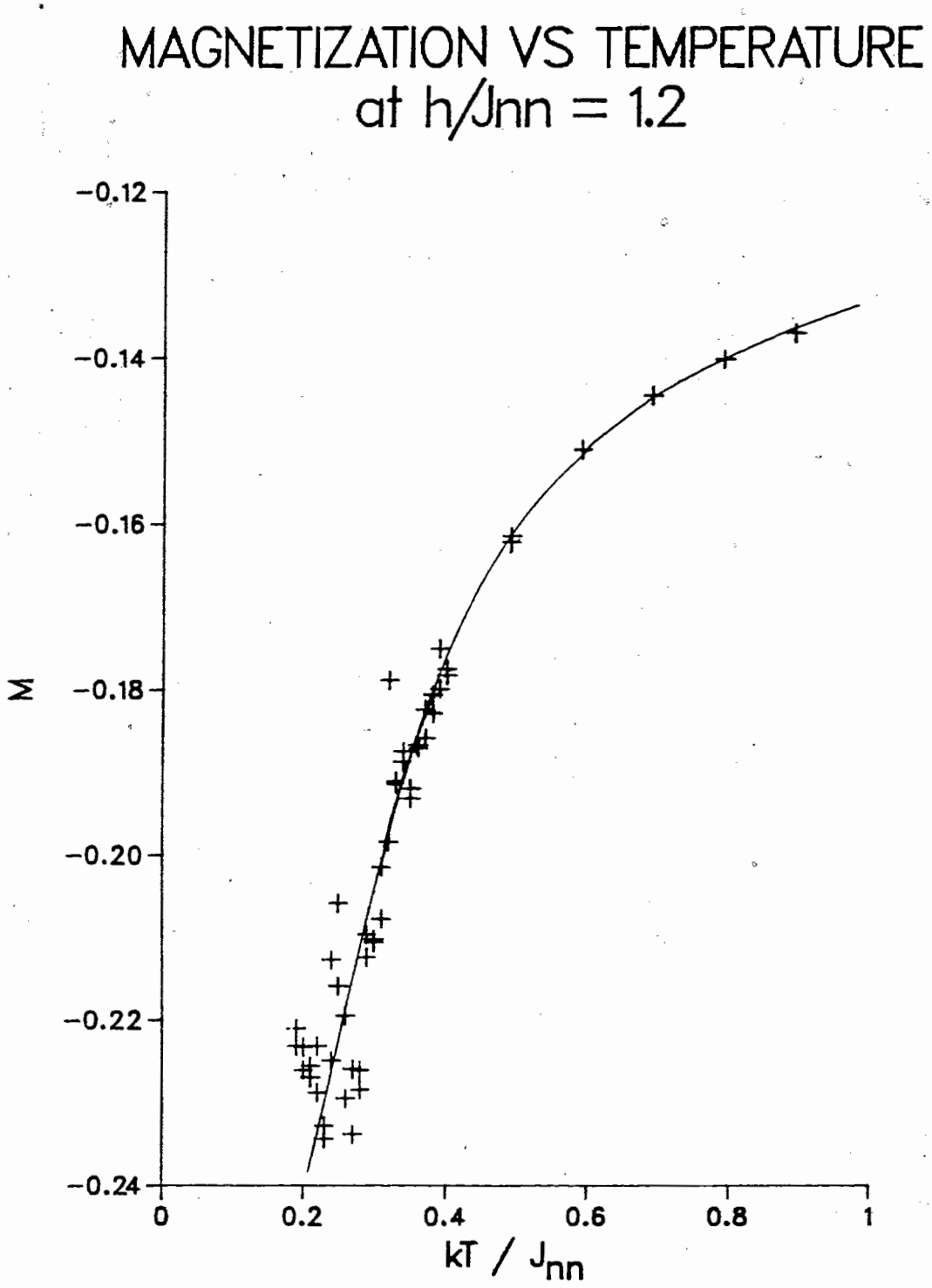
MAGNETIZATION VS TEMPERATURE
at h/Jnn = 1.2
−0.12
−0.14
−0.16
−0.18
−0.20
−0.22
−0.24
M
0
0.2
0.4
0.6
0.8
1
kT / Jnn

Figure 4.1.2

with suggestions how one might proceed to prove the result rigorously is found in the appendix A.

The second feature, the transition between the $\sqrt{3}\times\sqrt{3}$ phase and 2×2 phase can be seen by MCRG despite our initial reservation. When the blocking of Fig. 3.1a is used on a 2×2 structure, the 2×2 structure is mapped onto a paramagnetic phase. Similarly, when the blocking of Fig. 3.1b is used on a $\sqrt{3}\times\sqrt{3}$ structure, the $\sqrt{3}\times\sqrt{3}$ structure is mapped onto a paramagnetic phase. Because of this, the bifurcation of the flows can still be seen, though they are not useful for the calculation of exponents. This transition can also be seen in regular Monte Carlo sampling by observing the discontinuity in the magnetization. One last point that should be mentioned about the $T-h$ phase diagram is that the MCRG results are consistent with the ground state phase diagram.

We also show, in figure 4.1.1b a crude phase diagram in the T-M plane. This was calculated by computing the magnetization at the transition point in the $T-h$ plane. Since the calculation was not initially designed for accurate evaluation of the magnetization at the transition the results are somewhat speculative. The features to note on figure 4.1.1b are the coexistence regions; 2×1 + paramagnetic , 2×2 + paramagnetic, and $2\times2+\sqrt{3}\times\sqrt{3}$, as well as the gap between $M\approx-0.14$ and $M\approx-0.26$. In this region the paramagnetic state seems to persists to zero temperature.

4.2. Order of the Phase Transitions

In this section we discuss the results of the calculation of the free energy functional $F(\psi)$ as defined in chapter 3. In particular we try to infer the order of the transition by examining the structure of $F(\psi)$. In the following section the conclusions drawn from this section will be compared for consistency with more traditional method using hysteresis and time series analysis to determine the order of the phase transition.

We first discuss the transition from the 2×1 to the paramagnetic phase. From the sequence of figures 4.2.3a-c we can see the evolution of $F(\psi)$ as the temperature is

increased through the transition temperature. The feature to notice in the graphs is that the bump in the free energy persists through the transition temperature ($T_c \approx 0.581$). The persistence of this bump and the equal depth of the associated wells at T_c is a signal that the free energy of distinct phases of order and disorder are becoming equal. They are distinct in that one can make a definite association of a phase with either the low or high order parameter well. The above description is that of a first order transition and we conclude that this transition is first order.

Since we are dealing with a finite system the effect of lattice size needs to be considered. To check for finite size effects, $F(\psi)$ was calculated on one smaller lattice (24×18) and one larger lattice (36×54).

From figures 4.2.2-4.2.4 we notice that the transition temperature decreases with increasing lattice size though the change is less than 1%. The most intersting feature to consider is how the size of the bump scales with lattice size. From the 24×18 lattice to the 36×36 lattice the bump increases by over a factor of two. From the 36×36 to the 36×54 lattice the results are not completely clear. They are partly obscured since figure 4.2.4 does not show $F(\psi)$ quite at the transition temperature, therefore making direct comparison difficult. With increasing size the structure of $F(\psi)$ near the transition temperature becomes very sensitive to temperature changes, making it difficult to obtain a plot representive of $F(\psi)$ at T_c. From insight gained by watching the evolution of $F(\psi)$ with temperature for smaller systems one can make a qualitative extrapolation of figure 4.2.4 and conclude that the bump in $F(\psi)$ at the transition would for the 36×54 system be about the same size (perhaps slightly larger) as that of the 36×36 lattice. An even larger lattice (72×54) was used to calculated $F(\psi)$. The results are not presented because the increased sensitivity with size made it very difficult to calculate the free energy functional sufficiently close to T_c to manifest the equal depths of the wells at T_c. However there was some indication that the bump would be slightly smaller at the transition.

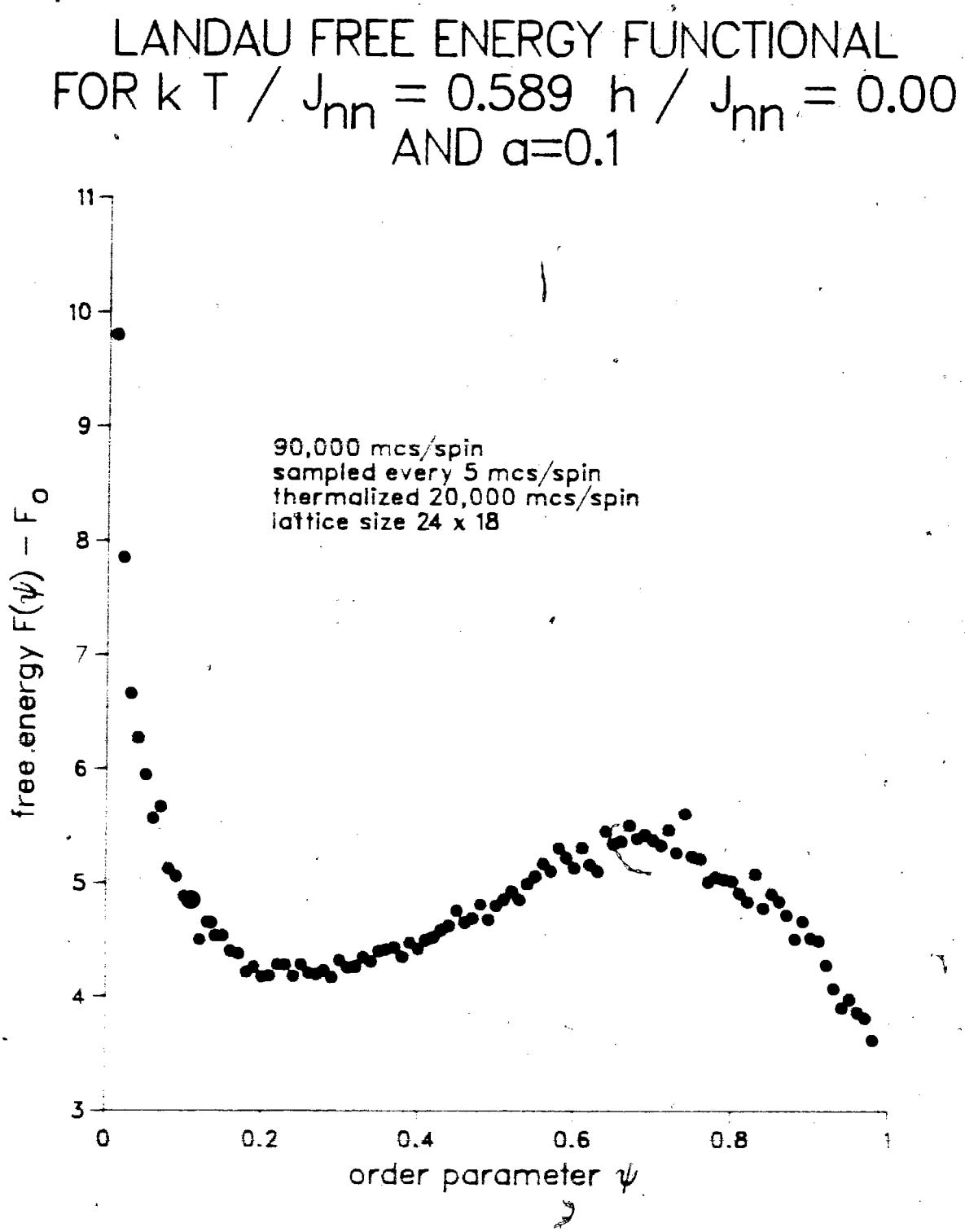
LANDAU FREE ENERGY FUNCTIONAL
FOR k T / J_{nn} = 0.589 h / J_{nn} = 0.00
AND a=0.1
90,000 mcs/spin
sampled every 5 mcs/spin
thermalized 20,000 mcs/spin
lattice size 24 x 18
free energy $F(\psi) - F_o$
order parameter ψ
11
10
9
8
7
6
5
4
3
0
0.2
0.4
0.6
0.8
1

Figure 4.2.2

LANDAU FREE ENERGY FUNCTIONAL FOR k T / J_{nn} = 0.580 h / J_{nn} = 0.00 AND a=0.1

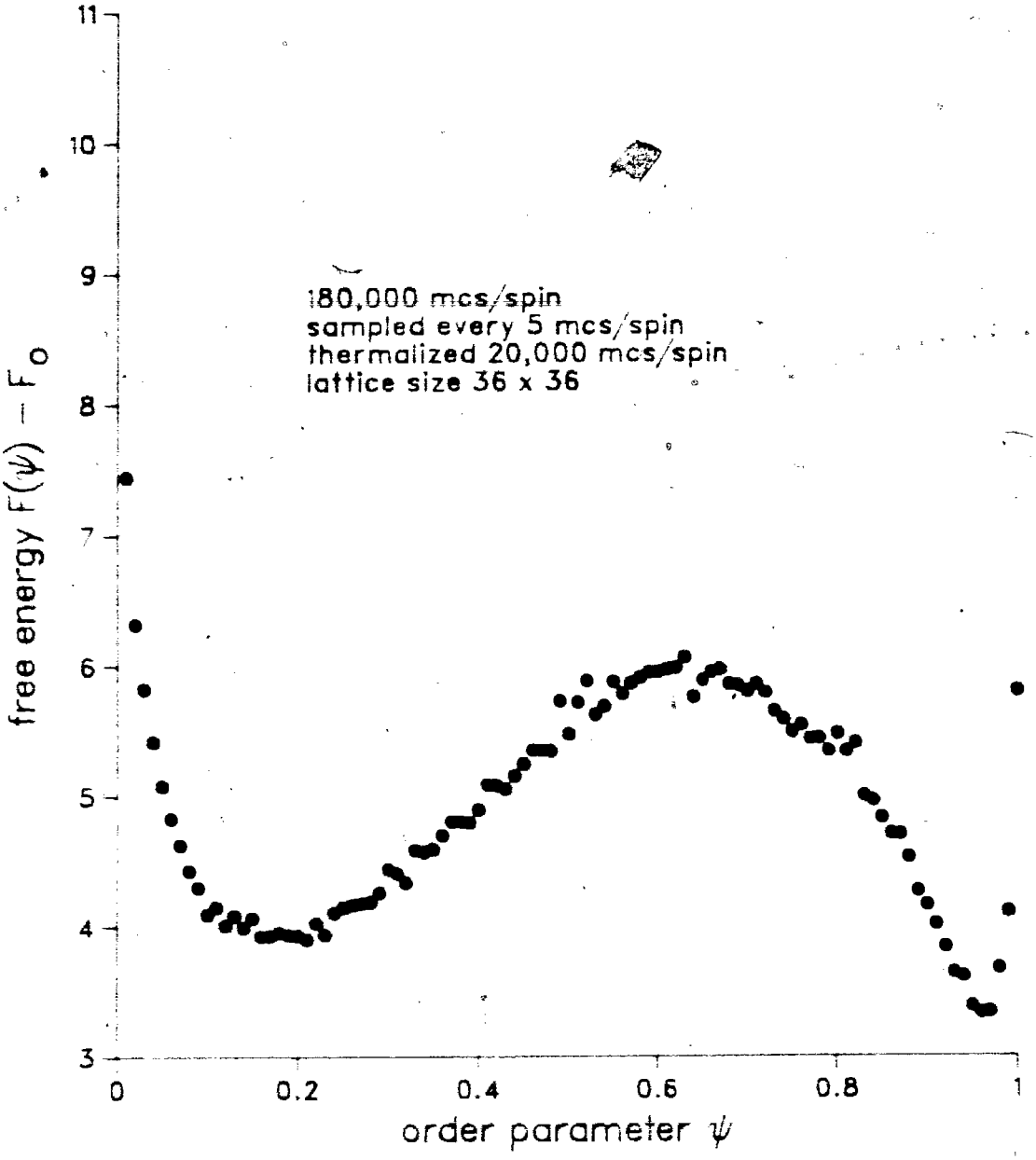

Figure 4.2.3a

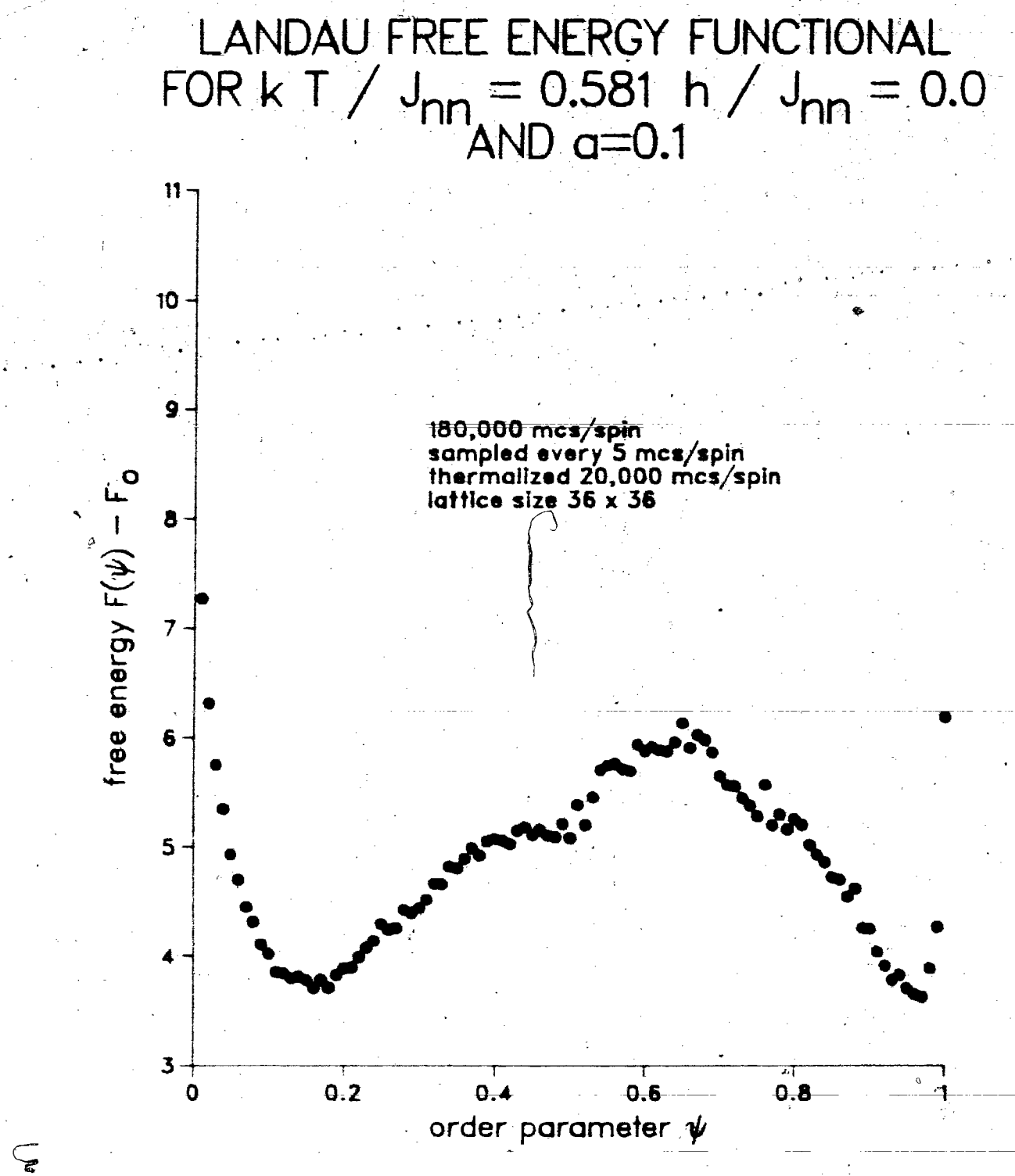
LANDAU FREE ENERGY FUNCTIONAL
FOR k T / J_{nn} = 0.581 h / J_{nn} = 0.0
AND a=0.1
180,000 mcs/spin
sampled every 5 mcs/spin
thermalized 20,000 mcs/spin
lattice size 36 x 36
free energy $F(\psi) - F_0$
order parameter ψ
11
10
9
8
7
6
5
4
3
0
0.2
0.4
0.6
0.8
1

Figure 4.2.3b

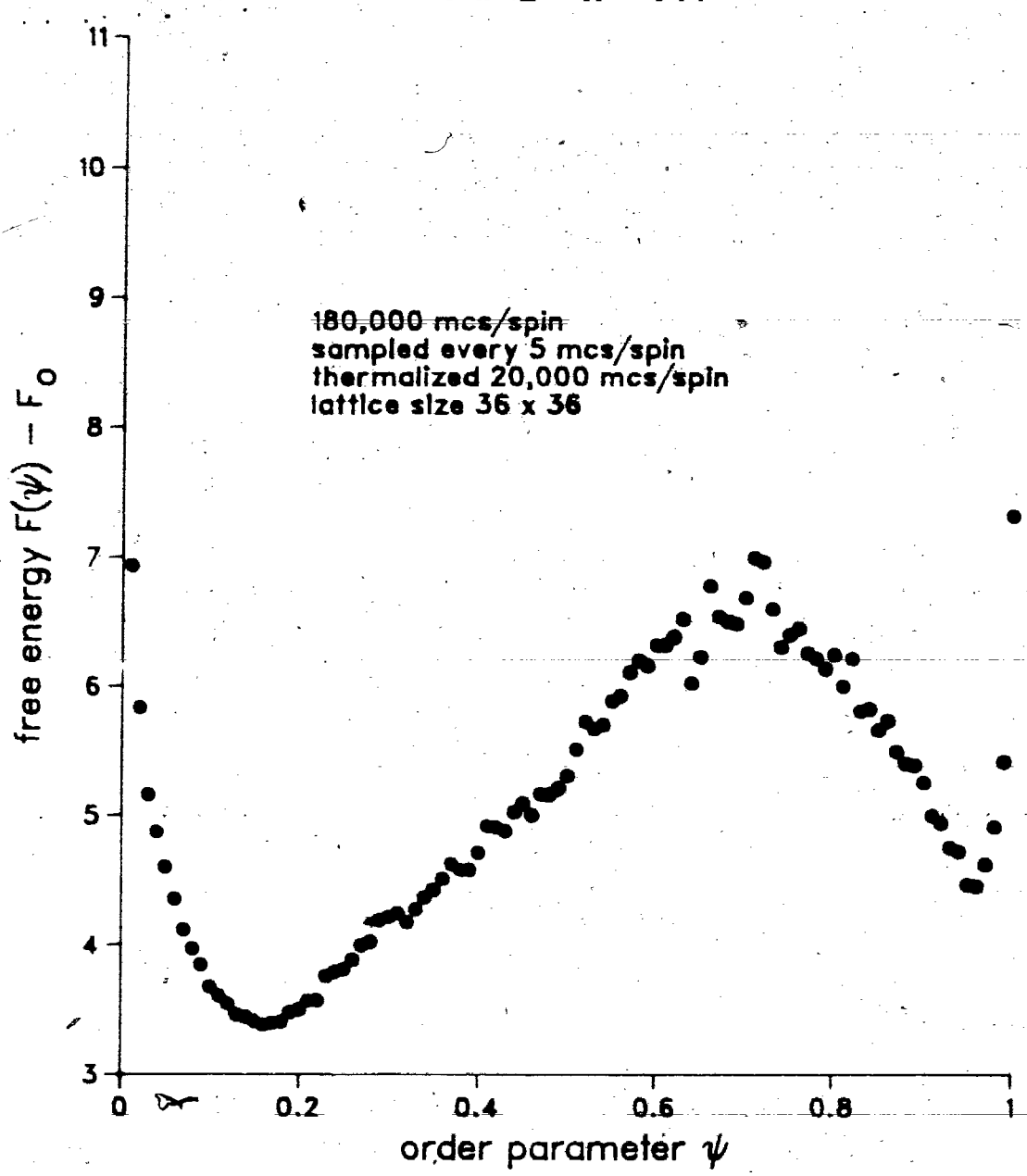
LANDAU FREE ENERGY FUNCTIONAL
FOR k T / J_nn = 0.582 h / J_nn = 0.00
AND a=0.1
180,000 mcs/spin
sampled every 5 mcs/spin
thermalized 20,000 mcs/spin
lattice size 36 x 36
free energy F(ψ) − F_0
order parameter ψ
11
10
9
8
7
6
5
4
3
0
0.2
0.4
0.6
0.8
1

Figure 4.2.3c

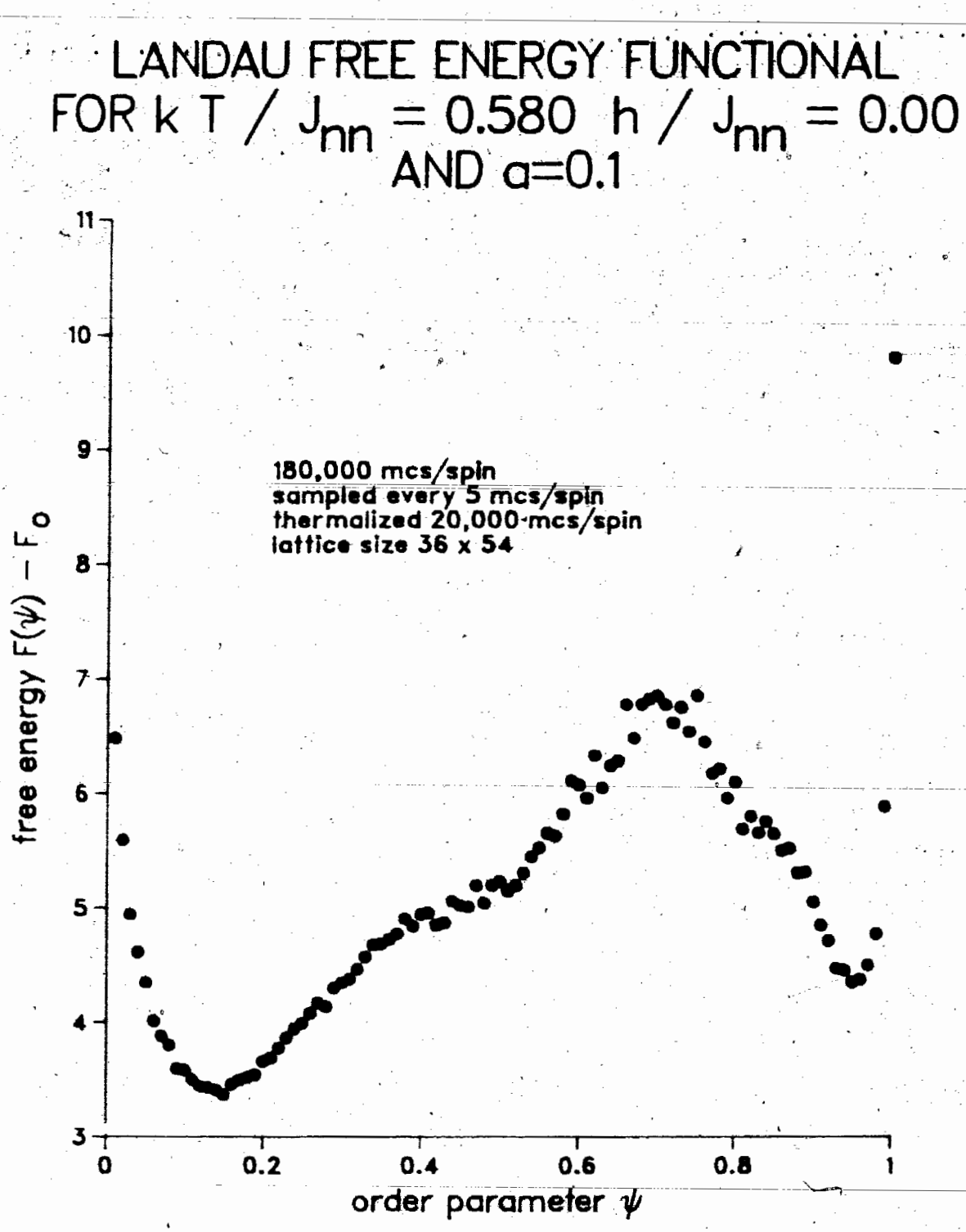
LANDAU FREE ENERGY FUNCTIONAL
FOR k T / J_{nn} = 0.580 h / J_{nn} = 0.00
AND a=0.1
180,000 mcs/spin
sampled every 5 mcs/spin
thermalized 20,000 mcs/spin
lattice size 36 x 54
free energy $F(\psi) - F_0$
order parameter ψ
11
10
9
8
7
6
5
4
3
0
0.2
0.4
0.6
0.8
1

Figure 4.2.4

From the above discussion, we see that what started out as a presumably clear signal of a first order transition has became somewhat dubious when finite size effects are considered. Though this result is somewhat disconcerting a plausible explanation which is consistent with an interpretation that the transition is first order can be found by examing the spin configuration of the system at steps along the Monte Carlo run. It was found that the system had a greater propensity to break up into regions of coexistence between various ordered and disordered phases as the size was increased. In a smaller system the coexistence was suppressed and the global order parameter was a good indication of the degree of order of a given phase. However the presence of coexistence between different ordered phases (as found in larger systems) made the global order parameter a poor indicator of the order in the system. For example the system may be broken up into two regions of different ordered phases with the magnitude of the order parameter nearly the same but with different signs. As a result the global order parameter would be very small though the system is completely ordered. It is this type of cancellation between coexisting ordered phases that we believe is responsible for the size of the bump diminishing for very large lattices.

The way around this problem would be to calculate a local order parameter over several regions of various size and check how these scaled with total size of the system. This was not done in this calculation because of time constraints but could prove to be an interesting investigation.

The above calculation was only for $h=0$ and we conclude that the transition is first order at least at $h=0$ in agreement with the conjecture stated in section 1.2. However from figures 4.1.1b and 4.3.1 we see that the coexistence region exists for nonzero fields indicating that the 2×1 order-disorder transition is first order even for nonzero fields. We conclude that the entire 2×1 boundary is first order.

We now discuss the free energy functional for the $\sqrt{3}\times\sqrt{3}$ order-disorder transition. We begin by considering $F(\psi)$ near the maximum transition temperature (T_c) which occurs as $h/J_{nn}=3.00$. The sequence of figures 4.2.6a-e for the 32×48 shows that there is no bump in $F(\psi)$ at T_c. The extreme flatness of the curve near its minimum is a good indication of a divergent susceptibility at T_c. The same results were found for the 64×48 and 64×96 lattices. We therefore conclude that the order-disorder transition at $h/J_{nn}=3.00$ is continuous.

At this point one is somewhat hesitant to conclude that the entire boundary is second order particularly since one end of the boundary is either a triple point, a critical endpoint or a multicritical point (see fig4.1.1a). By sampling $F(\psi)$ for $h/J_{nn}=4.2$ we see that the order-disorder transition is still continuous (see fig4.2.7) very near this point. Near the other end of the boundary no thorough investigation was made. However in a casual study no indication that the transition would be first order was found. We therefore feel confident that the entire $\sqrt{3}\times\sqrt{3}$ order-disorder transition is second order.

Finally we discuss the 2×2 to paramagnetic transition. This boundary has the most structure and for this reason we use it to compare the various methods of determining the order of a phase transition. Before doing so we describe the nature of the free energy functional $F(\psi)$ when evaluated on this boundary. $F(\psi)$ was calculated along the 2×2 boundary at $h/J_{nn}=4.75,\ 5.5,\ 6.0$. At $h/J_{nn}=4.75$, $F(\psi)$ for the 36×36 lattice (Figure 4.2.9) shows a distinct bump. When the lattice was increased to 36×54 the bump clearly decreased (figure 4.2.10) in magnitude. Such behaviour has been observed with model that are known to undergo a continuous transition (i.e. Blume-Capel and Baxter hard hexagons models) [20,28]. Associated with the diminishing bump in these systms is a decrease in the separation of the minima of $F(\psi)$. Such is not the case with this model. From figures 4.2.9-10 we notice that the minima are stationary with respect to changes in the systems size.

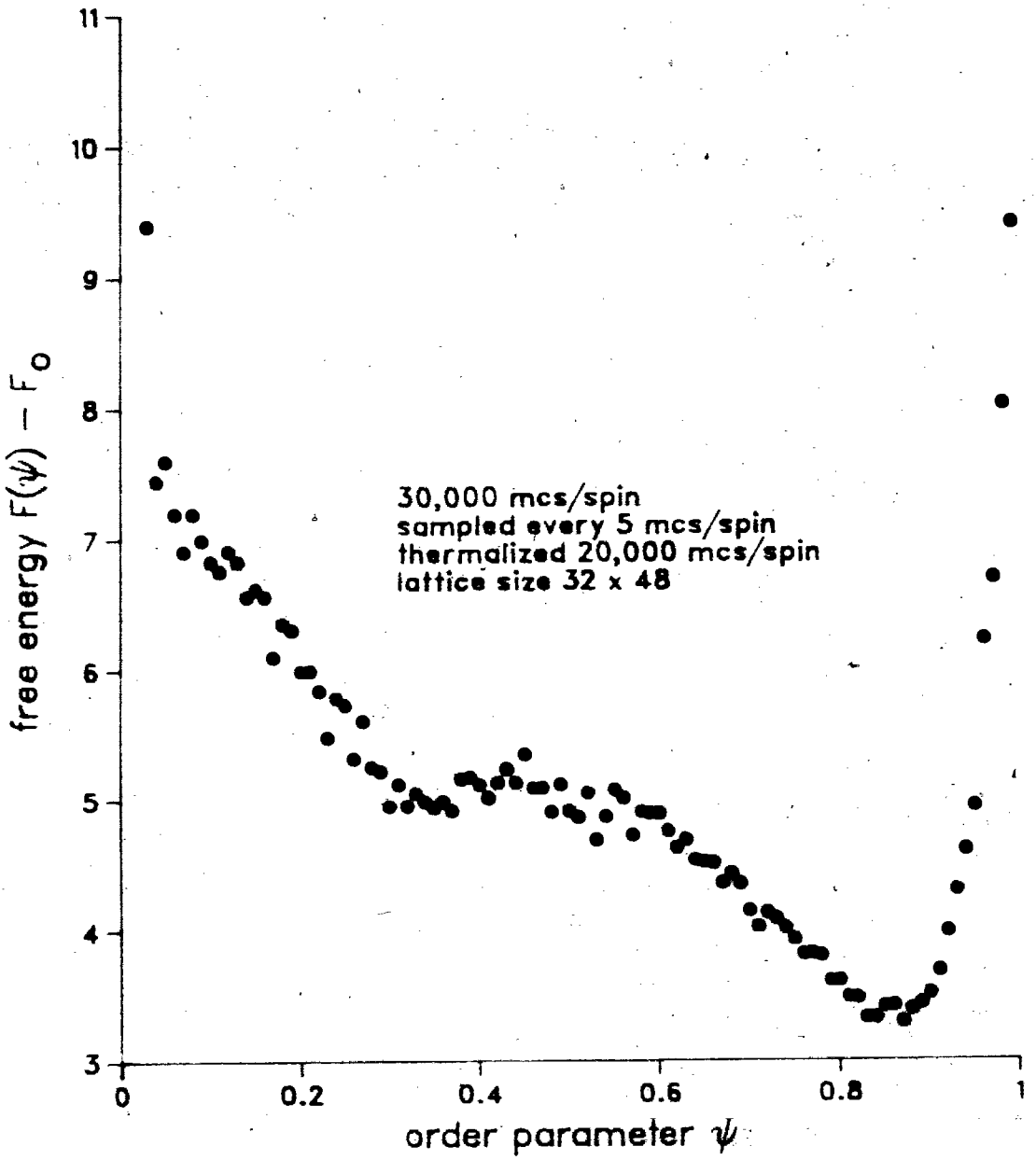
LANDAU FREE ENERGY FUNCTIONAL
FOR k T / J_{nn} = 0.820 h / J_{nn} = 3.0
AND a=0.1
free energy F(ψ) − F_o
order parameter ψ
30,000 mcs/spin
sampled every 5 mcs/spin
thermalized 20,000 mcs/spin
lattice size 32 x 48
11
10
9
8
7
6
5
4
3
0
0.2
0.4
0.6
0.8
1

Figure 4.2.6a

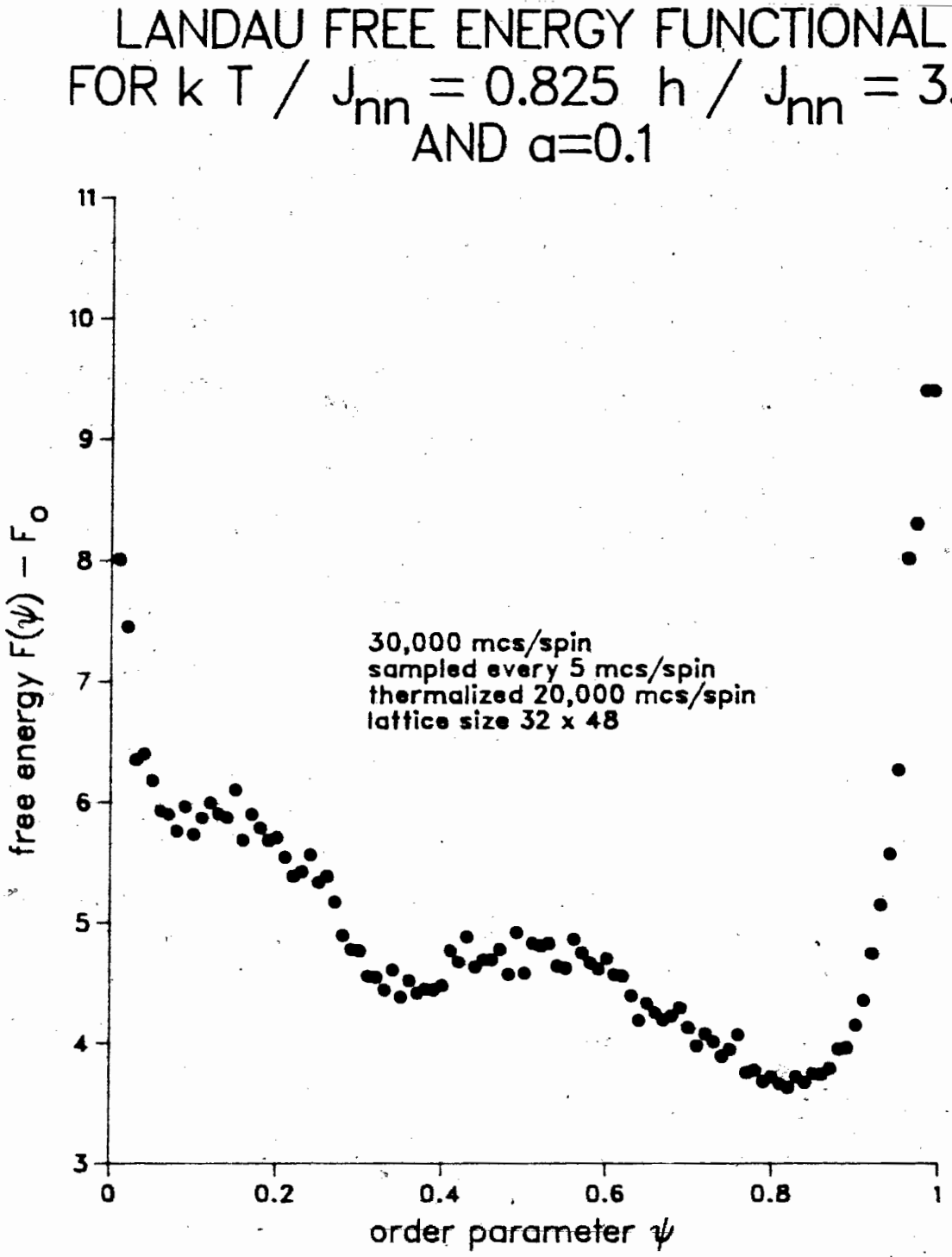
LANDAU FREE ENERGY FUNCTIONAL
FOR k T / J_{nn} = 0.825 h / J_{nn} = 3.0
AND a=0.1
free energy $F(\psi) - F_o$
order parameter ψ
30,000 mcs/spin
sampled every 5 mcs/spin
thermalized 20,000 mcs/spin
lattice size 32 x 48
11
10
9
8
7
6
5
4
3
0
0.2
0.4
0.6
0.8
1

Figure 4.2.6b

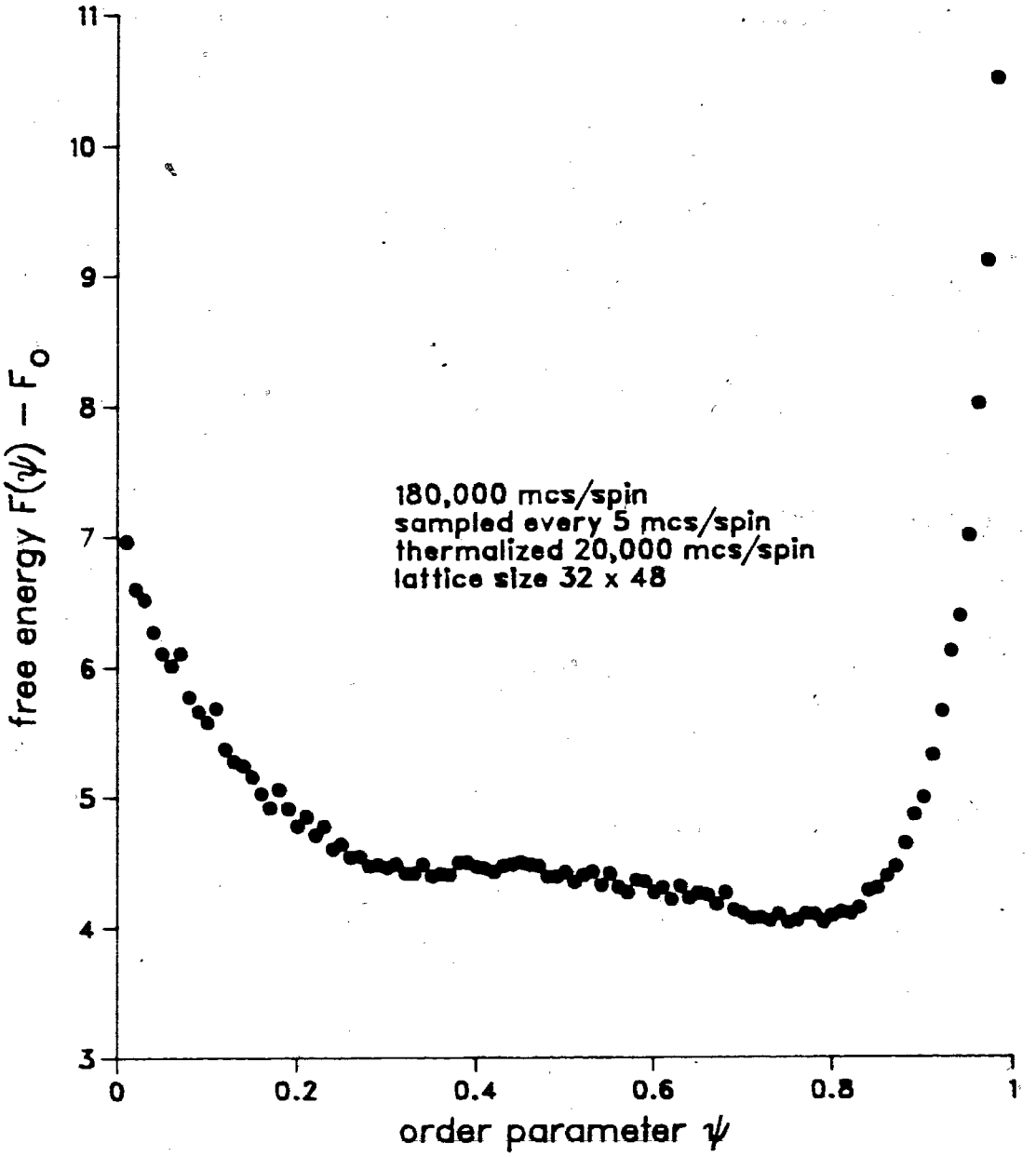
LANDAU FREE ENERGY FUNCTIONAL
FOR k T / J_nn = 0.831 h / J_nn' = 3.0
AND a=0.1
free energy F(ψ) − F_o
order parameter ψ
180,000 mcs/spin
sampled every 5 mcs/spin
thermalized 20,000 mcs/spin
lattice size 32 x 48
11
10
9
8
7
6
5
4
3
0
0.2
0.4
0.6
0.8
1

Figure 4.2.6c

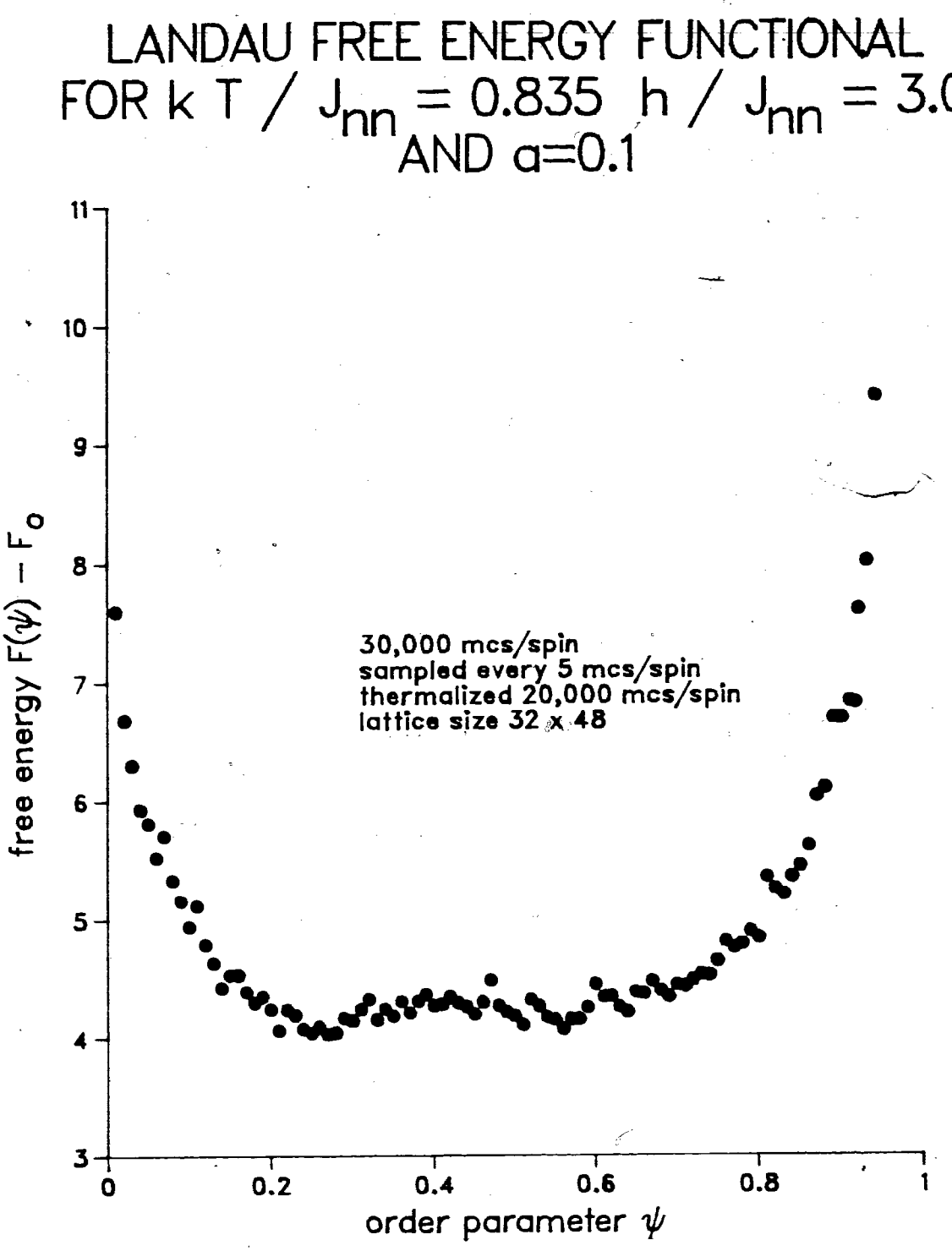
LANDAU FREE ENERGY FUNCTIONAL
FOR k T / J_nn = 0.835 h / J_nn = 3.0
AND a=0.1
free energy F(ψ) − F_o
order parameter ψ
30,000 mcs/spin
sampled every 5 mcs/spin
thermalized 20,000 mcs/spin
lattice size 32 x 48
11
10
9
8
7
6
5
4
3
0
0.2
0.4
0.6
0.8
1

Figure 4.2.6d

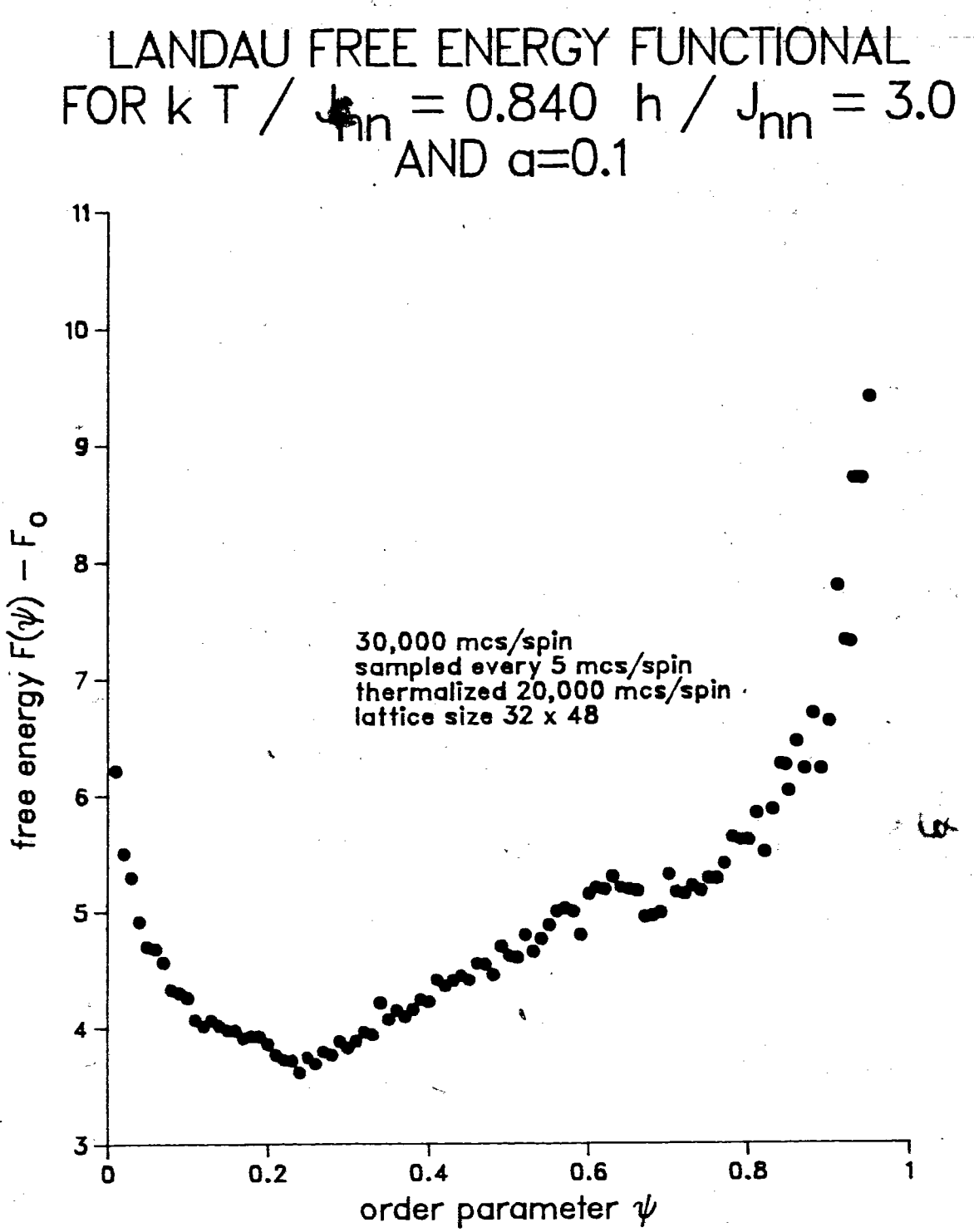
LANDAU FREE ENERGY FUNCTIONAL
FOR k T / J_nn = 0.840 h / J_nn = 3.0
AND a=0.1
free energy F(ψ) − F_o
order parameter ψ
30,000 mcs/spin
sampled every 5 mcs/spin
thermalized 20,000 mcs/spin
lattice size 32 x 48
11
10
9
8
7
6
5
4
3
0
0.2
0.4
0.6
0.8
1

Figure 4.2.6e

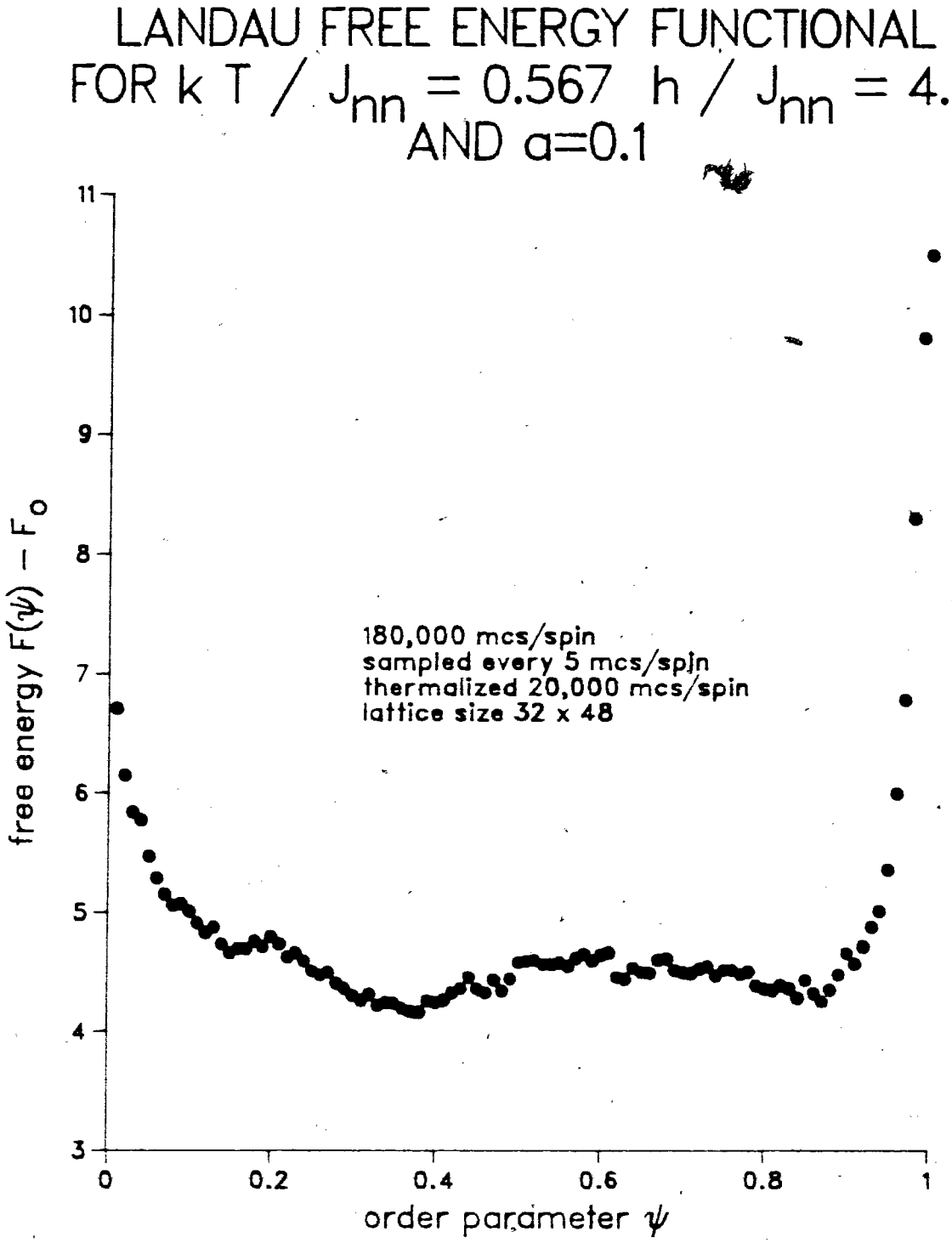
LANDAU FREE ENERGY FUNCTIONAL
FOR k T / J_nn = 0.567 h / J_nn = 4.2
AND a=0.1
free energy F(ψ) − F_o
order parameter ψ
180,000 mcs/spin
sampled every 5 mcs/spin
thermalized 20,000 mcs/spin
lattice size 32 x 48
11
10
9
8
7
6
5
4
3
0
0.2
0.4
0.6
0.8
1

Figure 4.2.7

We thereby appeal to the coexistence argument to explain the decrease and conclude that the transition is first order. The coexistence alluded to above was actually found in typical configurations of the Monte Carlo runs.

At h/J_{nn}=5.5 figures 4.2.11a-b indicate a small bump in $F(\psi)$ for the 24×18 lattice. For the same value of h/J_{nn} on the 36×36 lattice there was a marked increase in the size of the maximum but it was only 60% of the height of the bump on the same size lattice for h/J_{nn}=4.75. When the lattice was further increased to 36×54 the maximum nearly disappeared (fig 4.2.13a-b). For h/J_{nn}=6.0 on the 36×36 lattice the bump is approximately 1/3 of the bump for h/J_{nn}=5.5 (see fig 4.2.14). On a 36×54 lattice the results are obscured since $F(\psi)$ is not calculated sufficiently close to the transition. However there appears to be no significant change in the size of the maximum. It appears, therefore, that the entire 2×2 order-disorder transition is an example of a first order transition which is weakened or driven second order with increasing field. The conclusion is somewhat questionable in light of the finite size effects discussed. Therefore it becomes necessary to compare conclusions drawn from the free energy functional $F(\psi)$ with more traditional methods and we do this in the next section.

We conclude this section with a discussion of one additional transition namely the 2×2 to $\sqrt{3}\times\sqrt{3}$ transition. There is little question that this transition will be anything but first order. Although no data is presented here it was found that associated with the transition was a large degree of hysteresis. In fact this hysteresis made accurate location of the transition difficult. The presence of the hysteresis is a signal of the expected first order nature of the transition.

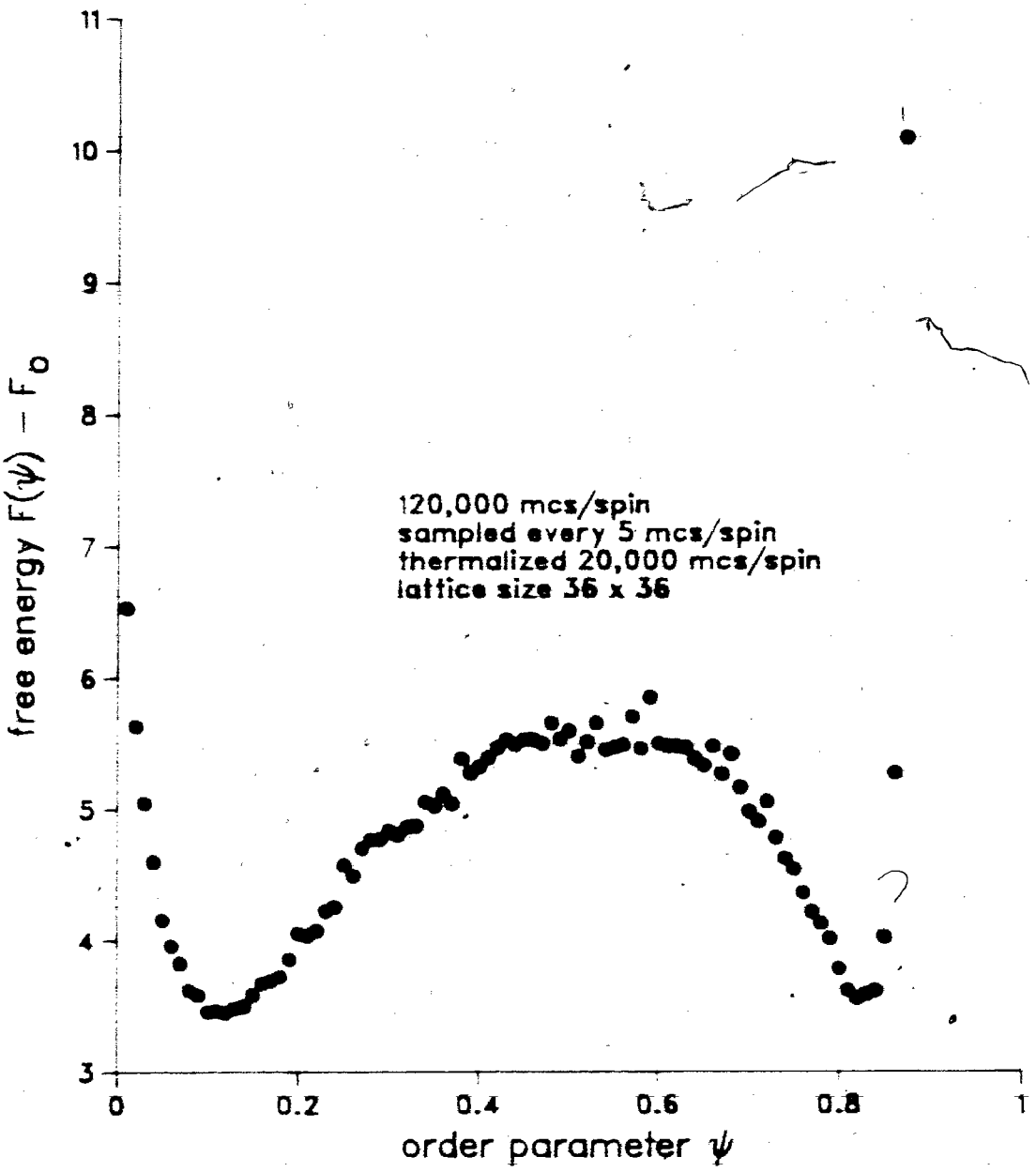
LANDAU FREE ENERGY FUNCTIONAL
FOR k T / J_{nn} = 0.615 h / J_{nn} = 4.75
AND a=0.1
free energy $F(\psi) - F_0$
order parameter ψ
120,000 mcs/spin
sampled every 5 mcs/spin
thermalized 20,000 mcs/spin
lattice size 36 x 36
11
10
9
8
7
6
5
4
3
0
0.2
0.4
0.6
0.8
1

Figure 4.2.9

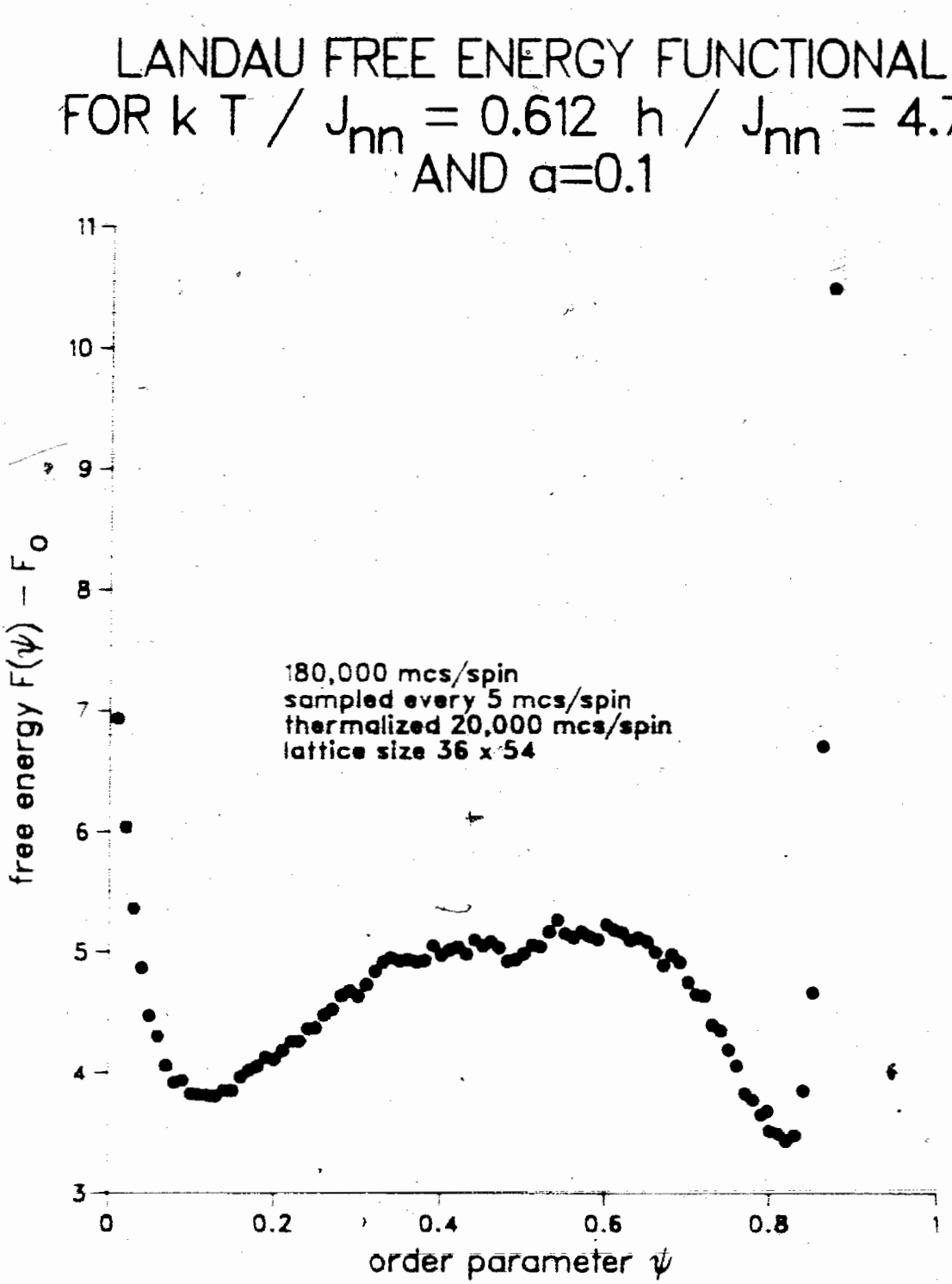
LANDAU FREE ENERGY FUNCTIONAL
FOR k T / J_nn = 0.612 h / J_nn = 4.75
AND a=0.1
180,000 mcs/spin
sampled every 5 mcs/spin
thermalized 20,000 mcs/spin
lattice size 36 x 54
free energy F(ψ) − F_0
order parameter ψ
11
10
9
8
7
6
5
4
3
0
0.2
0.4
0.6
0.8
1

Figure 4.2.10

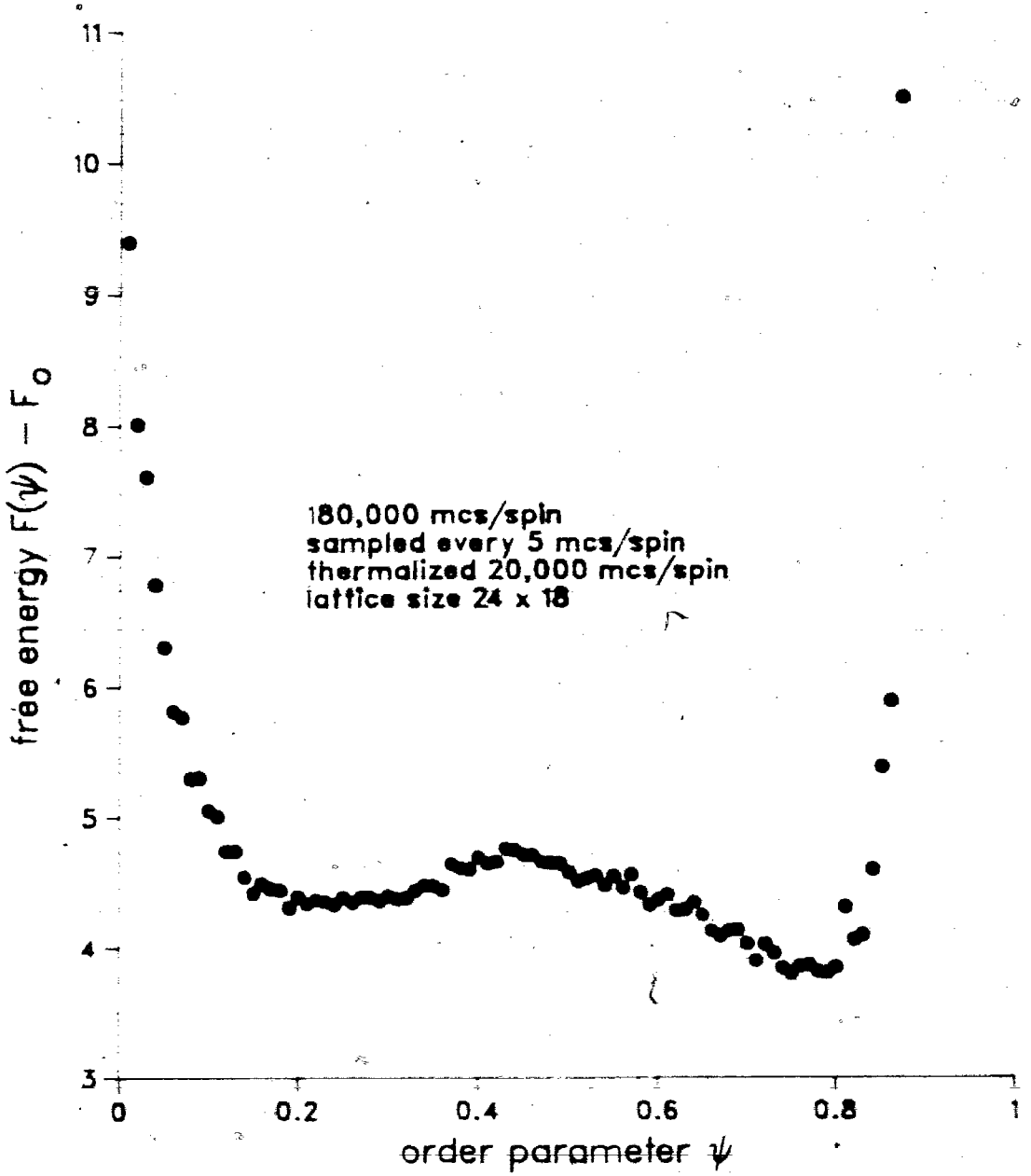

Figure 4.2.11a

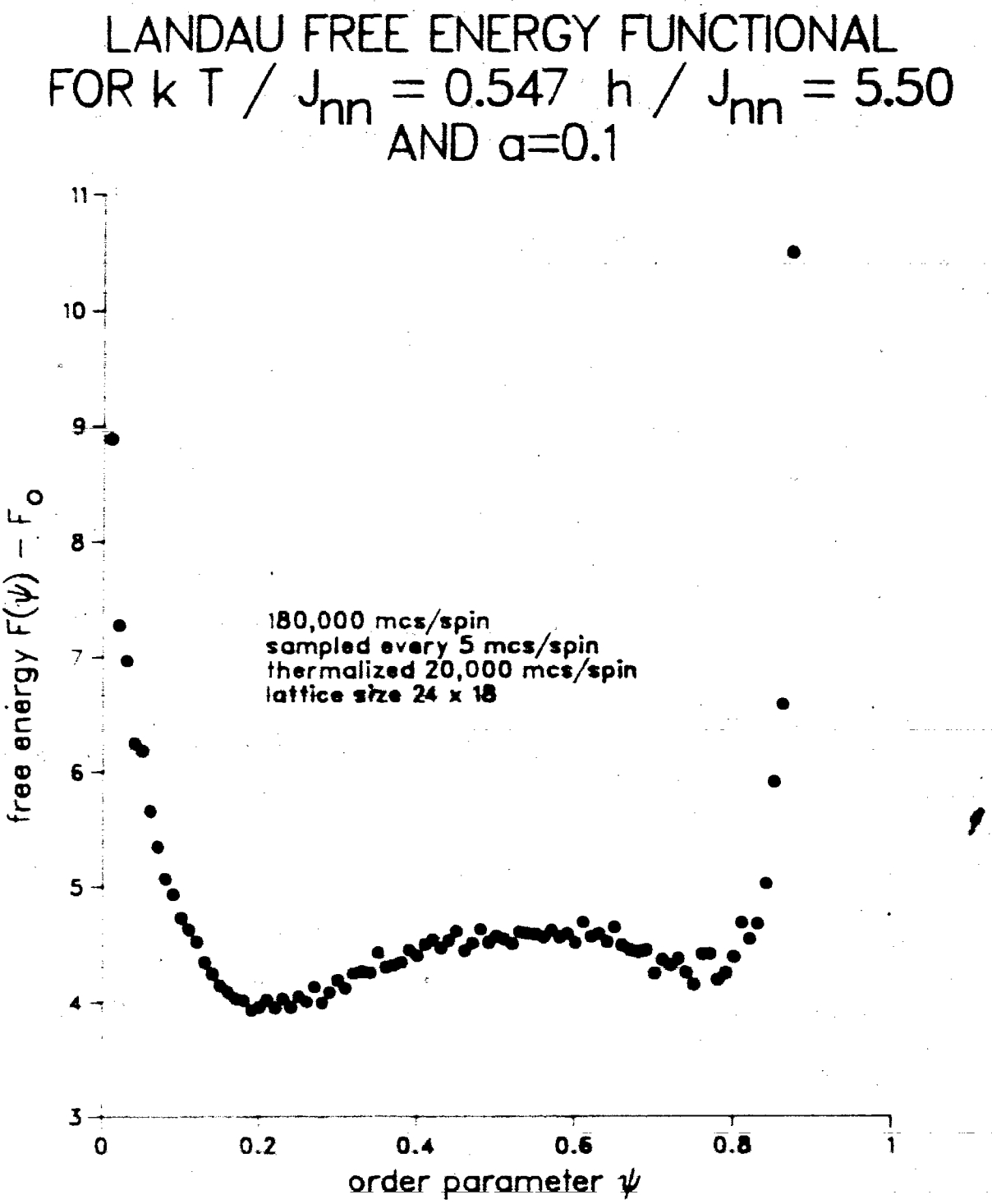

Figure 4.2.11b

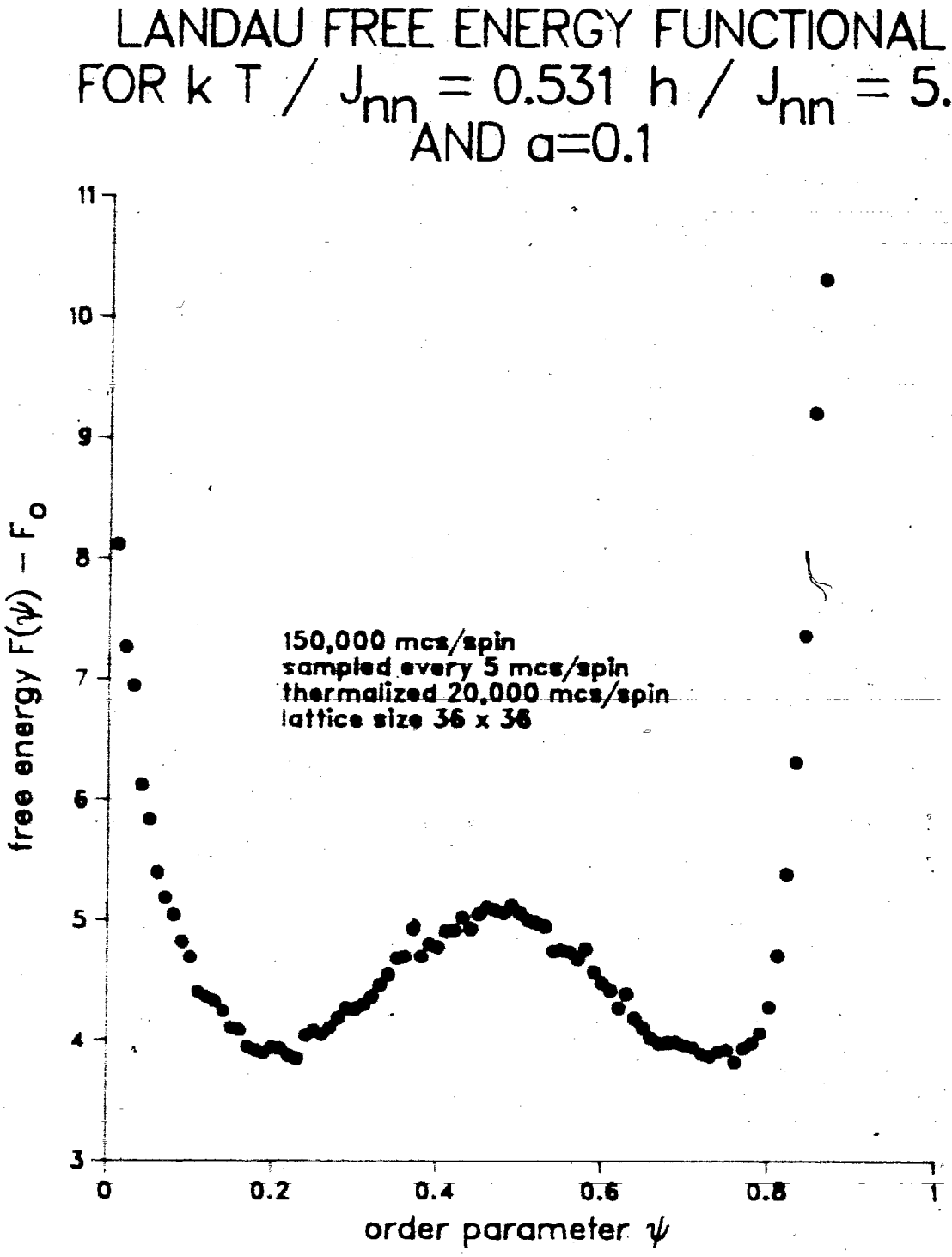
LANDAU FREE ENERGY FUNCTIONAL
FOR k T / J_nn = 0.531 h / J_nn = 5.5
AND a=0.1
free energy F(ψ) − F_o
order parameter ψ
150,000 mcs/spin
sampled every 5 mcs/spin
thermalized 20,000 mcs/spin
lattice size 36 x 36
11
10
9
8
7
6
5
4
3
0
0.2
0.4
0.6
0.8
1

Figure 4.2.12

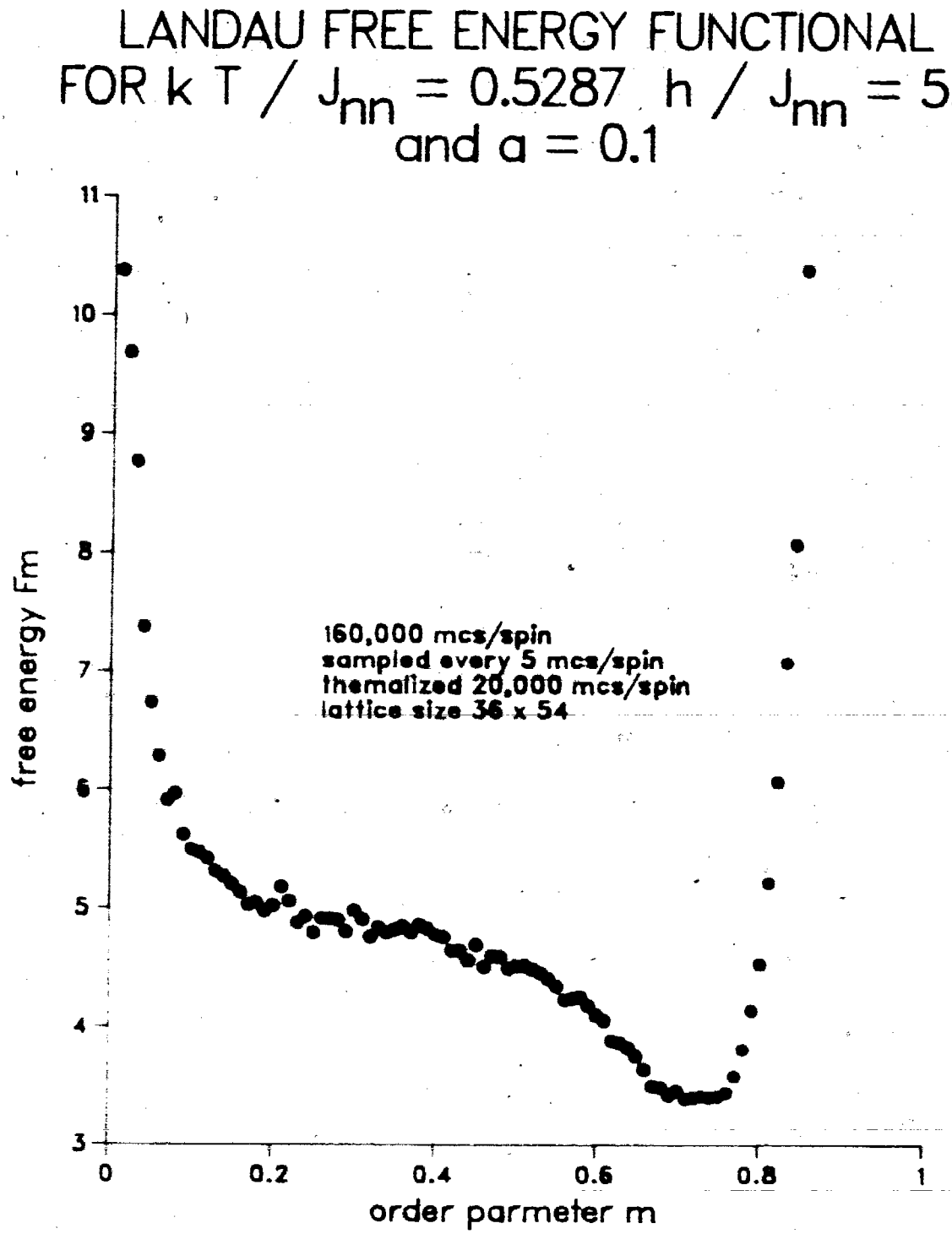

Figure 4.2.13a

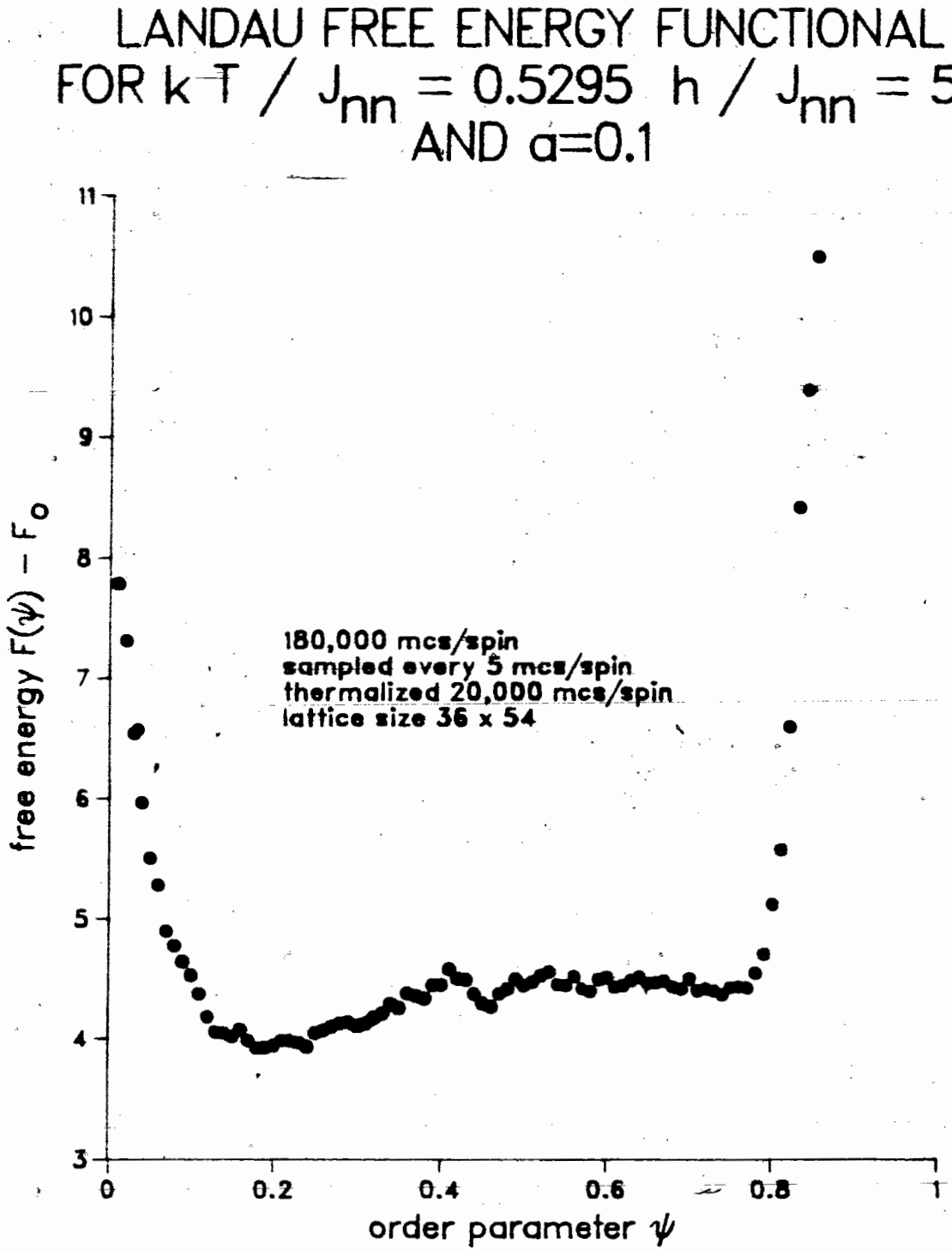

Figure 4.2.13b

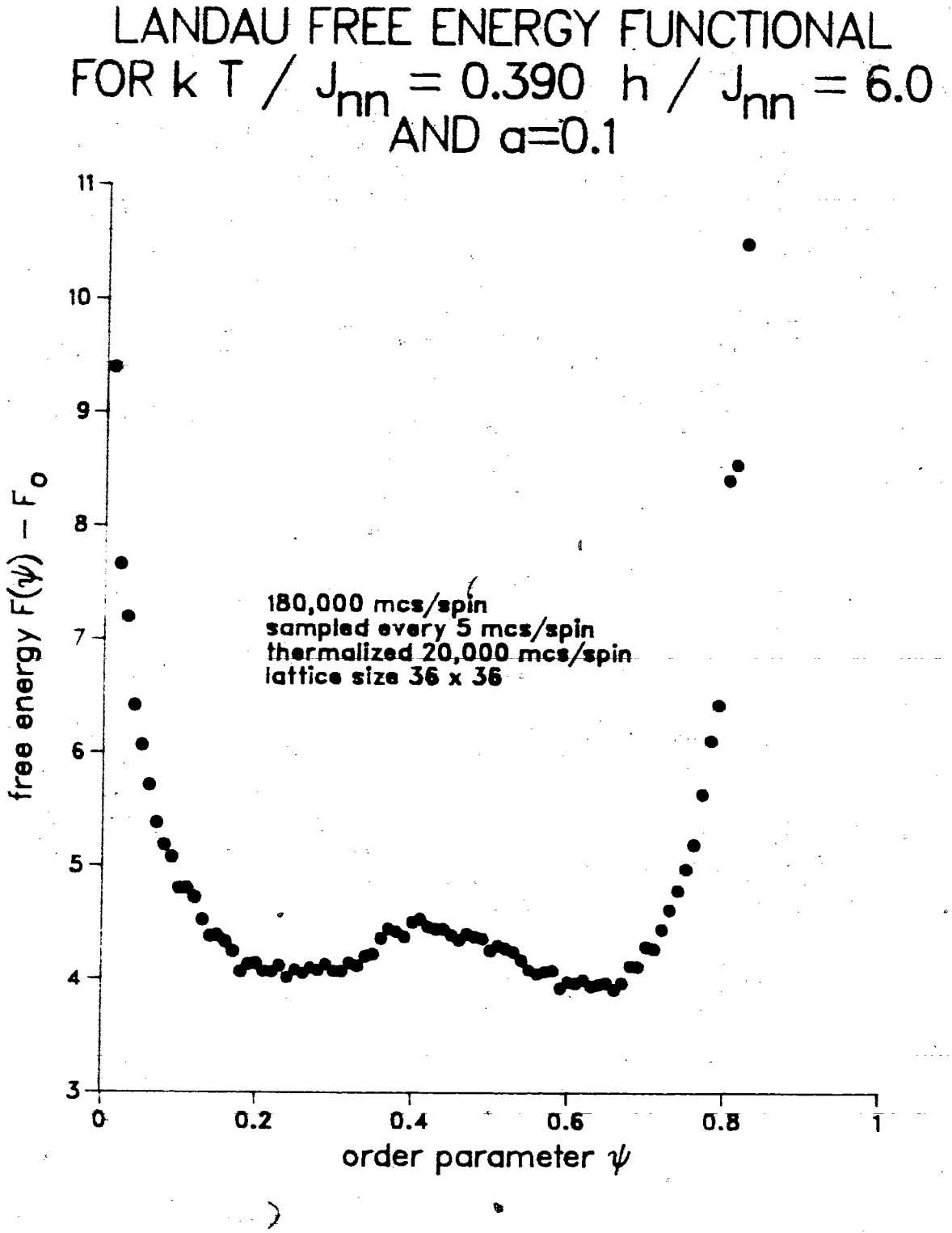
LANDAU FREE ENERGY FUNCTIONAL
FOR k T / J_nn = 0.390 h / J_nn = 6.0
AND a=0.1
180,000 mcs/spin
sampled every 5 mcs/spin
thermalized 20,000 mcs/spin
lattice size 36 x 36
free energy F(ψ) − F_o
order parameter ψ
11
10
9
8
7
6
5
4
3
0
0.2
0.4
0.6
0.8
1

Figure 4.2.14

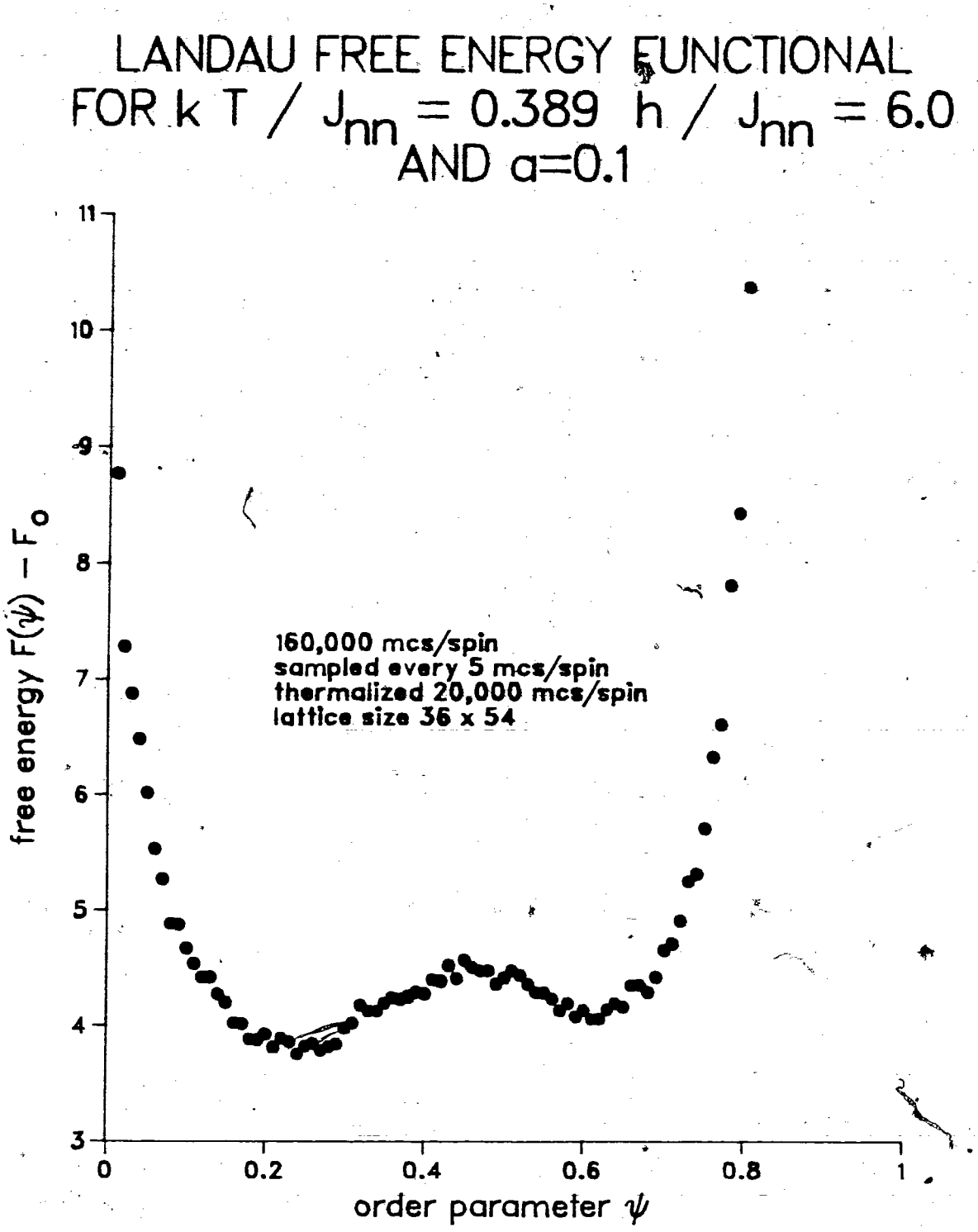

Figure 4.2.15a

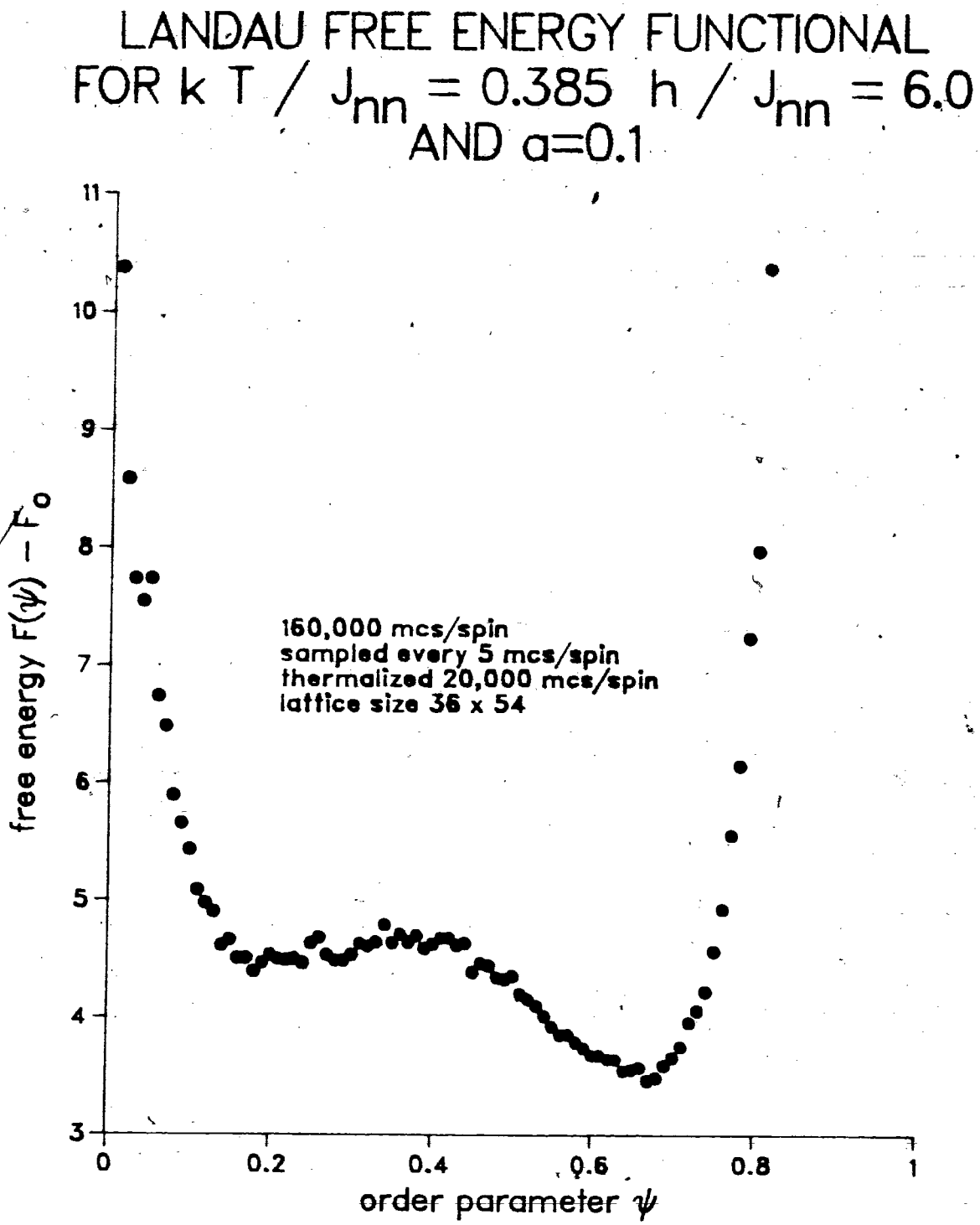

Figure 4.2.15b

4.3. Hysteresis and Time Series Study

We begin with discussing the results of the hysteresis calculation. Figures 4.3.2-6 show plots of energy and order parameter versus temperature for a sequence of increasing field values along the 2x2 order-disorder transition boundary. Figures 4.3.2-4 show a clear discontinuity in both the internal energy and the order parameter indicating that the transition is first order for $4.375 \leq h/J_{nn} \leq 4.625$. One may notice a slight increase in the scatter of the data as the field is increased from $h/J_{nn}=4.375$ to $h/J_{nn}=4.625$. This scatter becomes excessive when the field is further increased to 4.75. We believe that the reason for this excessive scatter is that the system is undergoing sufficient fluctuations to cause the the system to jump back and forth between the ordered and disordered phases during the sampling period . In an infinite system metastability would prevent such an oscillation. Therefore to mimic the infinite system more closely we increased the lattice size sufficiently to suppress these oscillations. Figures 4.3.5-6 show plots for fields $h/J_{nn}=4.75$ and $h/J_{nn}=5.5$ obtained from a calculation on a 72x54 lattice. From the figures 4.3.2-6 we see that there is significant hysteresis for $4.375 \leq h/J_{nn} \leq 4.75$. There appears to still be a hysteresis loop for $h/J_{nn}=5.5$ but this is not entirely clear. This indicates that the transition at the 2x2 boundary is first order but is becoming closer to a continuous transition as the field is increased. The increased scatter of the data with increasing field also suggests this conclusion.

Figure 4.3.7 is a plot of the width (ΔT) of the hysteresis loop and the magnitude (ΔE) of the discontinuity of the internal energy versus field (h/J_{nn}). Notice that both the gap's width and height of the gap decrease with field and appears to vanish at $h/J_{nn} \approx 6$, demonstrating the weakening of the first order transition. These conclusions are entirely consistent with the conclusions based on the functional $F(\psi)$ thus providing a check of this new method for the determination of the order of a transition.

Also consistent with all the above results are the time series calculations. In such calculations one plots coarse grained averages (i.e averages computed over a small segment of the total run) of the order parameter or internal energy as a function of "time" in the Markov chain. These calculations were initially suggested by Mouritsen, in a private conversation, as a good indication of a first order transition if one could sample sufficiently long to witness the sharp switching of the system from an ordered to a disordered phase or vice versa. Such switching was found for both the 2x1 and 2x2 transitions (see Fig4.3.8 and Fig4.3.10) from which we infer that at these point on the phase boundaries the transitions are first order . It is interesting to contrast the plots of figures 4.3.8 and 4.3.10 to a similar plot (figure 4.3.9) made for a point on the $\sqrt{3}\times\sqrt{3}$ boundary at which we believe the transition is continuous. The dramatic difference leads one to believe that the respective transitions must be qualitatively different.

In summary we conclude that the 2x2 transition is first order on the small field side of the curve and is weakened as the field is increased. However it is not clear if the transition remains first order for all values of the field. It may crossover to second order transition at sufficiently large values of the field. It appears that if the transition becomes continuous it will do so for $h/J_{nn} \geq 5.5$. It should be mentioned that this result contradicts the universality augments of Schick et al. based on a Landau theory. They predicted that this transition will always be second order for all values of the field.

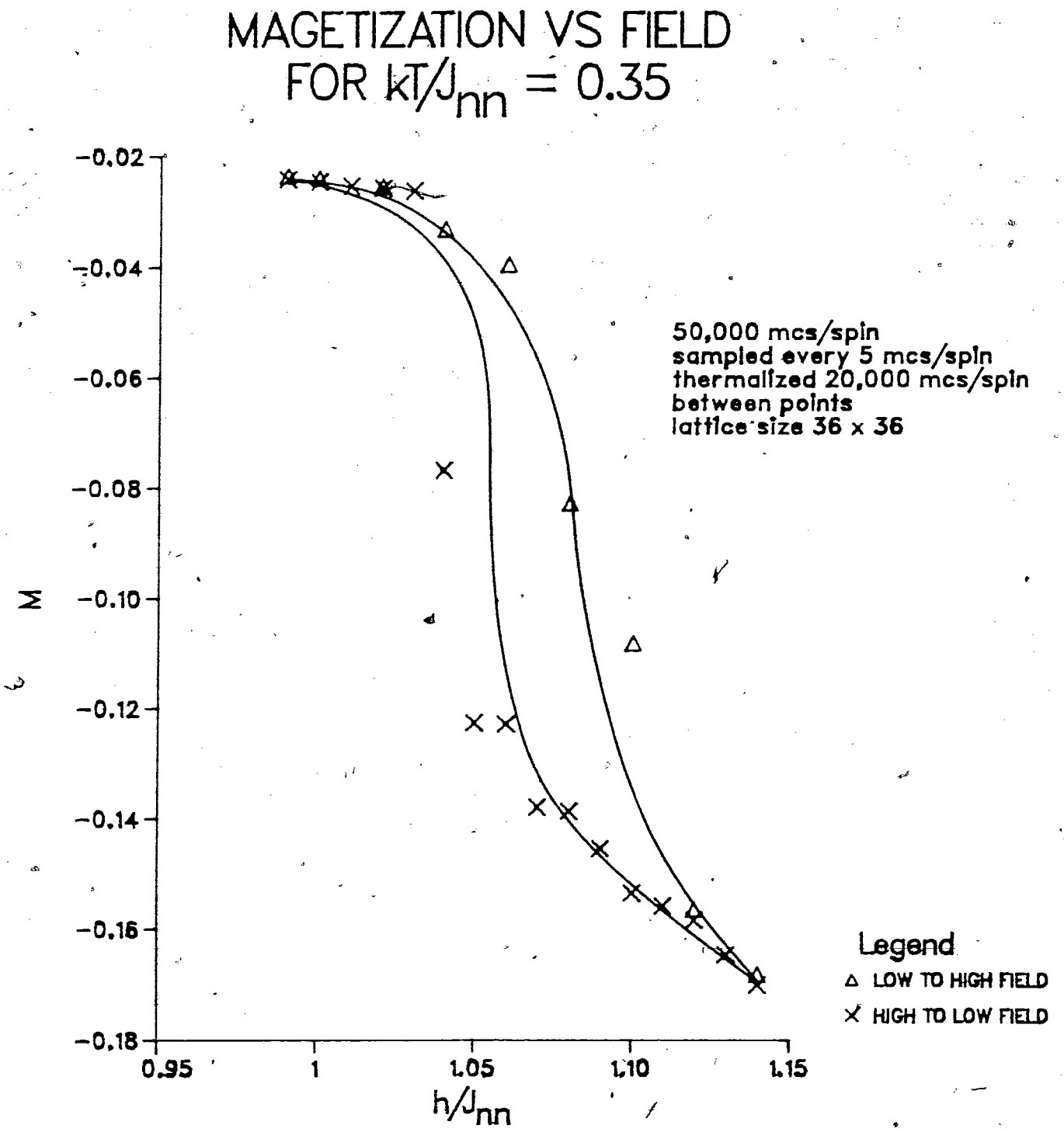
MAGETIZATION VS FIELD
FOR kT/J_nn = 0.35
-0.02
-0.04
-0.06
-0.08
-0.10
-0.12
-0.14
-0.16
-0.18
M
0.95
1
1.05
1.10
1.15
h/J_nn
50,000 mcs/spin
sampled every 5 mcs/spin
thermalized 20,000 mcs/spin
between points
lattice size 36 x 36
Legend
LOW TO HIGH FIELD
HIGH TO LOW FIELD

Figure 4.3.1

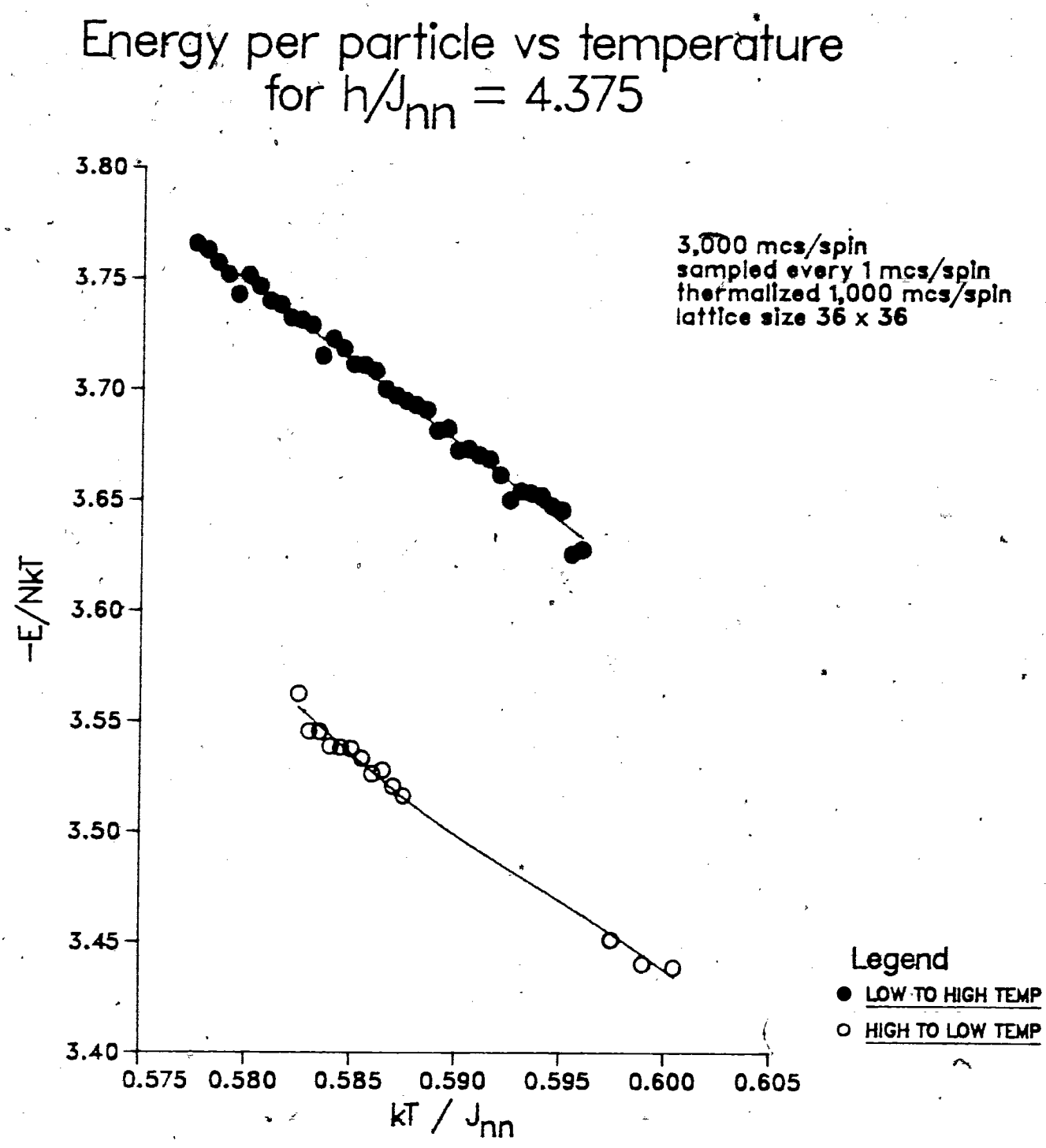
Energy per particle vs temperature
for h/J_nn = 4.375
3,000 mcs/spin
sampled every 1 mcs/spin
thermalized 1,000 mcs/spin
lattice size 36 x 36
-E/NkT
3.80
3.75
3.70
3.65
3.60
3.55
3.50
3.45
3.40
0.575
0.580
0.585
0.590
0.595
0.600
0.605
kT / J_nn
Legend
LOW TO HIGH TEMP
HIGH TO LOW TEMP

Figure 4.3.2a

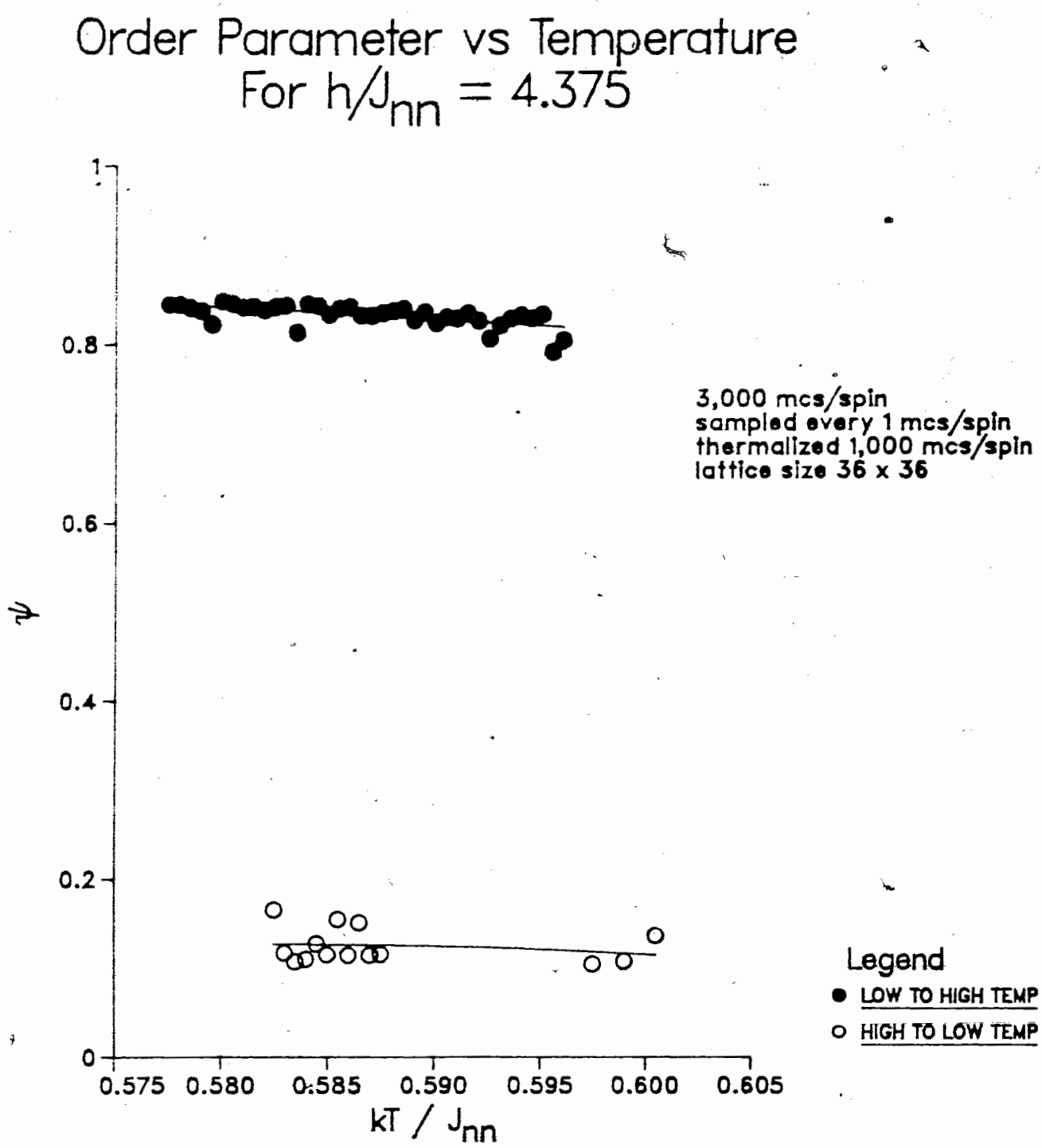
Order Parameter vs Temperature
For h/Jnn = 4.375
1
0.8
0.6
0.4
0.2
0
ψ
0.575
0.580
0.585
0.590
0.595
0.600
0.605
kT / Jnn
3,000 mcs/spin
sampled every 1 mcs/spin
thermalized 1,000 mcs/spin
lattice size 36 x 36
Legend
LOW TO HIGH TEMP
HIGH TO LOW TEMP

Figure 4.3.2b

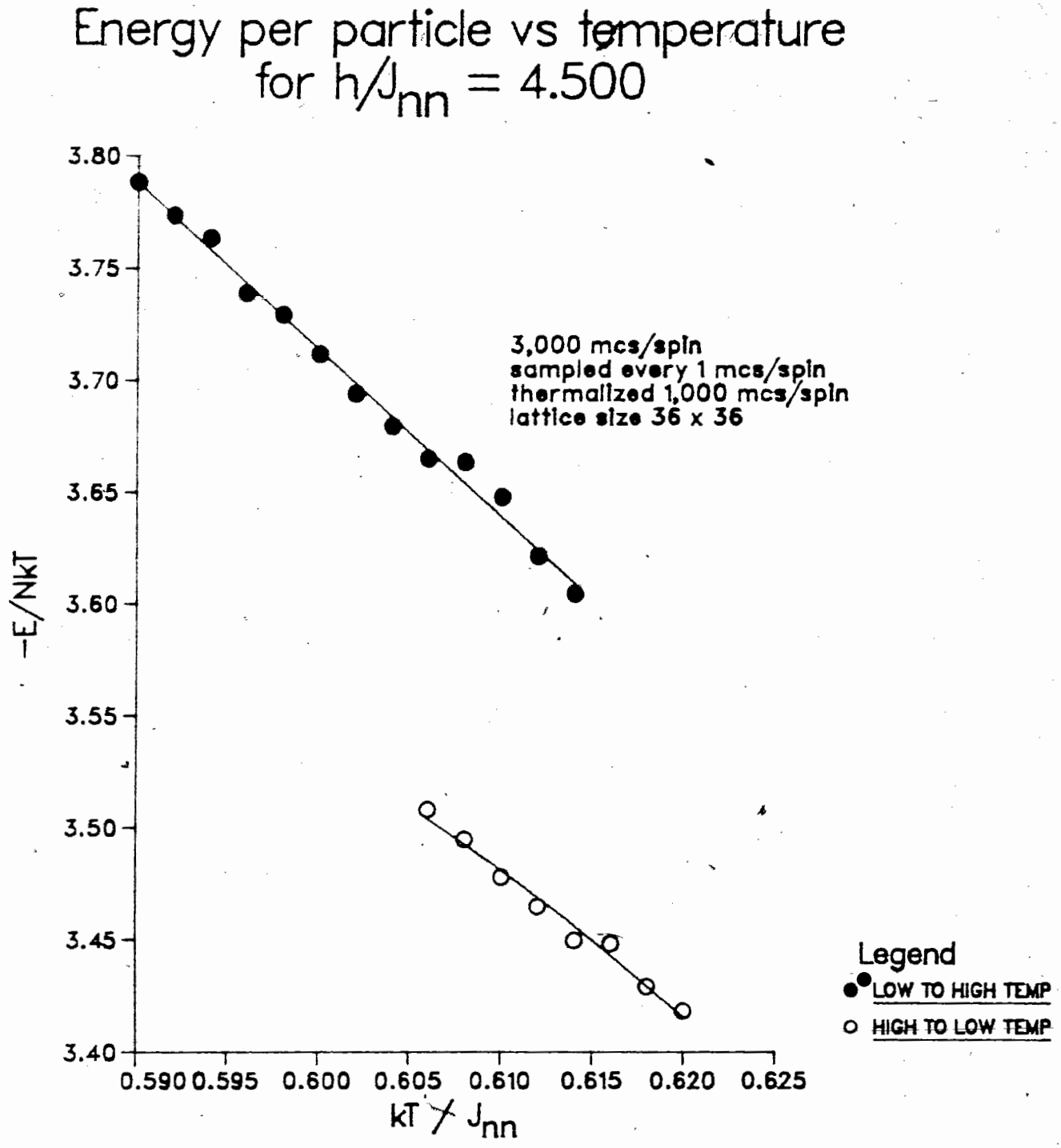
Energy per particle vs temperature
for h/J_nn = 4.500
3.80
3.75
3.70
3.65
3.60
3.55
3.50
3.45
3.40
-E/NkT
0.590 0.595 0.600 0.605 0.610 0.615 0.620 0.625
kT / J_nn
3,000 mcs/spin
sampled every 1 mcs/spin
thermalized 1,000 mcs/spin
lattice size 36 x 36
Legend
LOW TO HIGH TEMP
HIGH TO LOW TEMP

Figure 4.3.3a

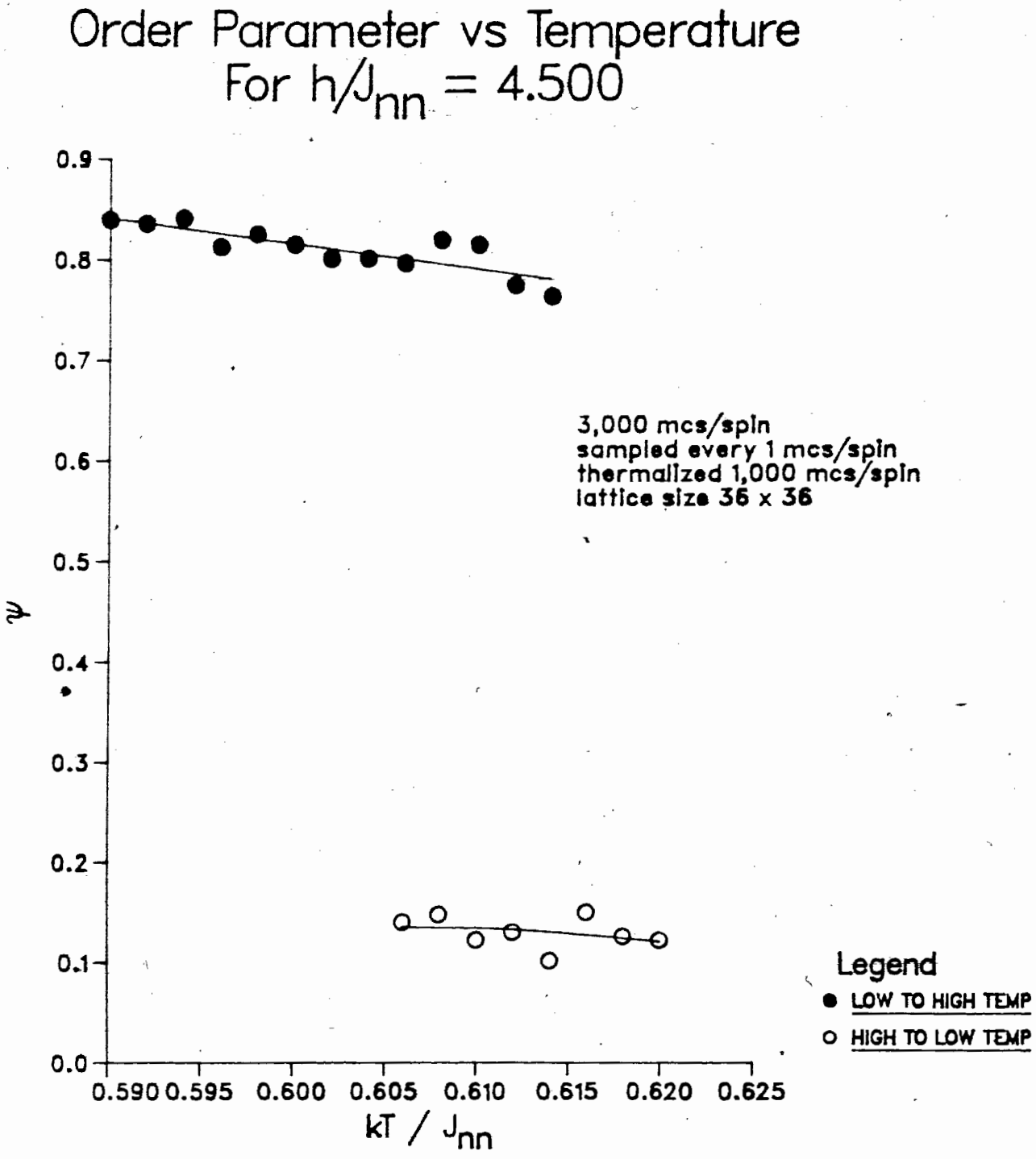
Order Parameter vs Temperature
For h/J_nn = 4.500
3,000 mcs/spin
sampled every 1 mcs/spin
thermalized 1,000 mcs/spin
lattice size 36 x 36
Legend
LOW TO HIGH TEMP
HIGH TO LOW TEMP
ψ
kT / J_nn
0.0
0.1
0.2
0.3
0.4
0.5
0.6
0.7
0.8
0.9
0.590
0.595
0.600
0.605
0.610
0.615
0.620
0.625

Figure 4.3.3b

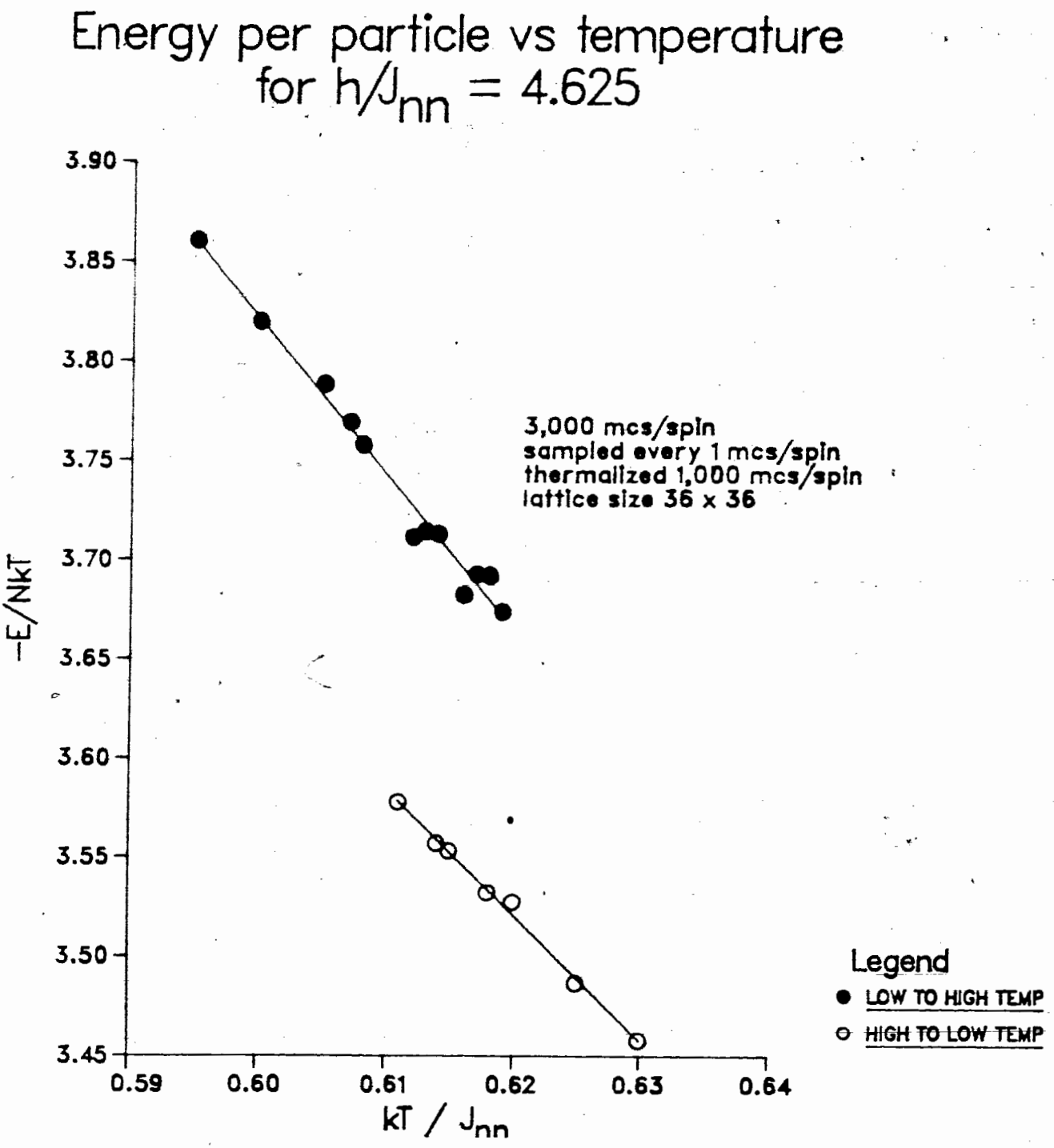
Energy per particle vs temperature
for h/J_nn = 4.625
3.90
3.85
3.80
3.75
3.70
3.65
3.60
3.55
3.50
3.45
-E/NkT
0.59
0.60
0.61
0.62
0.63
0.64
kT / J_nn
3,000 mcs/spin
sampled every 1 mcs/spin
thermalized 1,000 mcs/spin
lattice size 36 x 36
Legend
LOW TO HIGH TEMP
HIGH TO LOW TEMP

Figure 4.3.4a

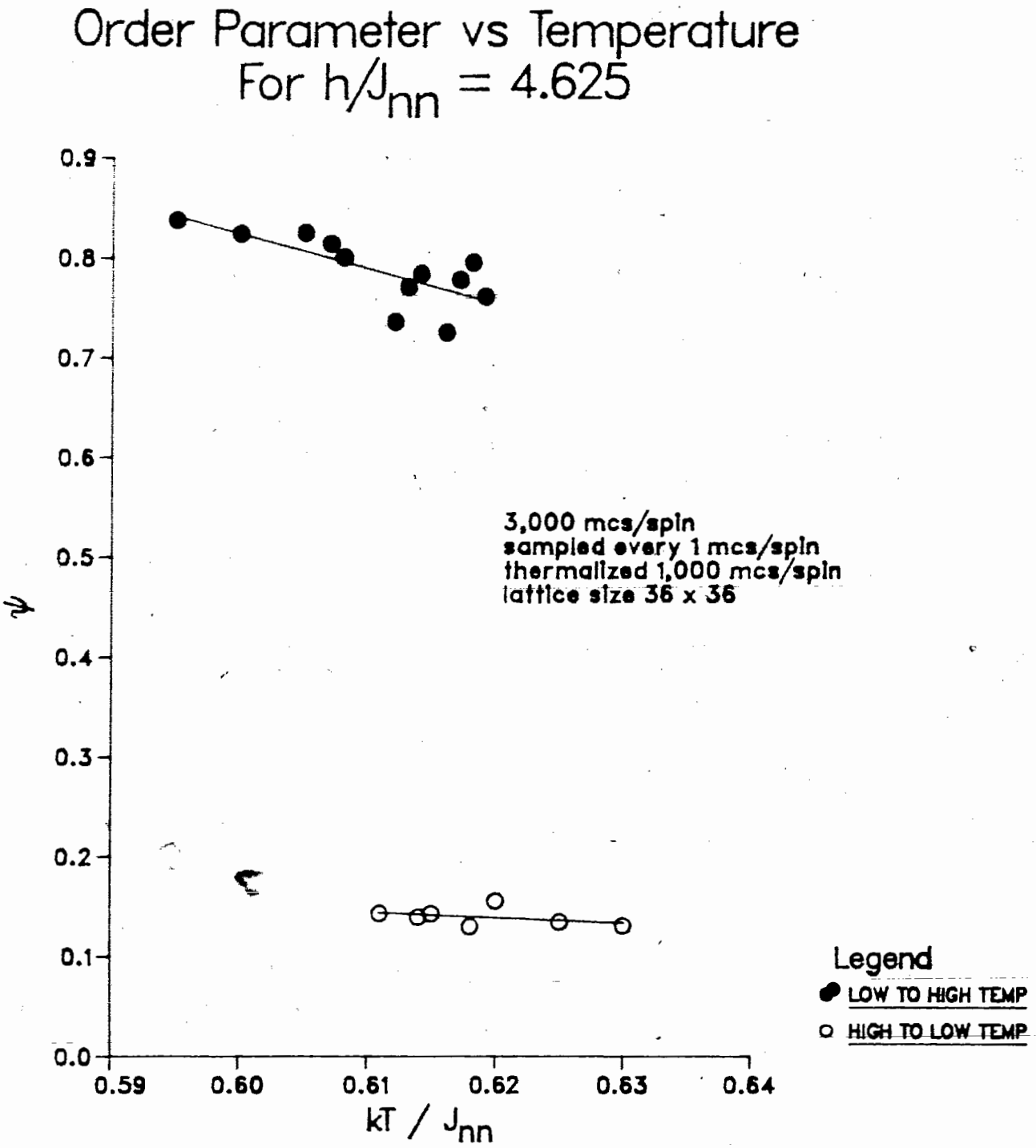
Order Parameter vs Temperature
For h/J_nn = 4.625
0.9
0.8
0.7
0.6
0.5
0.4
0.3
0.2
0.1
0.0
ψ
0.59
0.60
0.61
0.62
0.63
0.64
kT / J_nn
3,000 mcs/spin
sampled every 1 mcs/spin
thermalized 1,000 mcs/spin
lattice size 36 x 36
Legend
LOW TO HIGH TEMP
HIGH TO LOW TEMP

Figure 4.3.4b

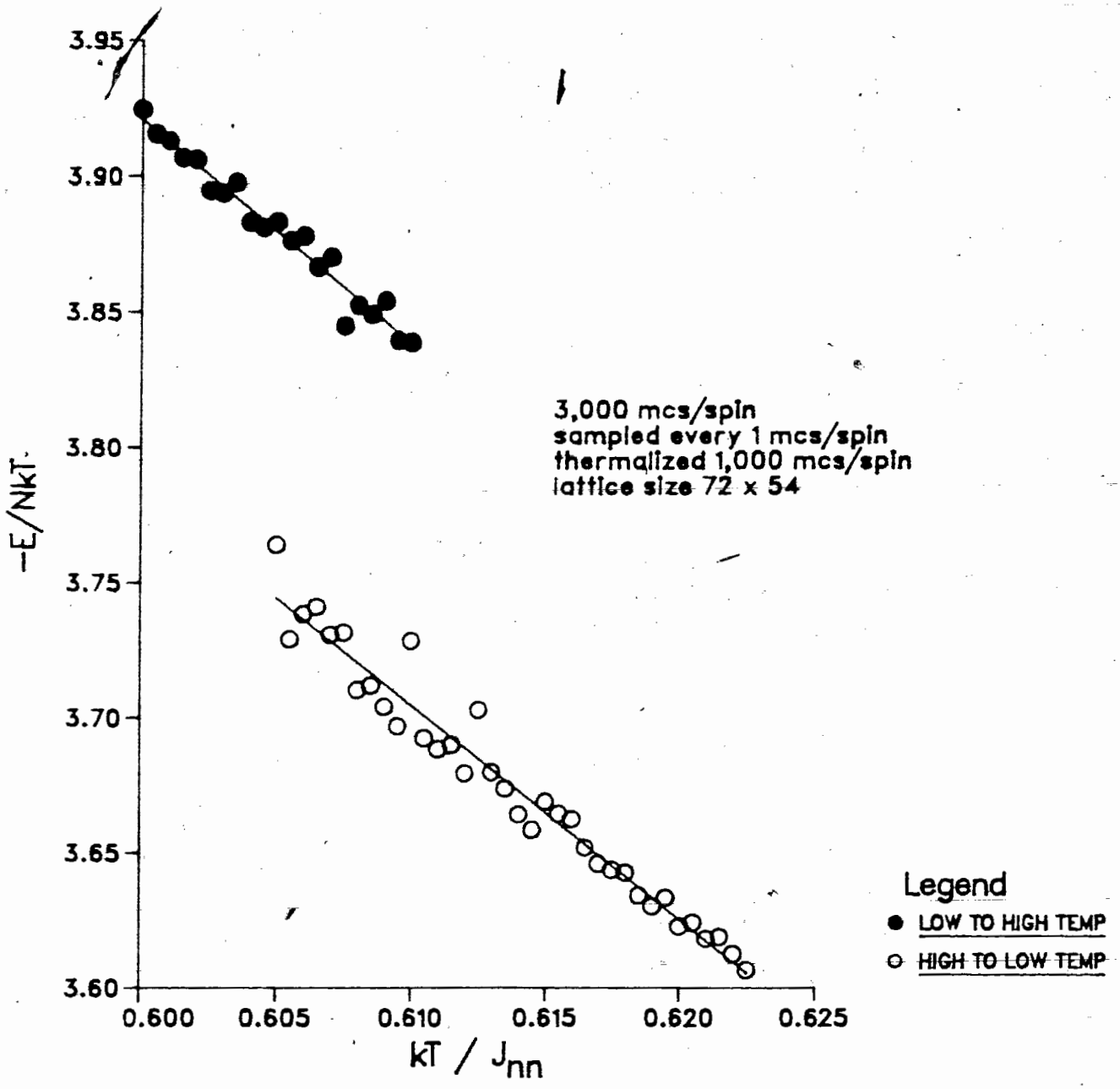
Energy per particle vs temperature
for h/J_nn = 4.750
3.95
3.90
3.85
3.80
3.75
3.70
3.65
3.60
-E/NkT
0.600
0.605
0.610
0.615
0.620
0.625
kT / J_nn
3,000 mcs/spin
sampled every 1 mcs/spin
thermalized 1,000 mcs/spin
lattice size 72 x 54
Legend
LOW TO HIGH TEMP
HIGH TO LOW TEMP

Figure 4.3.5a

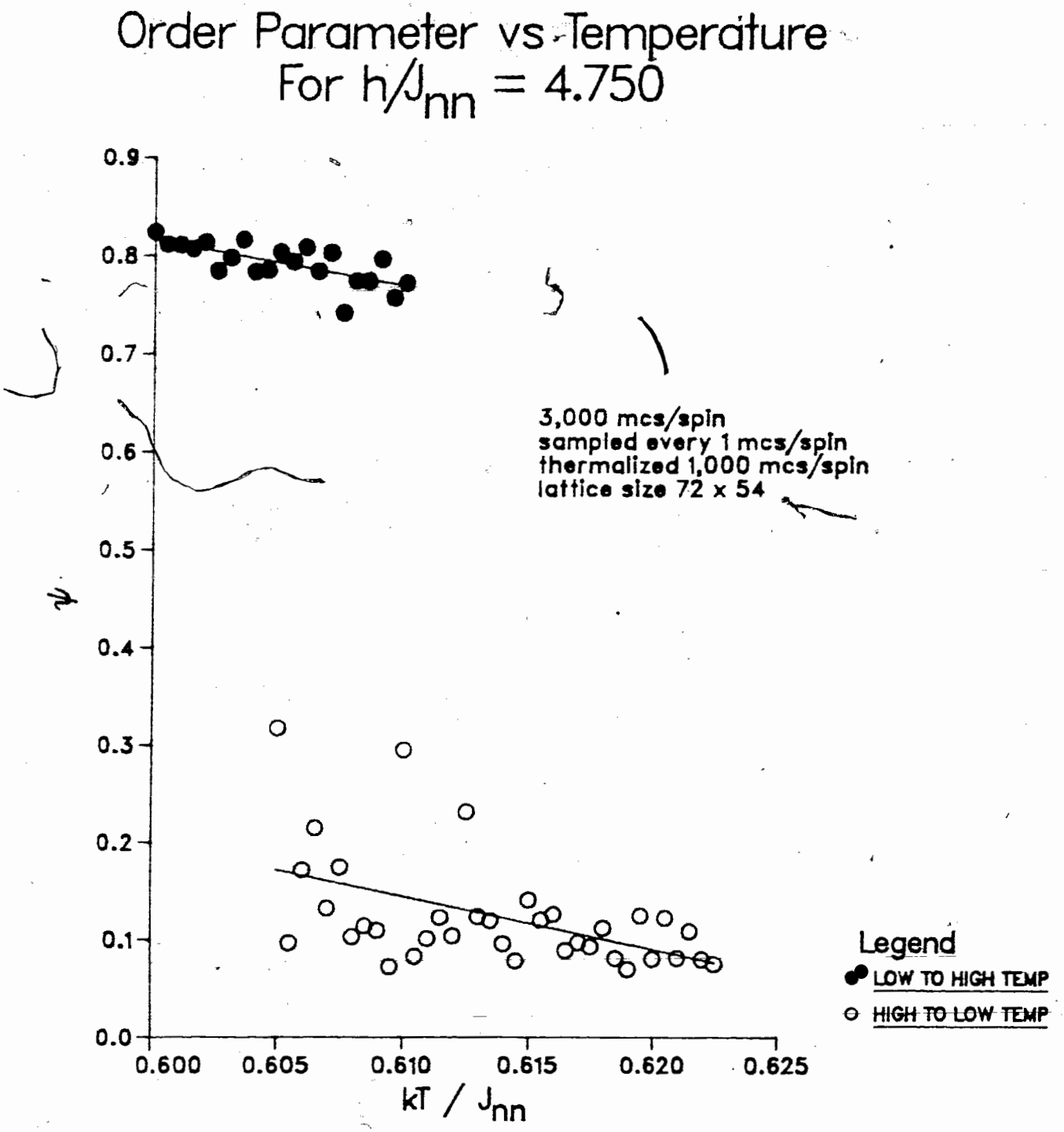
Order Parameter vs Temperature
For h/J_nn = 4.750
3,000 mcs/spin
sampled every 1 mcs/spin
thermalized 1,000 mcs/spin
lattice size 72 x 54
ψ
0.9
0.8
0.7
0.6
0.5
0.4
0.3
0.2
0.1
0.0
0.600
0.605
0.610
0.615
0.620
0.625
kT / J_nn
Legend
LOW TO HIGH TEMP
HIGH TO LOW TEMP

Figure 4.3.5b

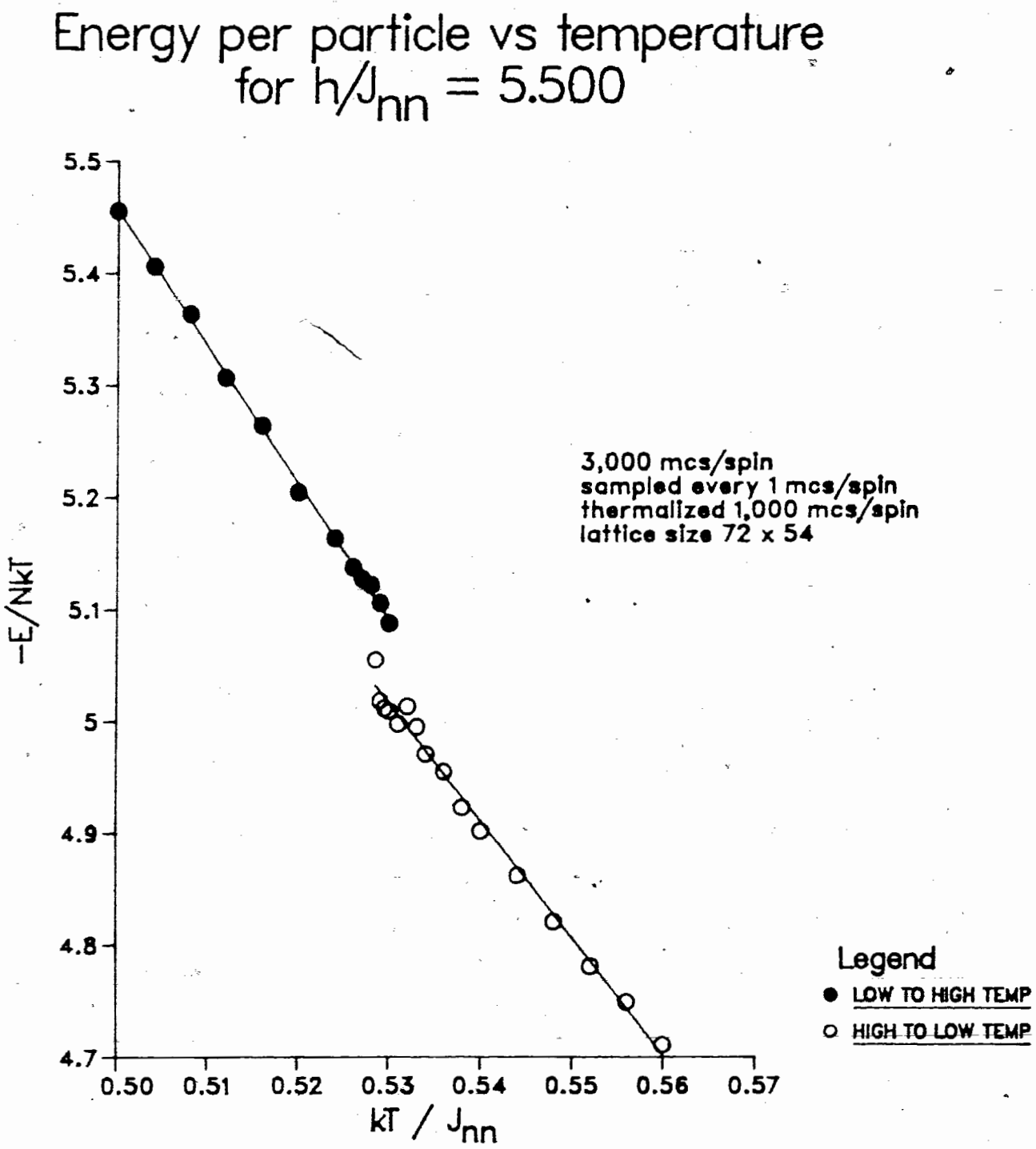
Energy per particle vs temperature
for h/J_nn = 5.500
5.5
5.4
5.3
5.2
5.1
5
4.9
4.8
4.7
-E/NkT
0.50
0.51
0.52
0.53
0.54
0.55
0.56
0.57
kT / J_nn
3,000 mcs/spin
sampled every 1 mcs/spin
thermalized 1,000 mcs/spin
lattice size 72 x 54
Legend
LOW TO HIGH TEMP
HIGH TO LOW TEMP

Figure 4.3.6a

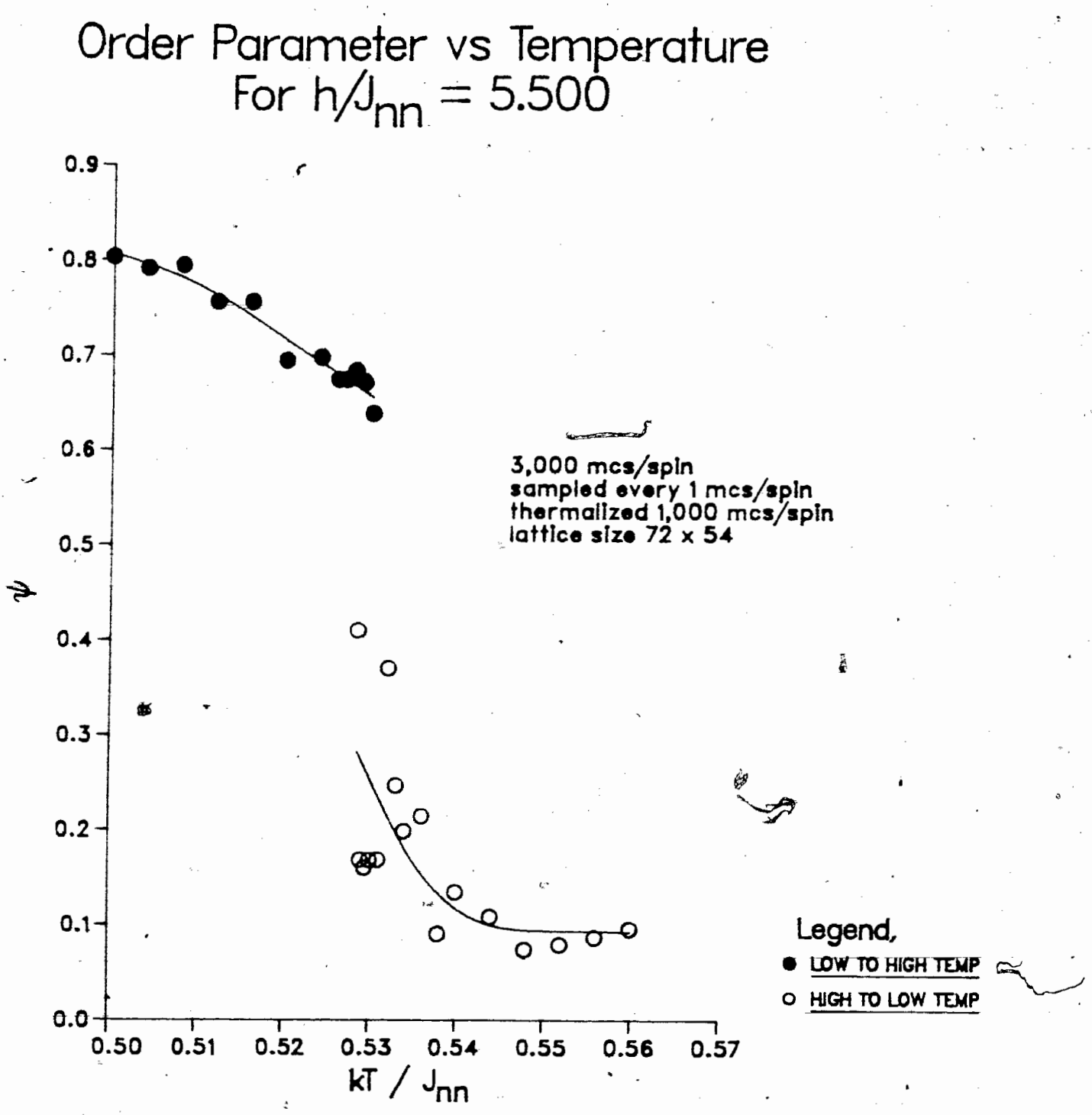
Order Parameter vs Temperature
For h/J_nn = 5.500
0.9
0.8
0.7
0.6
0.5
0.4
0.3
0.2
0.1
0.0
ψ
0.50
0.51
0.52
0.53
0.54
0.55
0.56
0.57
kT / J_nn
3,000 mcs/spin
sampled every 1 mcs/spin
thermalized 1,000 mcs/spin
lattice size 72 x 54
Legend,
LOW TO HIGH TEMP
HIGH TO LOW TEMP

Figure 4.3.6b

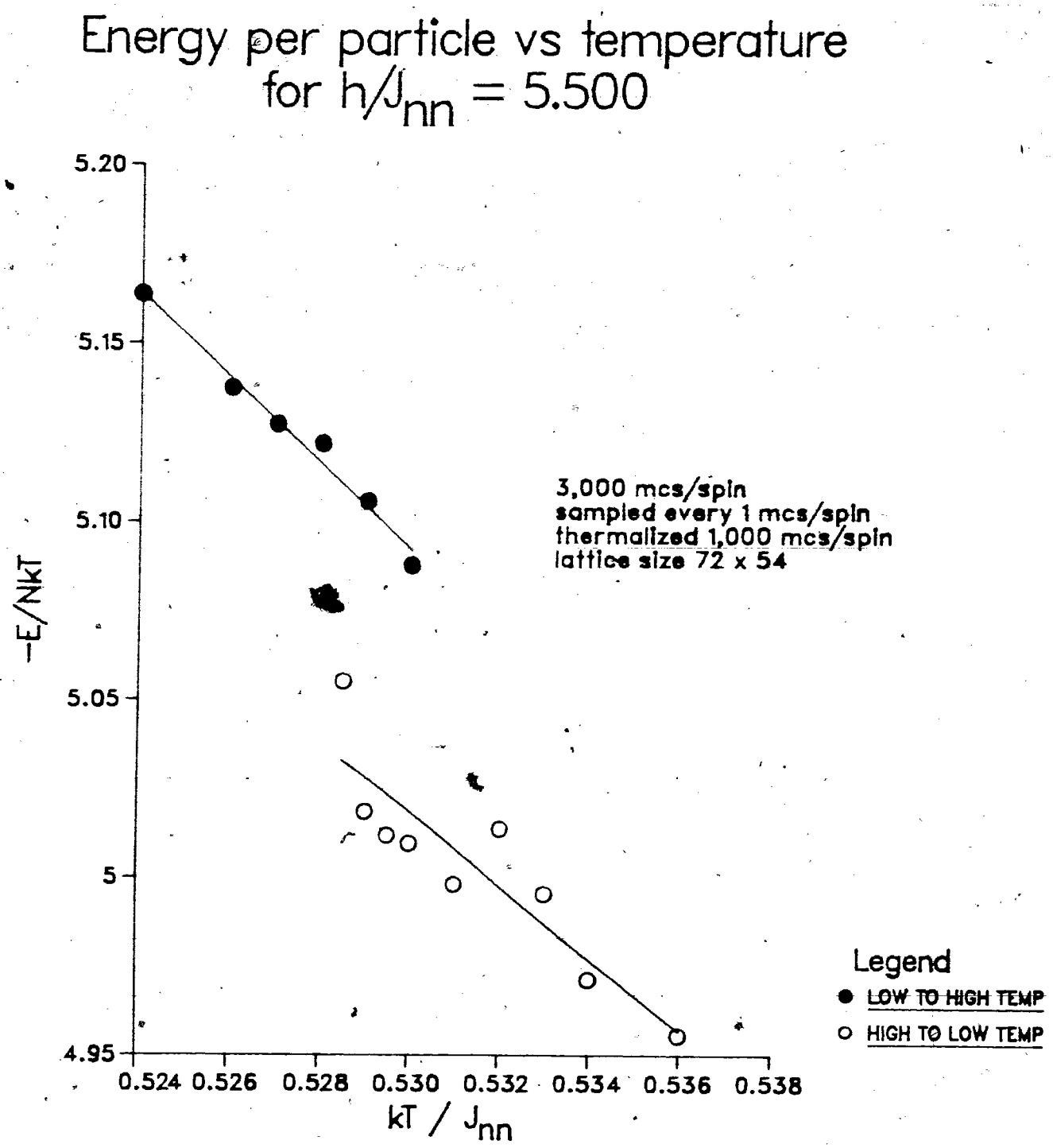
Energy per particle vs temperature
for h/J_nn = 5.500
5.20
5.15
5.10
5.05
5
4.95
-E/NkT
0.524 0.526 0.528 0.530 0.532 0.534 0.536 0.538
kT / J_nn
3,000 mcs/spin
sampled every 1 mcs/spin
thermalized 1,000 mcs/spin
lattice size 72 x 54
Legend
LOW TO HIGH TEMP
HIGH TO LOW TEMP

Figure 4.3.6c

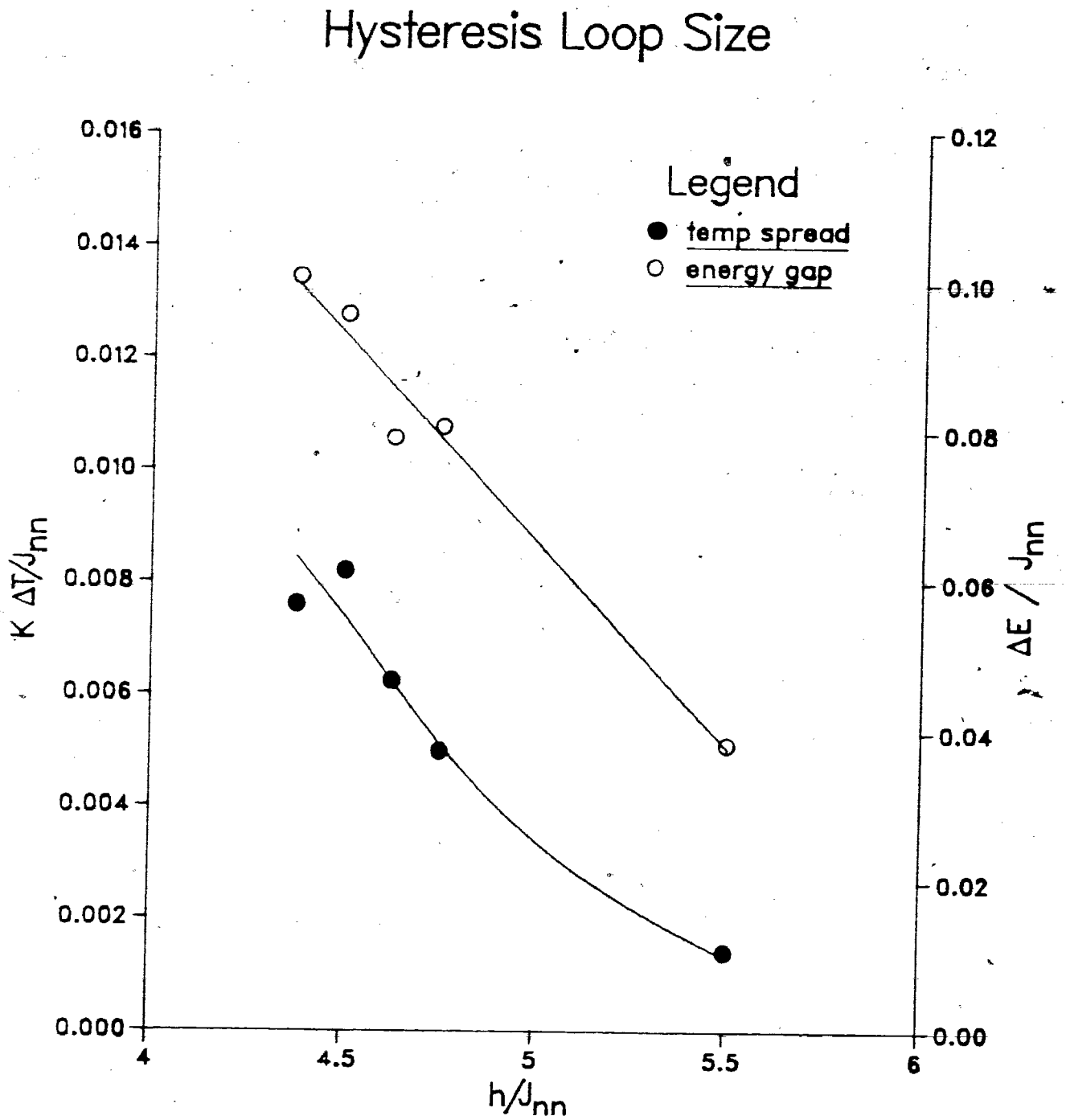
Hysteresis Loop Size
Legend
temp spread
energy gap
K ΔT/Jnn
ΔE / Jnn
h/Jnn
0.016
0.014
0.012
0.010
0.008
0.006
0.004
0.002
0.000
0.12
0.10
0.08
0.06
0.04
0.02
0.00
4
4.5
5
5.5
6

Figure 4.3.7

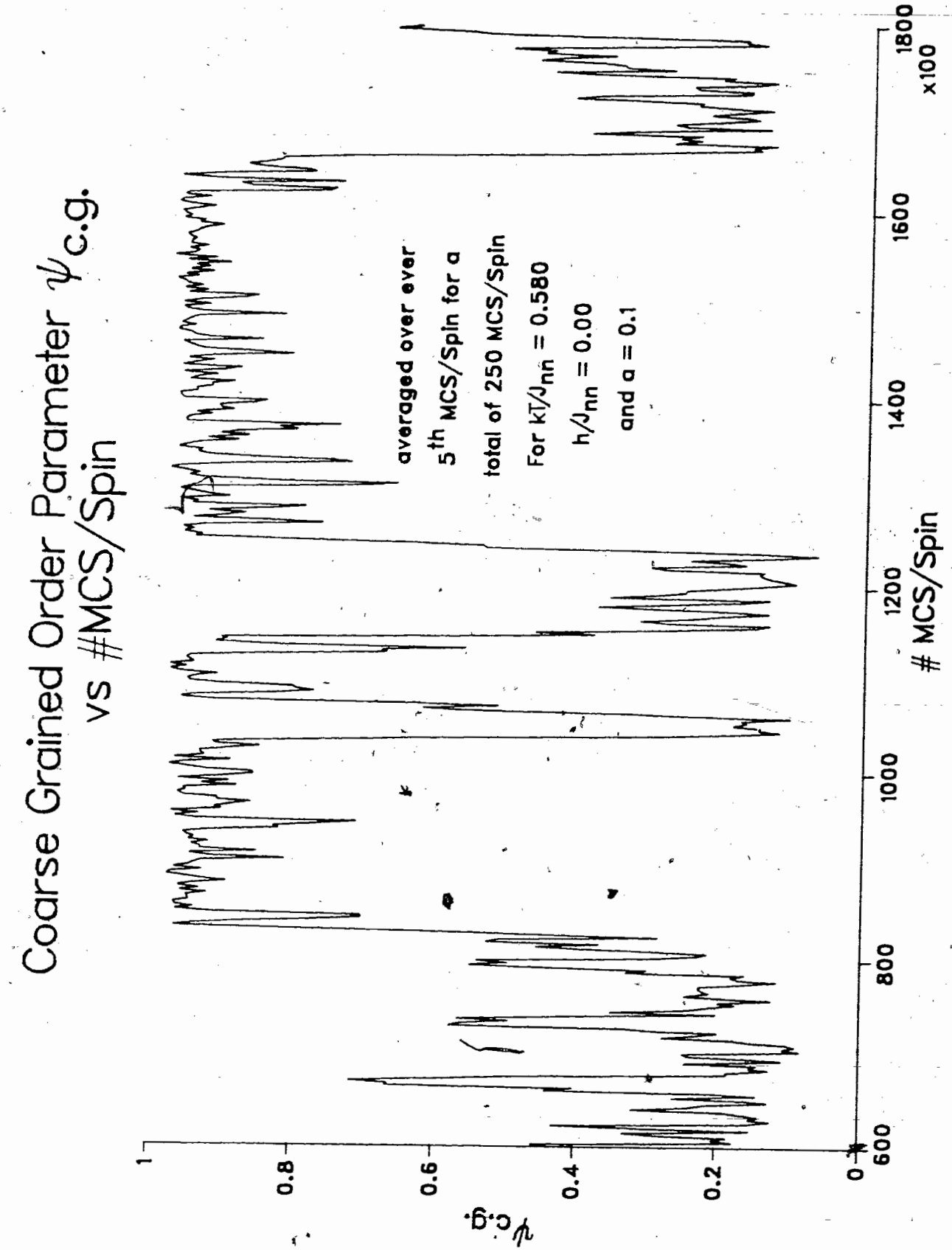
Coarse Grained Order Parameter $\psi_{c.g.}$
vs #MCS/Spin
averaged over ever
5th MCS/Spin for a
total of 250 MCS/Spin
For kT/J_{nn} = 0.580
h/J_{nn} = 0.00
and a = 0.1
$\psi_{c.g.}$
MCS/Spin
x100
0
0.2
0.4
0.6
0.8
1
600
800
1000
1200
1400
1600
1800

Figure 4.3.8

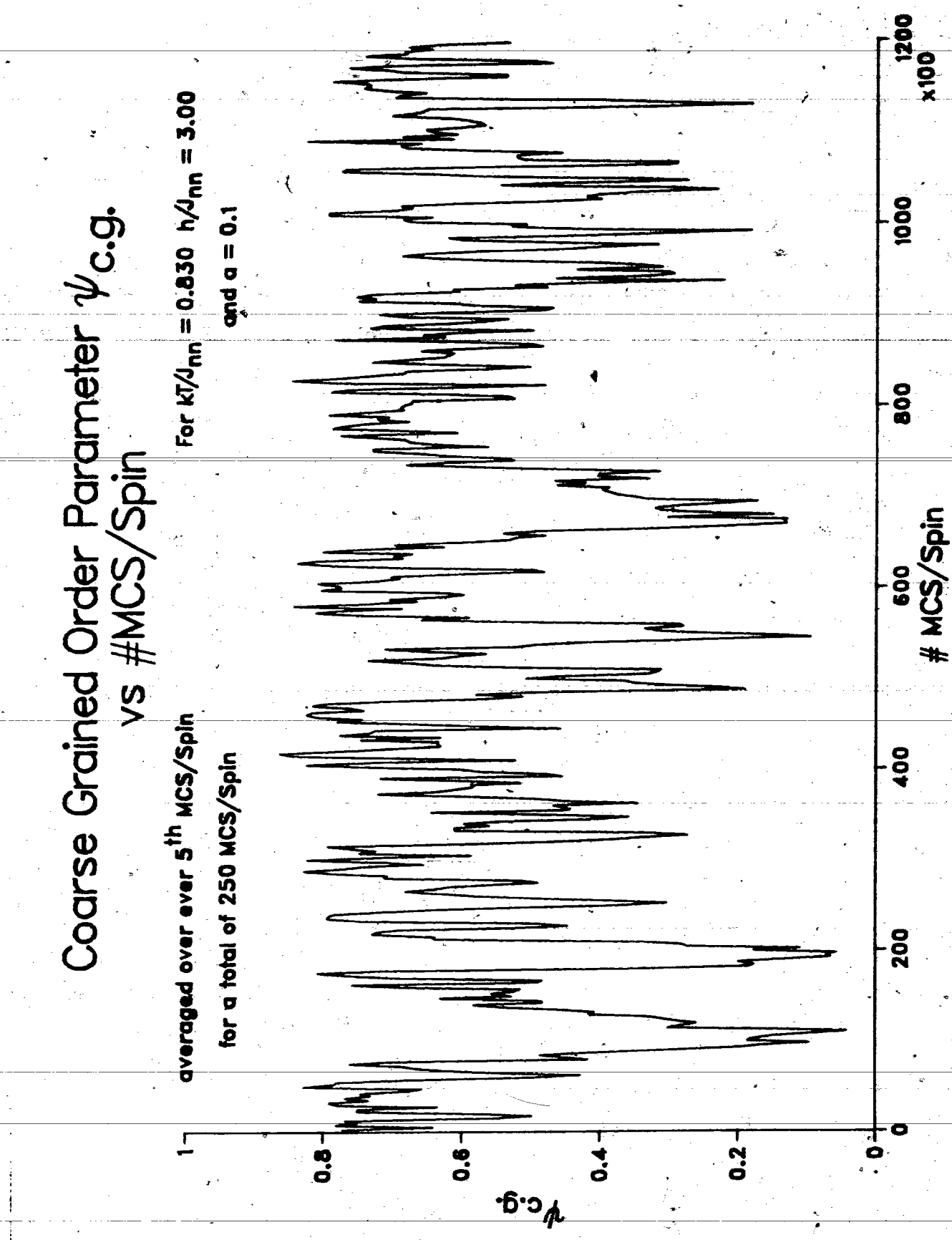
Coarse Grained Order Parameter $\psi_{c.g.}$
vs #MCS/Spin
For kT/J_{nn} = 0.830 h/J_{nn} = 3.00
and a = 0.1
averaged over ever 5th MCS/Spin
for a total of 250 MCS/Spin
$\psi_{c.g.}$
MCS/Spin
x100
0
0.2
0.4
0.6
0.8
1
200
400
600
800
1000
1200

Figure 4.3.9

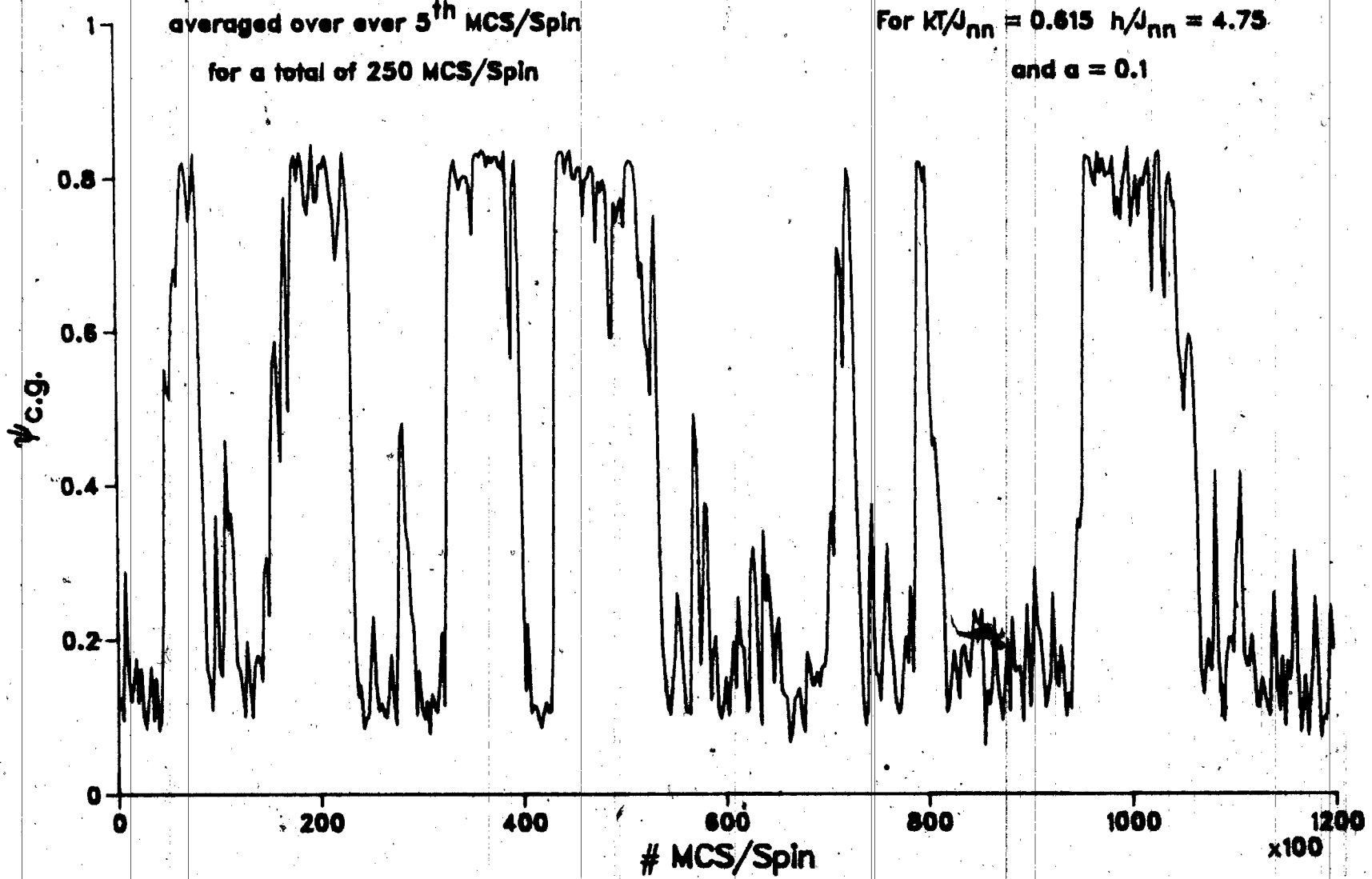
Coarse Grained Order Parameter $\psi_{c.g.}$
vs #MCS/Spin
averaged over ever 5th MCS/Spin
for a total of 250 MCS/Spin
For kT/J_{nn} = 0.615 h/J_{nn} = 4.75
and a = 0.1
$\psi_{c.g.}$
1
0.8
0.6
0.4
0.2
0
0
200
400
600
800
1000
1200
x100
MCS/Spin

Figure 4.3.10

4.4. Critical Exponents

Monte Carlo renormalization group calculation of critical exponents were performed for points on each of the three order to disorder transition boundaries. We will first discuss the calculation made at the maximum of the 2×1 boundary ($h/J_{nn}=0$). Then we will continue with a discussion of the results of the calculation near the maximum of the $\sqrt{3}\times\sqrt{3}$ boundary ($h/J_{nn}=3.00$). Finally we present an extensive discussion of the critical exponent calculations carried out at three different points on the 2×2 boundary ($h/J_{nn}=4.75$, 5.5, and 6.0). Typically all runs were allowed to thermalize for 20,000 MCS/spin before sampling every 5 MCS/spin along runs of various lengths that ranged from 60,000 MCS/spin to 1,800,0000 MCS/spin.

Although the 60,000 MCS/spin runs are too short to yield well converged values of the exponents do they allow one to observe trends in the results. The run of 1,800,000 MCS/spin is far longer than runs typically carried out by other workers and serves as a check on the results obtained from the shorter runs. We now discuss the specific calculations.

For the calculation on the 2×1 and 2×2 boundaries, we used the blocking scheme of figure 3.2 and kept four coupling constants, i.e. four correlation functions. These were; the single spin term •, the nearest neighbour spin-spin term •—•, the next nearest neighbour spin-spin term •—•—• and the nearest neighbour four spin term .

For the 2×1 boundary we do not present the exponents but only some qualitative observations. For both lattices used (24×18, $kT_c/J_{nn}=0.585$ and 36×54 $kT_c/J_{nn}=0.578$) we found that the exponents did not seem to converge or tend to any fixed point values.

The results of the calculation on the $\sqrt{3}\times\sqrt{3}$ boundary are summarized in Table 4.4.1. In this calculation we used the blocking scheme of figure 3.2 with four coupling terms. They were; the single spin term • , the nearest neighbour spin-spin term •—• , the next nearest neighbour spin-spin term •—•—•, and the nearest neighbour three spin term  . It

was found that the single spin and nearest neighbour spin-spin term were most important. The addition of the next nearest neighbour couplings produced a change of about 15% in exponents determined from the first set coupling constants.

The discrepancy decreased with successive iterations of the renormalization transformation. When the nearest neighbour three spin term was added changes of about 2-3% resulted in the first two iterations, but again the differences decreased with successive iterations. Additional terms were added (i.e. longer range spin-spin, longer range three spin, and nearest neighbour four spin) but all produced changes of less than 1%.

Table 4.4.1

Critical Exponents of $\sqrt{3}\times\sqrt{3}$ Order to Disorder Transition Boundary at h/J_{nn}=3.00			
Lattice Size		32×48	64×96
T_c		0.824	0.822
Iteration #	1	1.9195± 0.0004	1.9215± 0.0008
	2	1.893 ± 0.001	1.898 ± 0.002
y_1^e	3	1.876 ± 0.003	1.888 ± 0.002
	4	1.864 ± 0.007	1.877 ± 0.004
	5		1.86 ± 0.01
Conjectured Value	1.86666		
Iteration #	1	1.183 ± 0.003	1.190 ± 0.006
	2	1.339 ± 0.003	1.332 ± 0.006
y_1^s	3	1.268 ± 0.004	1.23 ± 0.01
	4	1.32 ± 0.02	1.13 ± 0.02
	5		Not Converged
Conjectured Value	1.200		
Iteration #	1	-1.93 ± 0.04	-2.02 ± 0.03
	2	-0.009 ± 0.03	-0.04 ± 0.02
y_2^s	3	-0.169 ± 0.005	-0.02 ± 0.02
	4	-0.00 ± 0.06	-0.02 Large
	5		Not Converged
Length of Run		180,000 MCS/spin	60,000 MCS/spin

From Table 4.4.1 we see that the largest odd exponent y_1^o seems to be converging slowly to its conjectured value of 28/15 . The slow convergence is consistent with the existence of a marginal direction indicated by y_2^o being nearly zero. A near marginal operator inhibits flow to the fixed point. Therefore, convergence of the exponents to their fixed point value is not a useful criterion for determination of the transition temperature in this model. We found that the flow of the near neighbour three spin correlation function was the most sensitive signal of T_c. The largest even exponent y_1^e seems to be also converging to its conjectured value of 1.2. The discrepancy between the calculated exponent and the conjectured value is much greater for y_1^e than for y_1^o.

The above conclusions would be made more convincing with increased running time for the 64×96 lattice. Also, one might try to find a parameter that couples strongly to the marginal direction, as Swendsen et al. [60] did with the four state Potts model. By varying this parameter one might be able to minimize the effects of the marginal direction. Our results for the direction of the flows are not sufficiently unambiguous to allow us to identify the appropriate interaction.

We now begin the discussion of the 2×2 boundary by examining the critical exponent for the point on the boundary at h/J_{nn}=5.5. The results for three different lattice sizes are given in table 4.4.2b. The general feature to notice is that the largest odd exponent y_1^o is not iterating towards its conjectured value of 1.875 but to some larger value (i.e. $y_1^o > 1.92$). At this point we conjecture that it is flowing towards a first order fixed point commonly called a discontinuity fixed point (i.e. $y_1^o = 2$)[19,41]. This conjecture is supported by the calculation at h/J_{nn}=4.75 on the 2×2 phase boundary which is summarized in Table 4.2.2a. This calculation was carried out only for a relatively small lattice (24×18) and should be compared with the corresponding column in Table 4.4.2b. The interesting feature is that y_1^o is substantially larger than for h/J_{nn}=5.5 but has the same general behaviour. It first iterates away from y_1^o =2 and then turns around to head towards it. It appears that by

Table 4.4.2a

Critical Exponents of 2×2 Order to Disorder Transition Boundary at h/J_{nn}=4.75		
Lattice Size		24×18
T_c		0.591
Iteration #	1	1.9716 ± 0.0001
y_1^t	2	1.9697 ± 0.0003
	3	1.9846 ± 0.0007
Conjectured Value	1.8750	
Iteration #	1	1.78 ± 0.01
y_1^t	2	1.52 ± 0.04
	3	1.56 ± 0.03
Conjectured Value	1.50	
Iteration #	1	-3.59 ± 0.08
y_2^t	2	-0.08 ± 0.03
	3	-0.03 ± 0.02
Conjectured Value	0.000	
Length of Run		855,000 MCS/spin

varying the field we in some sense move closer to the first order fixed point. The above results should be contrasted with the results of the calculation made on the boundary at h/J_{nn}=6.0 which are presented in Table 4.4.2c. Notice now that y_1^t seems to be converging to the conjectured value of 1.875 though it drops slightly on the last iteration. We believe that this drop is due to the fact that kT/J_{nn}=0.385 is slightly larger than the appropriate T_c. Finite size effects may also play a role. When the calculation was carried out on a smaller lattice we obtained basically the same results. The values of y_1^t are not very close to the conjectured value of 1.5 but do seem to iterate toward this value. Other workers have also been unable to determine y_1^t accurately [30,37,44,61].

In summary, we conclude that the 2×2 order-disorder transition for $h \leq 5.5$ is governed by a first-order fixed point and for $h \geq 6.0$ by a second order fixed point. This second order fixed point appears to be the same fixed point which governs the four state

Table 4.4.2b

Critical Exponents of 2×2 Order to Disorder Transition Boundary at h/J_{nn}=6.5				
Lattice Size		24×18	36×54	72×54
T_c		0.520	0.525	0.525
Iteration #	1	1.92459± 0.00002	1.916 ± 0.002	1.9134± 0.0001
	2	1.91840± 0.00006	1.907 ± 0.003	1.9033± 0.0003
y_1^f	3	1.93749± 0.00007	1.923 ± 0.003	1.913 ± 0.001
	4		1.930 ± 0.007	1.917 ± 0.001
Conjectured Value	1.8750			
Iteration #	1	1.379 ± 0.004	1.317 ± 0.005	1.334 ± 0.004
	2	1.31 ± 0.02	1.32 ± 0.02	1.27 ± 0.01
y_1^f	3	1.389 ± 0.008	1.42 ± 0.01	1.41 ± 0.02
	4		Not Converged	1.43 ± 0.07
Conjectured Value	1.50			
Iteration #	1	-5.49 ± 0.04	-4.94 ± 0.02	-5.5 ± 0.2
	2	-0.33 ± 0.06	-0.16 ± 0.01	-0.62 ± 0.02
y_2^f	3	-0.02 ± 0.06	0.10 ± 0.01	-0.253 ± 0.06
	4		Not Converged	-0.61 Large
Conjectured Value	0.000			
Length of Run		1,800,000 MCS/spin	60,000 MCS/spin	205,000 MCS/spin

Table 4.4.2c

Critical Exponents of 2×2 Order to Disorder Transition Boundary at h/J_{nn}=6.00		
Lattice Size		36×54
T_c		0.385
Iteration #	1	1.8728 ± 0.0002
	2	1.8757 ± 0.0005
y_t'	3	1.8767 ± 0.002
	4	1.8653 ± 0.002
Conjectured Value	1.8750	
Iteration #	1	1.059 ± 0.004
	2	1.16 ± 0.01
y_t'	3	1.22 ± 0.02
	4	1.09 ± 0.03
Conjectured Value	1.50	
Length of Run		200,000 MCS/spin

Potts and Baxter-Wu Models. From the above we expect a tricritical or multicritical point between h/J_{nn}=5.5 and h/J_{nn}=6.0 on the 2×2 boundary at which the transition crosses over from first order to second order. These conclusions are consistent with those obtained from the free energy functional, hysteresis and time series calculations reported in sections 4.2 and 4.3.

CHAPTER 5

Conclusions

In this section we wish to summarize the results for each portion of the phase diagram and compare with previous work. Also, possible additional work will be outlined.

The 2×1 order $\rightarrow$ disorder transition was found to be first order for the entire range of field h for which the 2×1 phase is stable. This is consistent with the work of Nienhuis et al. [40] who suggested that such a transition will always be fluctuation induced first order [25]. It also appeared that the transition temperature was depressed to zero as $h/J_{nn} \rightarrow 12s=1.2$. This point will be discussed later.

The $\sqrt{3}\times\sqrt{3}$ order $\rightarrow$ disorder transition was found to be continuous over its entire boundary, in agreement with the work of Schick et al. [51]. Schicks' work predicts that this model is in the same universality class as the three-state Potts and Baxter's hard hexagon models, for which the leading odd exponent $y_1^f = 28/15 \approx 1.867$ and leading even exponent $y_1^f = 6/5 = 1.2$ [2]. From the MCRG calculation on this model we found a y_1^f which agreed extremely well with the conjectured value (28/15). A y_1^f was also found a that that was within 5% of its conjectured value (6/5). The exponent y_1^f seemed not to have converged completely to its fixed point value. The slow convergence might be due to a marginal direction indicated by $y_2^f \approx 0$. Like the $2\times1\rightarrow$ disorder transition, this transition is also depressed to zero as $h/J_{nn} \rightarrow 12s=1.2$.

The $2\times2 \rightarrow$ disorder transition appeared to have a crossover from discontinuous to continuous as the field (h) was increased. The crossover took place between $h\approx5.5$ and $h\approx6.0$, indicating the existence of a multicritical point in this range. In the region $4.28 \leq h \leq 5.5$ the leading odd exponent y_1^f seemed to flow to a discontinuity value of 2. The value of y_1^f had not converged to its fixed point value. In the region where the

transition appeared to be continuous y_1^t iterated towards its conjectured four-state Potts value of 1.875, but y_1^t was quite far from its corresponding value of 1.5 [3]. This could be caused by the marginal direction associated with this universality class which has hampered similar calculations on the four-state Potts model [48].

We also see that there exists a finite temperature transition between the $\sqrt{3}\times\sqrt{3}$ and 2×2 phases, which is first order as expected. This transition boundary, as well the boundaries for the $\sqrt{3}\times\sqrt{3}$ and 2×2 order to disorder transitions all terminate on a common point at $kT/J_{nn}=0.513$ and $h/J_{nn}=4.28$, which appears to be a critical end point.

The last feature of the phase diagram to be discussed is the absence of a transition between the 2×1 and the $\sqrt{3}\times\sqrt{3}$ phases. From the Monte Carlo data it appears that transition temperatures for both phases are depressed to zero as $h/J_{nn}\rightarrow1.2$. we conjecture that the paramagnetic phase is stable down to $T=0$ at this field value; however, there is the possibility that the paramagnetic phase might give way to a sequence of modulated phases [21,54] as the temperature is decreased. The presence of such phases is hard to detect by Monte Carlo methods.

Additional work which may be done includes the following:

1) an analytic analysis of the nature of the phase diagram in the neighbourhood of the point $T=0$ and $h/J_{nn}=12a$.

2) accurate location of the crossover point on the 2×2 boundary as well as determination of its exact nature.

3) introduction of vacancy-like fields [40,42] to improve convergence of exponents on the continuous portion of the 2×2 phase boundary.

4) investigate the finite size scaling of the local Landau-like free energy and its usefulness in determining the order of a transition.

APPENDIX A

Degeneracy of Ground State at $|h|/J_{nn}=12a$

Within this appendix we wish to consider the nature of the phase diagram of the Hamiltonian 3.1 in the vicinity of the point $T=0$ and $h/J_{nn}=12a$. From the Monte Carlo calculation it appeared that no direct transition exists between the 2×1 and $\sqrt{3}\times\sqrt{3}$ at finite temperature. We were unable to demonstrate this rigorously. We did however, find a set of transformations that involved flipping columns of spins that cost no energy at $T=0$ and $h/J_{nn}=12a$. These transformations were sufficient to show that the surface tension between the various ordered states vanishes at this point, suggesting that the 2×1 and $\sqrt{3}\times\sqrt{3}$ are unstable for $T>0$ at $h/J_{nn}=12a$. If this is the case, there is no direct transition between these two phases.

To begin this discussion, recall from section 1.2 that the 2×1 and the $\sqrt{3}\times\sqrt{3}$ phases are degenerate at $|h|/J_n=12a$, however the degeneracy is greater that just this. To see the degeneracy of the ground state consider the Hamiltonian defined on a $2m\times\infty$ lattice with periodic boundary conditions in the m direction (i.e. $m+1^{th}$ row is the same as the 1^{st} row). In figure A2 the system is shown in a pure $\sqrt{3}\times\sqrt{3}$ phase. On this drawing notice the shaded triangles each containing three spins. Imagine that the triangles which point up extend infinitely to the right and the ones which point down extend infinitely to the left. Notice, only triangles in a given column will interact with each other since our model is restricted to 1^{st} and 2^{nd} neighbour interactions between spins.

It will be of some interest to consider the interaction that spins of a given triangle have with their neighbouring spins. To facilitate this we have shown in figure A1 the bonds that these spins make with their neighbours. The bonds have been categorized into three types (a,b and c). The a type bonds are between spins of a given triangle and their

first and second neighbour that are also in a triangle. The b type bonds are between spins of the given triangle and their first neighbour not in any triangle.

The c type bonds are between the spins of the given and their second neighbours that are also not in any triangle.

Now consider the energy change if the spins of a given column of triangles are all flipped. It is clear that the energy of the a type bonds are unchanged.

The net energy change of the b type is also unchanged because there are the same number of favourable and unfavourable b type bonds. The change of the c type bonds produce a decrease of energy of $2\times3\times4mJ_2$. The only remaining contribution to the energy change is due to the field which produces a increase of the energy of $2\times mh$. Hence the total energy change is;

$$\Delta E=2m(h-12J_{nn})$$

but $h/J_{nn}=12$, therefore $\Delta E=0$.

In summary there is no energy cost to flip a column of triangles. In fact all orientations of these columns are degenerate with each other since there is no interaction between them.

Now consider the configuration produced if all columns of upward pointing triangles of figure A2 are flipped. The result is shown in figure A3. Notice the right hand side of the lattice is now in a pure 2×1 phase and the left and side is in a pure $\sqrt{3}\times\sqrt{3}$ phase. Since this configuration was produced by a series of zero energy flips of columns, this coexisting state will be degenerate with the pure $\sqrt{3}\times\sqrt{3}$ or the pure 2×1 phase.

Now flip all the remaining downward pointing triangles. The result is shown in figure A4 This is a coexisting state between a two different 2×1 phases. By construction, it too must be degenerate with both the pure 2×1 and $\sqrt{3}\times\sqrt{3}$ phases by the same reasoning as above.

Now we wish to construct a coexisting state between two different $\sqrt{3}\times\sqrt{3}$ phase. Begin with a system in a pure 2×1 phase as shown in figure A5. Then flip all triangles (they extend infinitely to the right and left). The result is shown in figure A6 and is a state of coexistence between two different $\sqrt{3}\times\sqrt{3}$ phases. Since only flipping of the the special columns was involved in going from the 2×1 to this coexistence state, the state must be degenerate with the pure 2×1 phases and hence the pure $\sqrt{3}\times\sqrt{3}$ phase.

We conclude this discussion of the degeneracy by summarizing the results. We found that the ground state of the pure 2×1, pure $\sqrt{3}\times\sqrt{3}$, coexisting 2×1 and $\sqrt{3}\times\sqrt{3}$ phases, coexisting 2×1 phases, and coexisting $\sqrt{3}\times\sqrt{3}$ phases are all degenerate at $|h|/J_{nn}=12a$.

Now we return to our surface tension discussion. At $T=0$ the only contribution to the free energy comes from the internal energy. Therefore the surface tension at zero temperature is merely the energy difference between a state of coexistence and the pure phases. Thus, from the above discussion we conclude that the surface tensions $\sigma_{2\times1,2\times1}$, $\sigma_{\sqrt{3}\times\sqrt{3},\sqrt{3}\times\sqrt{3}}$, and $\sigma_{\sqrt{3}\times\sqrt{3},2\times1}$ all vanish at $|h|/J_{nn}=12a$ and $T=0$. This is highly suggestive that these surface tensions vanish at finite temperature at this field. If this were true both the 2×1 and $\sqrt{3}\times\sqrt{3}$ phases would be unstable at $|h|/J_{nn}=12a$ for all finite temperatures, from which we could conclude that there does not exist any finite temperature transition between these two phases. The nature of the conjectured intermediate phase is not known. We speculate that it would be paramagnetic to zero temperature. However one might find that for low temperature the paramagnetic phase gives way to a sequence of modulated phases of the form found by Fisher and Selke while investigating the ANNNI model [36].

To clarify the exact nature of the phase diagram in the vicinity of the point $T=0$ and $|h|/J_{nn}=12a$, more work will have to be done. One might try to proceed as Fisher and Selke [21] did with the ANNNI model by constructing a low temperature expansion. This approach, however might be hampered by convergence problem for d=2. A more likely method, might be a domain wall transfer matrix approach [37,44,62].

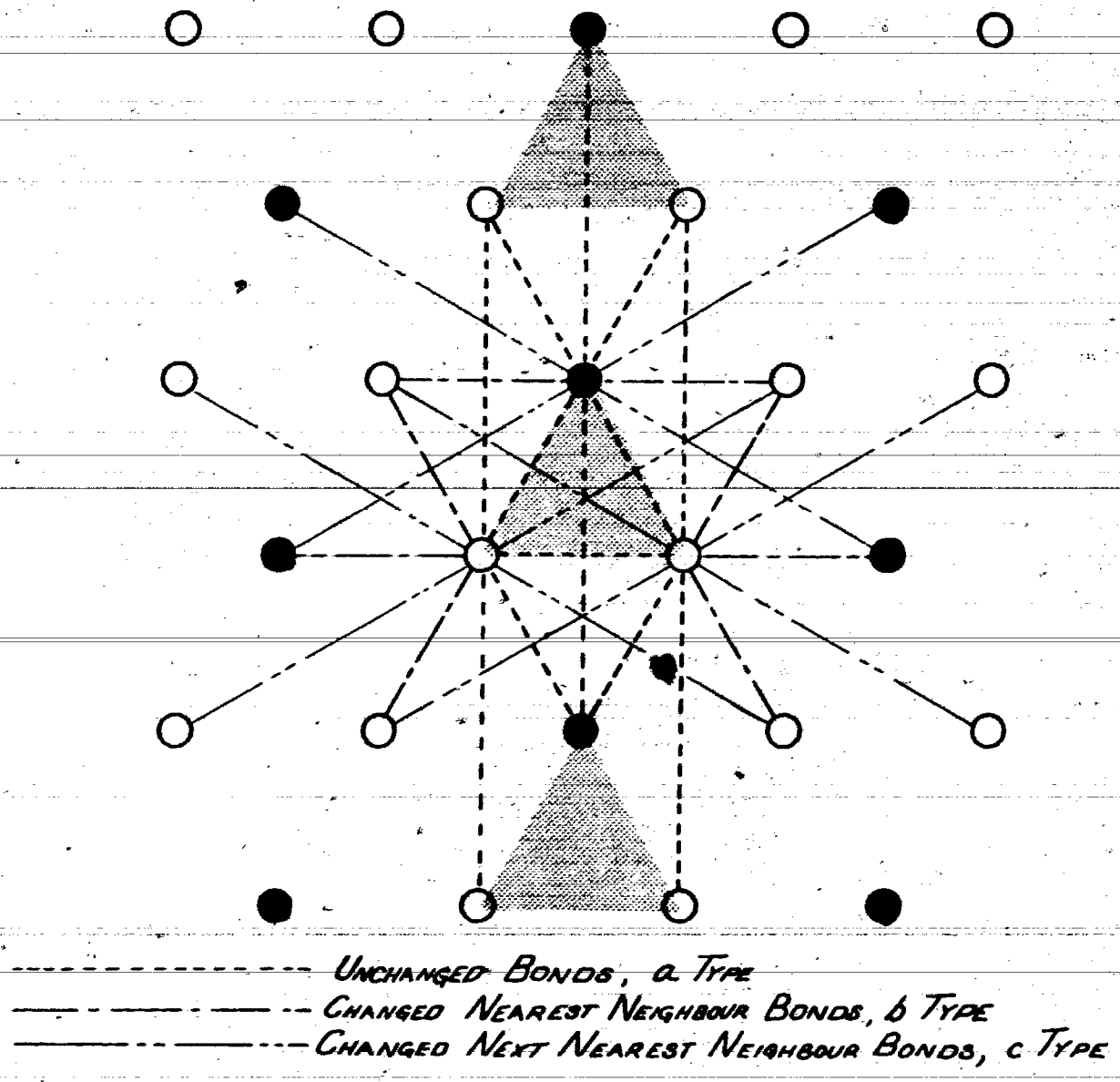

Figure A1

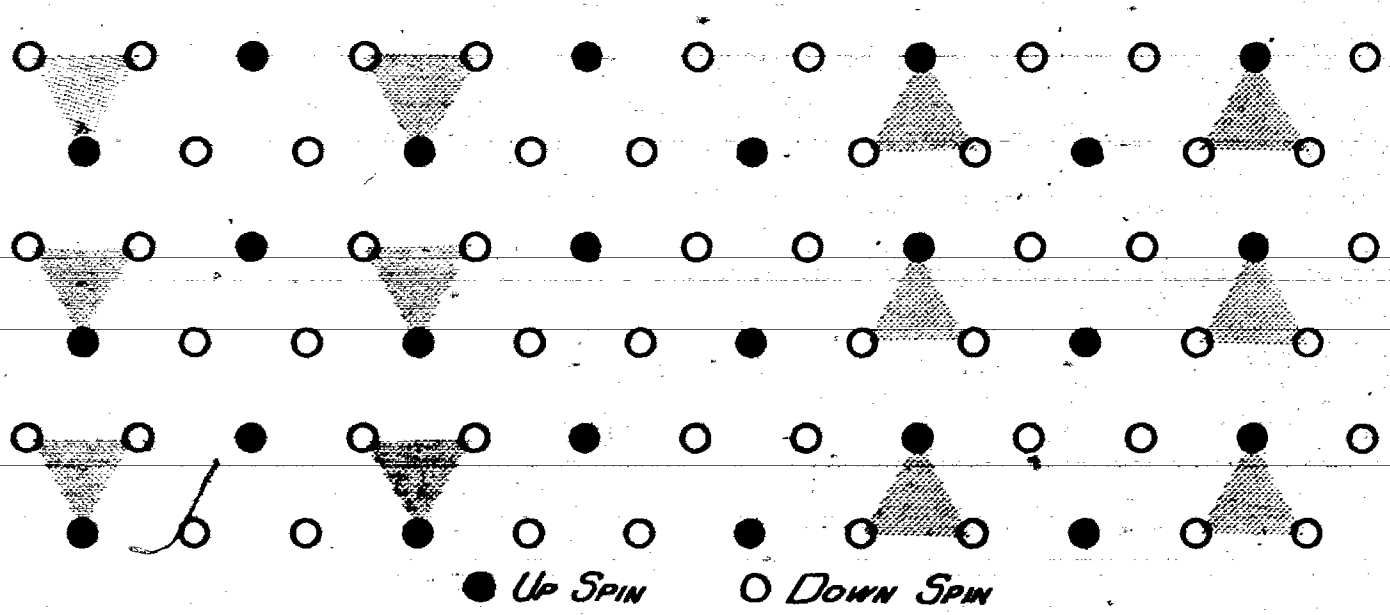

Figure A2

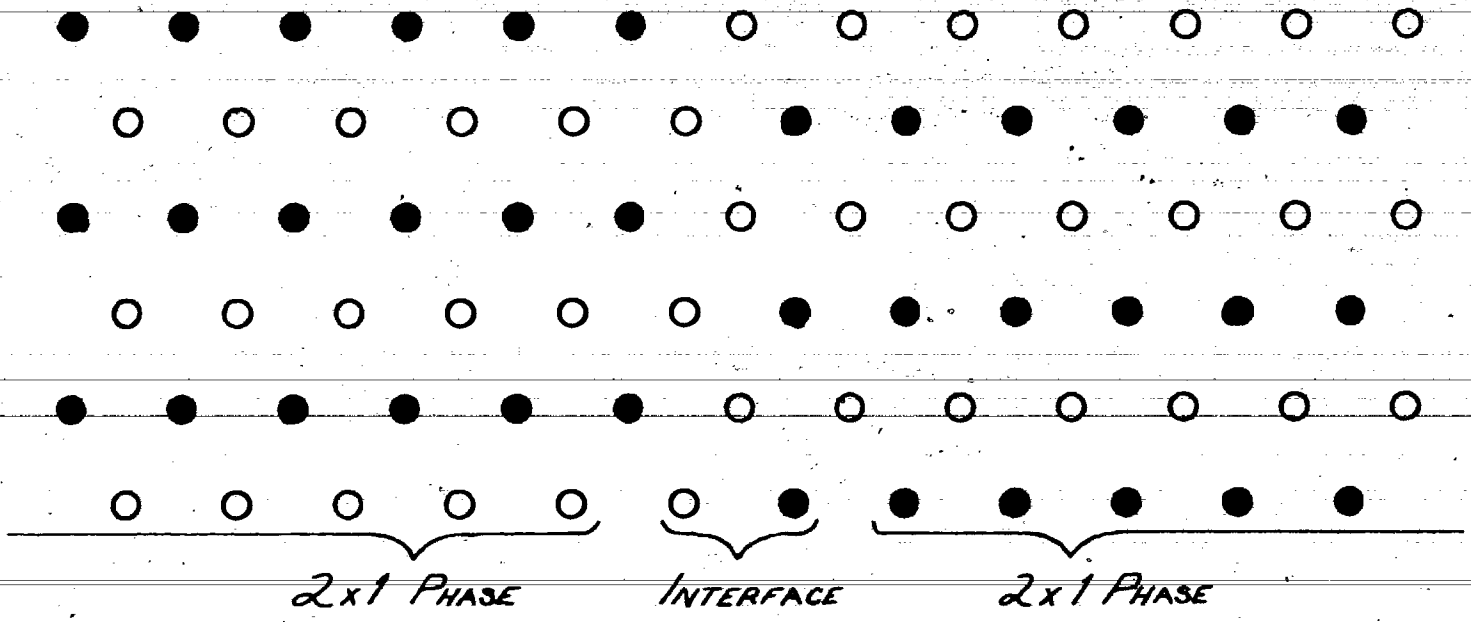

Figure A4

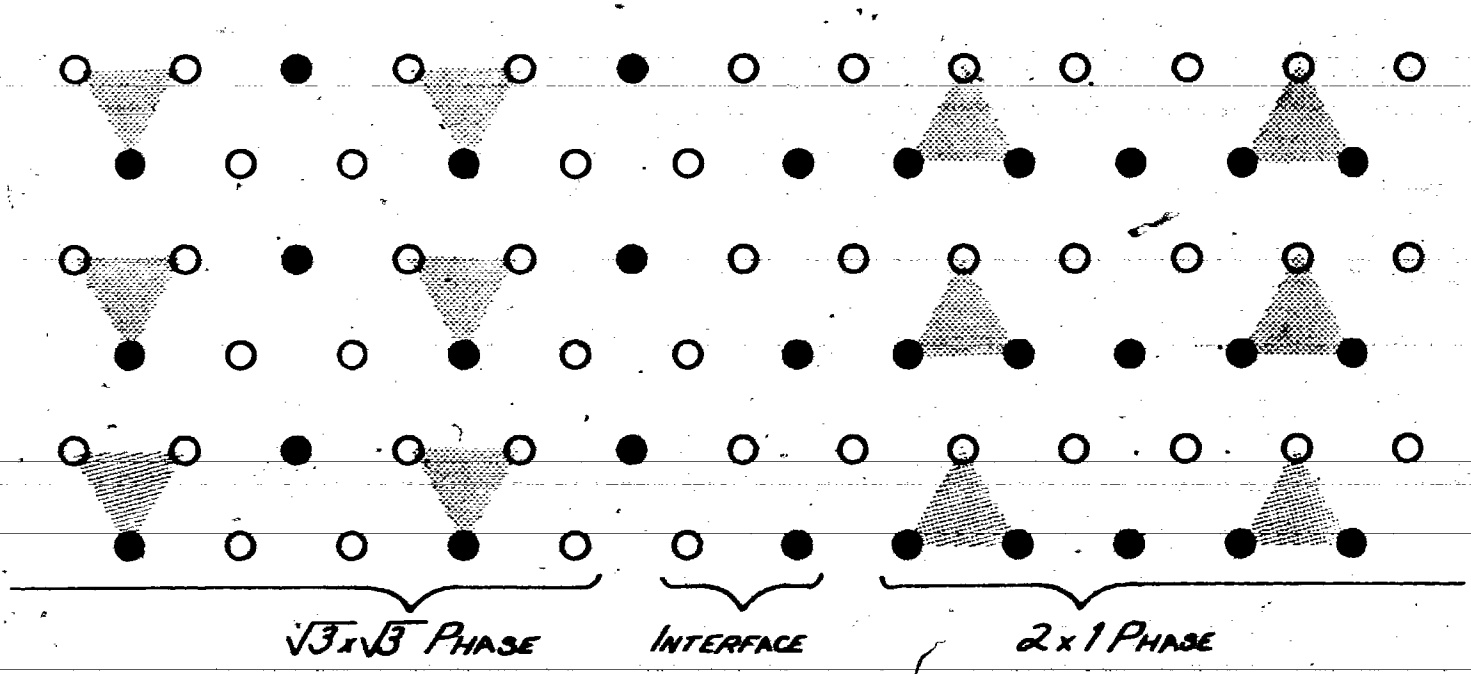

Figure A3

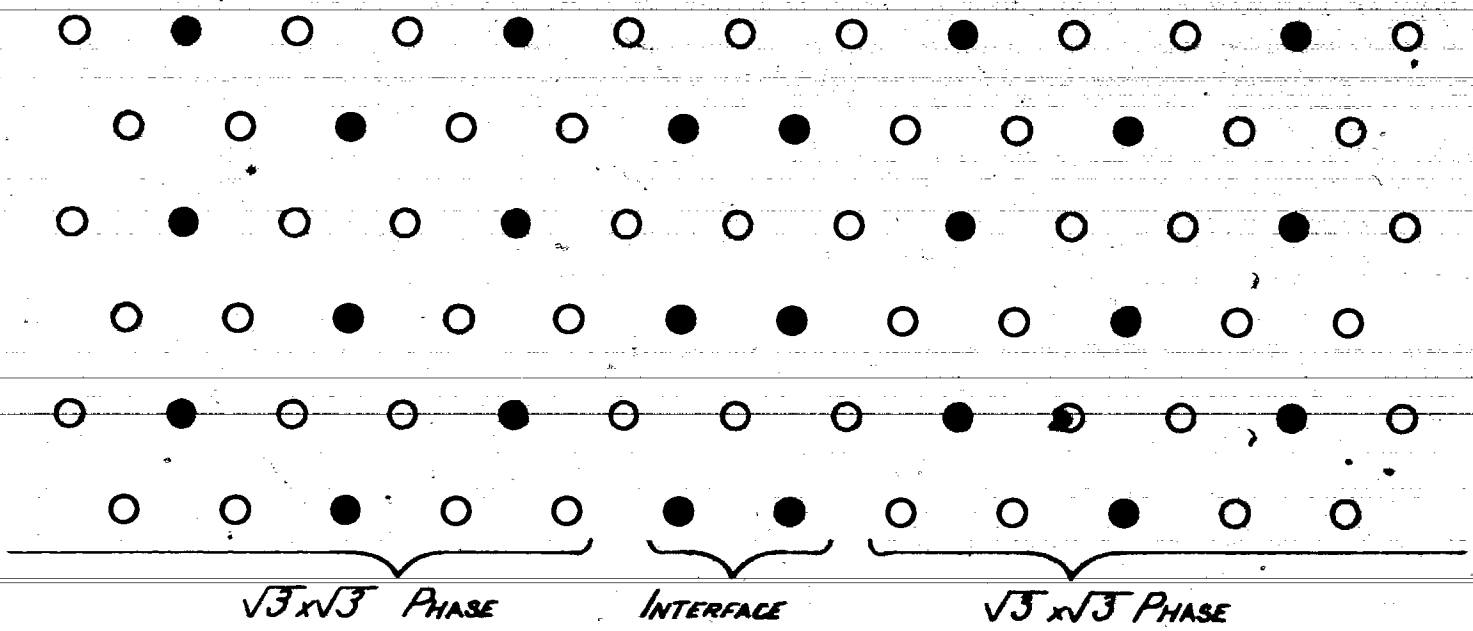

Figure A6

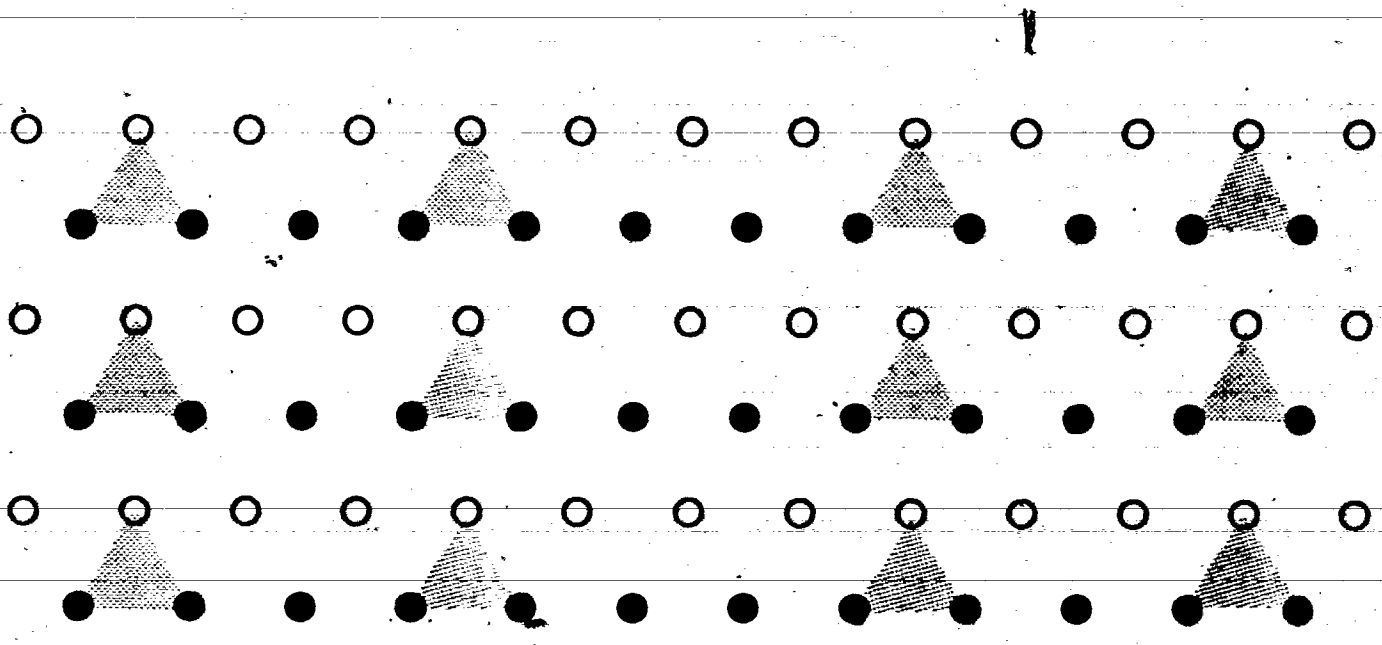

Figure A5

REFERENCES

1) M.N. Barber, Phys. Reports 59, 377 (1980)

2) R. J. Baxter, J. Phys. A 13, L61 (1980)

3) R.J. Baxter and F.Y. Wu, Phys. Rev. Lett. 31, 1294 (1978)

4) K. Binder (ed.):Monte Carlo Methods in Statistical Physics (Springer-Verlag 1979)

5) K. Binder, Phys. Rev. Lett. 47, 693 (1981)

6) K. Binder, Z. Phys. B 43, 119 (1981)

7) M. Bretz and J.G. Dash, Phys. Rev. Lett. 27, 647 (1971)

8) M. Bretz, J.G. Dash, D.C. Hickernell, E.O. Mclean and O.E. Vilches, Phys. Rev A 8, 1589 (1973)

9) T.W. Burkhardt, Z. Physik B 39, 159 (1980)

10) T.W. Burkhardt and J.W.J van Leeuwen (eds.): Real space Renormalization (Springer-Verlag 1983)

11) G. W. Cunningham, J. of Comp. Phys. 20, 50 (1976)

12) J.G. Dash Phy. Rep. 38, 177 (1978)

13) J. G. Dash, Endeavour, New Series, 6, 15 (1981)

14) E. Domany, M. Schick, J. Walker and R. Griffiths, Phys. Rev. B 18, 2209 (1978)

15) E. Domany and M. Schick, Phys. Rev. B 20, 3828 (1979)

16) C. Domb and M.S. Green (eds.): Phase Transitions and Critical Phenomena, Volume 6, (Academic New York 1976)

17) R.L. Elgin and D.L. Goodstein, Phys. Rev. A 9, 2657 (1974)

18) M.E. Fisher, Rep. Prog. Phys. 30, 615 (1967)

19) M. E. Fisher and A. N. Berker, Phys. Rev B 26, 2507 (1982)

20) M. E. Fisher and David A. Huse, Melting, Localization and Chaos, (Elsevier Sc. Pub. Inc. 1982)

21) M.E. Fisher and W. Selke, Philo. Trans. Roy. Soc. A 302, 1 (1981)

22) R.B. Griffiths, Physcia 106A, 59 (1981)

23) K. Huang, Statistical Mechanics, Wiley, New York (1963)

24) L. Kadanoff, Phys. 2, 263 (1966)

25) M. Kerszberg and David Mukamel, Phys. Rev. B 23, 3943 (1981)

26) S.J. Knak Jenson, O.G. Mouritsen, E. Kjaersgaard Hansen and Per Bak, Phys. Rev. B 19, (1979)

27) D.P. Landau, Phys. Rev. B 13, 2997 (1976)

28) D.P. Landau and R.H. Swendsen, Phys. Rev. Lett. 46, 1437 (1981)

29) R. Leonelli, M. Plischke, and J.C. Irwin, Phys. Rev. Lett. 45, 1291 (1980)

30) K.Y. Lin and F.Y. Wu, Z. Phys B 33, 181 (1979)

31) B.D. Metcalf Phys. Lett. 45A, 1 (1973)

32) B.D. Metcalf Phys. Lett. 46A, 325 (1974)

33) B. Mihura and D.P. Landau, Phys. Rev. Lett. 38, 977 (1977)

34) B. Mihura and D.P. Landau, Phys. Rev. Lett. 38, 977 (1977)

35) O.G. Mouritsen and A.J. Berlinsky, Phys Rev Lett 48, 181 (1982)

36) O.G. Mouristen S.J. Knak Jensen and Per Bak, Phys Rev Lett 39, 629 (1977)

37) E. Muller-Hartmann and J. Zittartz, Z. Phy. B 27, 261 (1977)

38) M. Nauenberg and B. Nienhuis, Phys. Rev. Lett. 33, 1598 (1974)

39) Th. Niemeijer and J.M.J. van Leeuwen, Phys. Rev. Lett. 31, 1411 (1973)

40) B. Nienhuis, A.N. Berker, E.K. Riedel and M. Schick, Phys. Rev. Lett 43, 737 (1979)

41) B. Nienhuis and M. Nauenberg, Phys. Rev. Lett. 35, 477 (1975)

42) B. Nienhuis, E.K. Riedel and M. Schick, J. Phys A 13, L31 (1980)

43) J. Oitmaa, J. Phys. A: Math. Gen. 15, 573 (1982)

44) S. Ostlund, Phys. Rev. B 24, 398 (1981)

45) S. Ostlund and A.N. Berker, Phys. Rev. Lett. 42, 843 (1979)

46) S. Ostlund and A.N. Berker, Phys. Rev. B 21, 5410 (1980)

47) M. Plischke, K.K. Bardhan, R. Leonelli, and J.C. Irwin Can. J. Phys. 61, 397 (1979)

48) C. Rebbi and R.H. Swendsen, Phys. Rev. B 21, 4094 (1980)

49) Y. Saito, Phys. Rev. B 24, 6652 (1981)

50) Y. Saito, Supp. Prog. Theor. Phys., 69 (1980)

51) M. Schick, Prog. Surface Science 11, 245 (1981)

52) M. Schick, J.S. Walker and M. Wortis, Phys. Rev. B 16, 2205 (1977)

53) L.S. Schulman, J. Phys. A 13, 237 (1980)

54) W. Selke and M.E. Fisher, Phys. Rev. B 20, 257 (1979)

55) R.L. Siddon and M. Schick, Phys. Rev. A 9, 907 (1974)

56) K.R. Subbaswamy and G.D. Mahan, Phys. Rev. Lett. 37, 642 (1976)

57) R.M. Suter, M.W. Shafer, P.M.Horn, and P. Dimon, Phys. Rev. B 26, 1495 (1982)

58) R.H. Swendson, Phys. Rev. Lett. 42, 859 (1979)

59) R.H. Swendsen, Phys. Rev. B 20, 2080 (1979)

60) R.H. Swendsen, D. Andelman and A.N. Berker, Phys. Rev. B 24, 6732 (1981)

61) R.H. Swendsen and S. Krinsky, Phys. Rev. Lett. 43, 177 (1979)

62) J. Villain and P. Bak, J. Physique 42, 657 (1981)

63) J.S. Walker and M. Schick, Phys. Rev. B 20, 2088 (1979)

64) B. Widom, J. Chem. Phys. 43, 3892 and 3898 (1965)

65) K.G. Wilson, Phys. Rev. B 4, 3174 (1971)

66) K.G. Wilson, Phys. Rev. B 4, 3184 (1971)